Modelling Cancellous Bone Screw Performance using Finite Element Models

A thesis submitted for the degree of Doctor of Philosophy

Antony T. Piper

Brunel University London

College of Engineering, Design and Physical Sciences
Department of Mechanical, Aerospace and Civil Engineering

August 2015

Abstract

Implants such as intramedullary nails or cancellous screws are used to mechanically stabilize fractures in bone. They provide reinforcement to the bone if they find good purchase in cancellous bone. Not all implants hold enough loads for mechanical stability and pull-out or cut-out may happen in some cases. This is linked to the interface between the bone and the implant.

Computer modelling techniques are used to investigate both the effects of cut-out in a femur model, and the pull-out forces of cancellous bone screws. The bone geometry was based on CT scanned cancellous bone and converted using Mimics® software. The finite element models were produced in ANSYS®.

Simple bone models were used to examine a fractured femur under standard gait loading. These models were continuum models and idealised the screw to bone interface in order to ease computational demand. The models were used to investigate the ideal positions of intramedullary devices lag screws on an anterior-posterior view of the implant location. In accordance with literature, an inferior-central or central-central position was the best position of the lag screw, while a superior-anterior or inferior-anterior position was adverse. The introduction of multi-scale modelling in order to investigate cut-out with a discrete bone model was not achieved.

Discrete cancellous bone models were used to examine some of the cancellous screw characteristics, including pitch, inner diameter and proximal half angle, while a cancellous screw was also studied using a model of cancellous bone with a range of bone densities. The calculated reaction force for a pull-out of 0.2mm shows the influence of some parameters. Change in the proximal half angle increased the stiffness and strength by about 15% in line with the experimental findings of others, while apparent density changes of 2.5% increased

the forces threefold. A significant reduction in reaction force was observed when a particular screw geometry in lower apparent density bone was modelled and rotated through 180° on a plane. Examination of the geometry of the bone/screw interface shows that in certain positions there is very little cancellous bone to support the implant. This will lead to low strength and is very difficult to predict.

The same models were used to examine the effect of increasing bone stiffness adjacent to the implant and the use of a cement layer to augment the screw model. The increasing stiffness concluded that an increase in pull-out stiffness can be achieved, even in low quality bone, while the cement augmentation showed a significant increase in pull-out strength, though it was idealised as bonded to the bone and screw.

Acknowledgements

I would like to thank Chris J. Brown for his guidance and supervision, as well as his support to give me the opportunity to carry out this project. Phillip Procter and Stryker for their data and input to the research. My family for their support during this project.

I would like to thank Ledean A. Cooper for her patience and for the ‘A.’ that describes her.

Declaration

I confirm that the intellectual content of this research presented in this thesis is the original work of the author, save for any express acknowledgements, references and bibliographies cited in the work. This work or any part thereof has not previously been presented in any form to any institutional body whether for another degree, award or other purposes.

This project was carried out at the Department of Mechanical, Aerospace and Civil Engineering, College of Engineering, Design and Physical Sciences, Brunel University, under the supervision of C. J. Brown.

Contents

List of Figures

List of Tables

Acronyms and Abbreviations Used

AP – Anteroposterior (View or Position)

BV/TV – Bone Volume/Total Volume

BMD – Bone Mineral Density

BMI – Body Mass Index

CaP – Calcium Phosphate

CAD – Computer Aided Design

CT – Computed Tomography

GPa – Giga-Pascal (Unit)

HPC – High Performance Computing

FEA – Finite Element Analysis

FEM – Finite Element Method

MRI – Magnetic Resonance Imaging

PLA – Polylactide

PLDLLA – Poly(L-lactide-co-D,L-lactide)

PMMA – Polymethylmetharcrylate

STP – Stress Transfer Parameter

WHO – World Health Organisation

µCT – Micro Computed Tomography

Equations

$$F_s = S \times A_s = \left(S \times L \times \pi \times D_{major}\right) \times \{0.5 + 0.57735[d/p]\}$$

$$Where: F_s = Predicted\ shear\ failure\ force\ (N)$$

$$S = Material\ ultimate\ shear\ stress\ (MPa)$$

$$A_s = Thread\ shear\ area\ (mm^2)$$

$$L = Length\ of\ thread\ engagement\ (mm)$$

$$D_{major} = Major\ diameter\ (mm)$$

$$d = Thread\ depth\ (mm)$$

$$p = Thread\ pitch\ (mm)$$

$$Pure\ Penalty:\ F_{normal} = k_{normal} x_{penetration}$$

$$Augmented\ Lagrange:\ F_{normal} = k_{normal} x_{penetration} + \lambda$$

$$F_{normal} = Force\ (N)$$

$$k_{normal} = constant$$

$$x_{penetration} = displacement\ (m)$$

$$\lambda\ is\ an\ internally\ calculated\ term\ that\ augments\ the\ penalty\ calculation$$

1) Chapter 1 – Introduction

Approximately 100 million bone screws are used each year. With a failure rate of at least 1%, this leads to around 1 million screws failing with each potentially leading to further surgery (Procter, 2013).

Two principal failure modes of bone implant consist of cut-out and pull-out. The concept of screw pull-out failure is based on the shear failure of an interface between the screw and the bone where the screw will shear bone, carrying material between the threads (Lyon, Cochran and Smith, 1941). The concept of cut-out of lag screws is defined as *"the collapse of the neck-shaft angle into varus, leading to extrusion of the screw from the femoral head"* (Bojan et al., 2013). This thesis describes the use of computer modelling techniques to investigate the interface between the bone and the implant and consider the variability in pull-out force as well as an attempt to understand one or improve the other mode of failure via augmentation.

Intramedullary devices are used in femur fractures when mechanical strength and reinforcement is needed. These devices are used to support most of the load in the femur proximal region which reaches the order of 1700N from the hip joint alone (Bergmann et al., 2001). As such, the occurrence of cut-out of the lag screw will compromise the entire mechanical stability if the fracture is not healed.

Cancellous bone screws are used to achieve good pull-out characteristics when connected to cancellous bone alone. The vertical load in reference to the screw at which the screw fails is called pull-out. A general equation for screw pull-out can be used in a continuum of any size, but this equation is not as appropriate when analysing a cancellous open, porous bone structure. The pull-out force is thought to be strongly determined by the screw outer diameter and length of engagement, as defined by Chapman *et al.* (1996) and this has been widely accepted.

Implant pull-out or cut-out leads to further surgery as the failed device must often be removed and replaced. This failure may occur many months after the initial surgery and can be very distressing and painful for the patient, if not fatal in some cases. By further research of the bone and implant interface and the implant's performance in bone, the aim is to improve the holding power of bone implants, reducing the incidence of failure by the two modes described.

Intramedullary devices can be improved if the phenomenon of cut-out is better understood and avoided by either changing the bone environment or changing the design of the device. In the case of lag screws, an ideal positioning inside the femur head will improve the strength of surrounding bone and overall performance of the device (Nishiura, Nozawa and Morio, 2009).

For cancellous screws, pull-out may be improved by the same approaches; either change the bone environment or change the screw design. Gausepohl *et al.* (2001) considers the latter and concluded that a narrow pitch will increase the pull-out force. Other parameters of the cancellous screw may have an effect on pull-out and this will be examined in this thesis.

In addition to varying screw parameters, the second approach of improvement by changing the bone environment will be investigated by modifying the properties of bone adjacent to the screw, increasing the elastic modulus of a cylinder of bone around the screw, and by cement augmentation. Two types of bone cements, Polymethylmetharcrylate (PMMA) and calcium phosphate (CaP), have been available for some time. PMMA is usually unpopular due to its heat generation upon curing which results in cell death (Gundapaneni and Goswami, 2014). Calcium Phosphate is a more recently developed product, but it is primarily defined as non-load bearing. In spite of this, early trial show positive results from its use as a void filler in critical areas around screws in cancellous bone. Cement augmentation may improve holding strength of bone implants, but the considerable variation in screw performance in practice has shown that they may not always lead to improvement (Procter *et al.*, 2015).

The main objectives of this research can be summarised as the following points:

- Create a model that can approximate in vivo or in vitro testing appropriately, in order to reduce investigation time of parameters, easily changed on a FEA model.
- Examine the performance of lag screws in low density bone by use of multi-scale models.
- Select the best position in the femur for the lag screw of an intramedullary nail, comparing the results to existing literature.
- Finding the best cancellous screw parameters for pull-out forces and asserting the importance of each.
- Investigating the effect of cement augmentation and reaching conclusions about its effectiveness in improving pull-out.

1.1. Body of Knowledge Contribution

- A novel method of modelling cancellous bone with frictional contacts at varying volume densities and the description of its implementation as a 3D mesh for use in FEA simulation.
- A positional FEA analysis of an intracapsular fracture. A confirmation of the ideal location for the lag screw of intramedullary implants.
- An FEA study of the parameters of a cancellous screw.
- A study of the use of cement augmentation to show how its use can improve the holding power of implants.
- Simulation of an Arthrex Pushlock implant and a comparative study with sonic fusion and a threaded anchor.

1.2. Outline

This thesis contains 8 chapters. Cut-out and intramedullary devices are investigated first and then the implant and bone interface is examined and analysed.

Chapter 2 provides all the background information needed to set this project into the current knowledge. Bone properties and histology, bone weaknesses and bone implants will be explained as background for the thesis.

Chapter 3 covers the modelling methods and techniques available and used as well as the software and hardware background.

Chapter 4 shows the initial work and simple bone models performed. These models are aimed at investigating cut-out and the bone-implant interface.

Chapter 5 follows a parametric study of a cancellous screw in bone. It investigates the volume fraction, the screw pitch, inner diameter and the proximal half angle.

Chapter 6 looks at the use of augmentation, by changing local material properties and adding idealised cement to the FEA models.

Chapter 7 compares an Arthrex Pushlock implant to a sonic fusion model and a Bio Mini-Revo implant.

Chapter 8 summarises the findings of the previous chapters, discussing the results and observations, and recommends the path further work could follow.

2) Chapter 2 – Review of Literature

2.1. Overview

This thesis addresses the use of mechanical implants for the fixation of bone fractures, by investigating the importance and interactions of bone to implant interfaces. Using implants to fix bone fractures is a process called osteosynthesis. This process was imagined as early as 1850 by the French surgeon Rigaud of Strasburg who precognised the use of screws in bone fixation, but who only used ivory intramedullary and pinning methods in practice. Aside from fixation with ivory, fractures were fixed by metal sutures. It is also important to note that these fixations were performed very late after the trauma, and often involved mortality by infection until 1862 and the breakthrough in infection control. The discovery of X-Rays in 1895 by Roentgen was the second breakthrough for osteosynthesis and greatly enhanced the fixation of bone by giving an image prior to operation, as opposed to relying on the sense of touch to analyse the type of fracture (Vichard and Gagneux, 1995).

In order to investigate the importance and interactions of bone to implant interfaces, the background of understanding needs to be explained. As such, this chapter has been split into sections that will cover different aspects of knowledge:

First of all, the human skeletal system will be described with relevant depth and attention will be given to the human femur as an example of structure for bones in which implants are used. The physiology of the bone is described in relevance to receiving implants, as understanding the whole system is of importance to a good healing outcome.

The mechanical properties of the bone will then be described as the material receiving the implants, which is of importance to any mechanical analysis of the interaction between the two.

The next section will cover weakened bone. Osteoporosis, fractures and cut-out (which is a consequence of fracture fixation) all affect the strength of the system analysed and are principal reasons for the use of devices or major affecting factors when the devices have been implemented.

Finally, the last section will cover the bone implants that are the subject of this thesis and literature surrounding previous research on devices. This section will be split into intramedullary devices and the more general concept of screws within bones.

2.2. Skeletal system

The human body is built around the skeletal structure. It is the biological frame upon which the muscles are attached and it is the primary structure which composes the human body. In the early stages of human life, the bones are softer and incomplete upon birth. Once the human body has reached a certain age, the growth and hardening of the bones is ended by gonad hormones, especially oestrogen in both sexes as it shuts down at epiphyseal (growth) plates, causing bone elongation to cease (Tortora and Derrickson, 2013). As the body ages further, bone mass then decreases due to factors, some of which are explained later in section 2.4. This decrease is seen mainly in women aged 50 to 60 years old (Riggs and Melton, 1986).

Almost all of the bones in the human body can be classified into four primary groups, although this classification may vary between authors. The human body is composed of:

- Long bones – These bones are longer than they are wide and circular, typically have two condyles (rounded connection surfaces) at either end. Some examples include the femur (thigh), tibia, fibula (leg), humerus (arm), ulna, radius (fore-arm) and phalanges (finger & toes)
- Short Bones – These bones are somewhat cuboid in shape: they are of nearly equal width and length. Some examples are usually found in most wrist and ankle bones.
- Flat Bones – These bones are usually thin, but provide protection for internal organs. They also provide large surfaces for muscle attachment and contain mostly red marrow, which makes them one of the largest producers of blood cells. Some examples include the cranial bones, the sternum, the ribs, and the scapulae (shoulder blades).
- Irregular Bones – These bones are of complex shapes which cannot be grouped in any of the previous categories. Some examples of irregular bones include the vertebrae, hip bones, and some facial bones.

- Sesamoid bones – These bones develop within certain tendons where friction, tension and physical stress are high. They are not always completely ossified and may vary in number depending on the individual. They are typically a few millimetres in diameter apart from the kneecap, large sesamoid bones that are normally present in everyone. Functionally, these serve as protection from wear and tear of the tendon, in addition to changing the direction of pull of the tendon, in order to improve the mechanical advantage of the joint.
- Sutural bones – These small bones vary greatly in number between individuals. They are small bones located in sutures between certain cranial bones.

In addition to support and blood cell production, the skeletal system provides the body with a mineral storage in order to provide the body with a balance of critical minerals (homeostasis) and storage for triglycerides (fats): the yellow bone marrow. Only red bone marrow exists in the new-born, but with increasing age, most of the red marrow changes to yellow (Tortora and Derrickson, 2013).

2.3. Femur Structure

As the principal long bone studied in this thesis, the femur is the large bone located within the thigh and above the tibia, fibula and knee. It is the longest bone in the body and is composed of two ends *(epiphysis)* and a shaft *(diaphysis)*. The two ends are called proximal, closest to the torso, and distal, most distant from the torso, where the proximal end (Figure 2-1) is composed of a head, a neck, a greater trochanter and a lesser trochanter. The head is approximately two thirds of a sphere and is connected to the pelvis. The neck is oblique and is the curved upper end of the femur shaft. Across the intertrochanteric crest from neck is greater trochanter, which is an outcrop to which the gluteus medius is attached. On the posterior surface of the bone the lesser trochanter can be found, which is where the iliopsoas finds attachment.

The distal end is composed of two condyles, the lateral and medial condyles, projections which articulate with the tibia. These condyles are separated on the anterior by a flat surface called the patellar surface (Tortora and Derrickson, 2013).

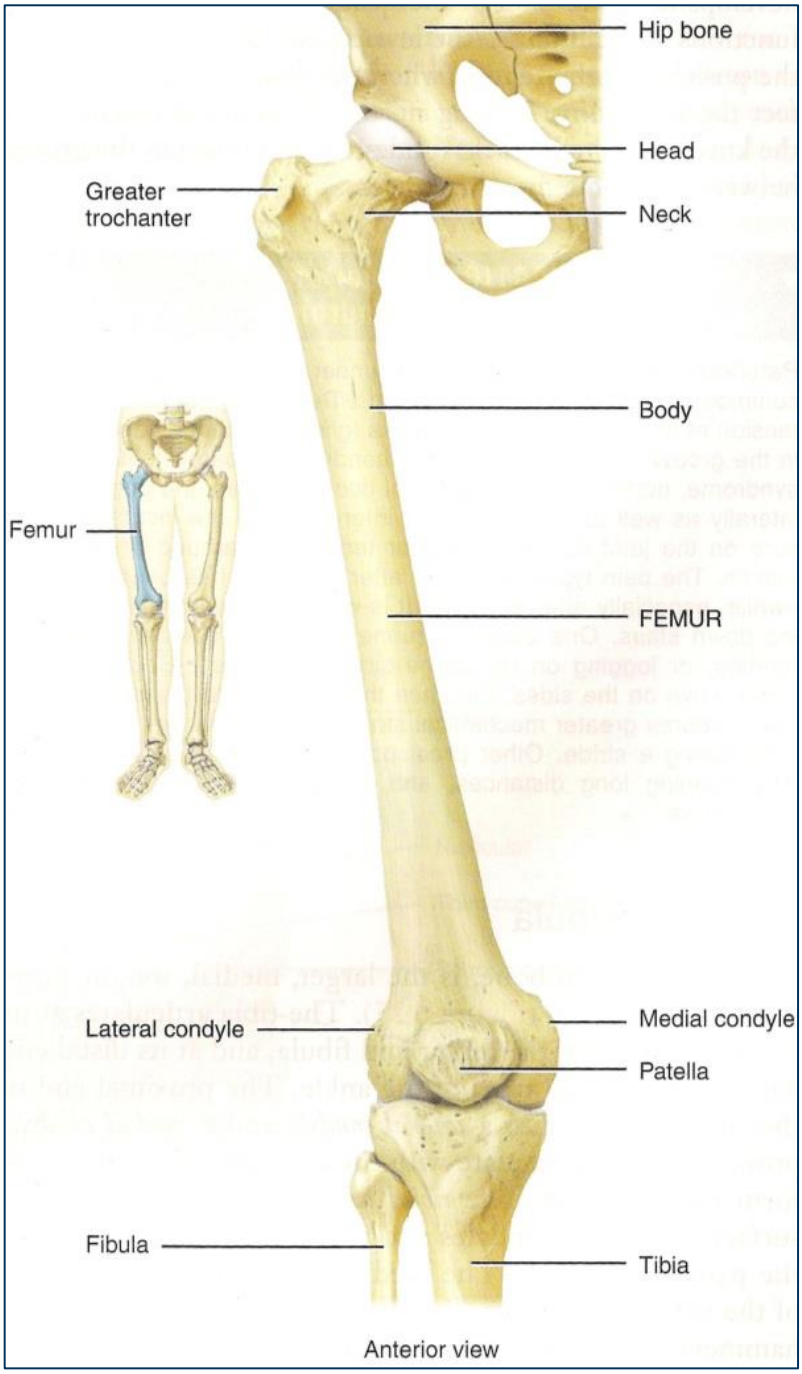

Figure 2-1: Structure of the Femur (Tortora and Derrickson, 2013).

2.4. Femur Physiology

The femur is composed of both cortical (compact) and cancellous (spongy) bone. The shaft is mainly composed of cortical bone, while both epiphyses are composed of a cortical shell with a cancellous interior. The outer layer is called the 'periosteum' while the inner section is called the 'endosteum'.

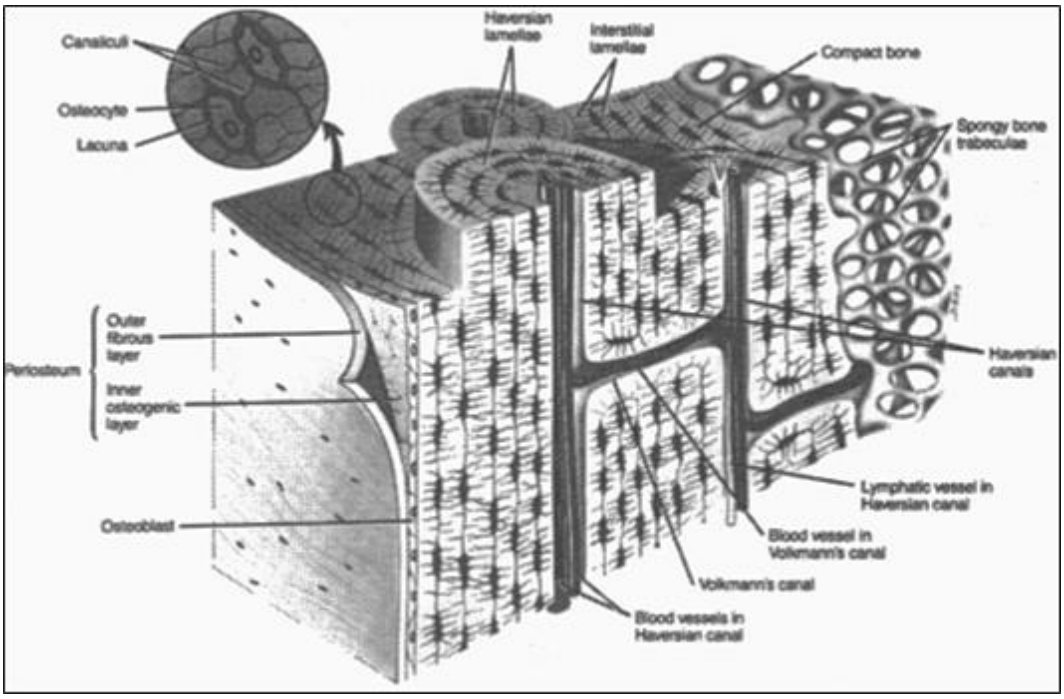

Figure 2-2: Diagram of a sector of the shaft of a long bone showing the different types of cortical bone, trabecular bone, and the various channels (Tortora and Derrickson, 2013).

2.4.a. Cortical bone

Cortical bone comprises approximately 80% of the skeletal mass. It is a compact layer of collagen fibres which forms the outer shell of a bone. For the average male adult, it is around 10mm thick in the shaft of a femur but much thinner on the epiphysis, where it can be less than 1mm thick (Jee, 2001). Cortical bone can be composed of woven bone or lamellar (Haversian) bone. Woven bone is found in the new-born and fractures where new bone is generated rapidly. It is then replaced by lamellar bone (at age 2 and 3 years in human long bones) which is a longer process, but produces osteons and layers of lamellae, both interstitial and circumferential. Osteons are typically around 200µm in diameter and run parallel to the long axis of the bone. Haversian bone is mechanically much stronger than

woven bone as the osteons contain multiple layers of lamellae which are approximately 3 to 7 µm thick and run in approximately the same direction, although these axes can differ by as much as 90° in adjacent units. The centres of these osteons contain nerve fibres, blood vessels and lymphatics. They are connected radially by Volkmann's canals (Figure 2-2) (Jee, 2001).

2.4.b. Cancellous bone

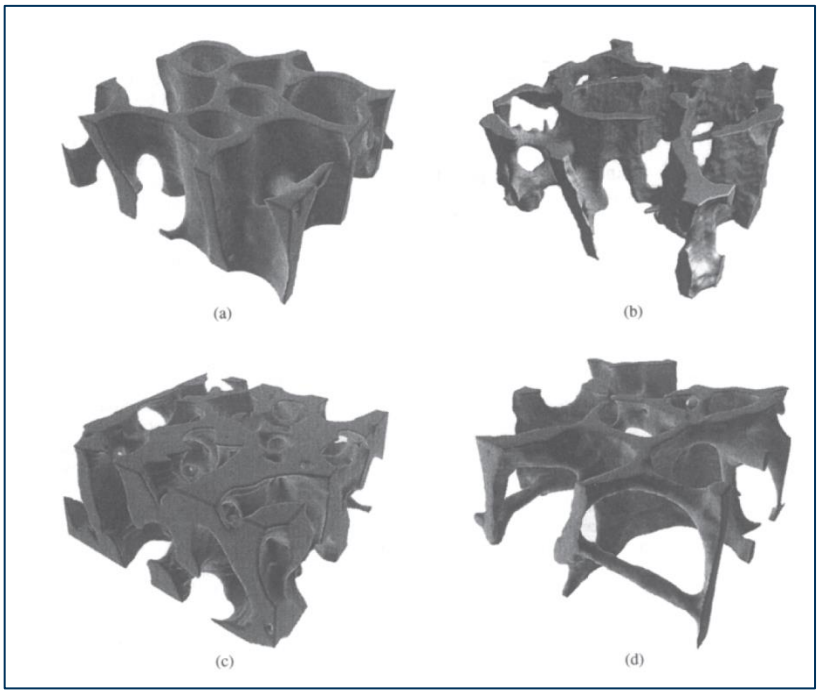

Figure 2-3: Three-dimensional reconstructions of trabecular bone from the (a) bovine proximal tibia, (b) human proximal tibia, (c) human femoral neck, (d) human vertebra. Each volume is 3 × 3 × 1 mm3 (Cowin, 2001).

The second type of bone, cancellous bone, also known as 'Spongy bone' or 'trabecular bone' approximates to a structure of struts and plates which contain wide spaces. This structure is made of units called trabeculae. Cancellous bone can therefore be thought of as an open-cell solid. As such, cancellous bone shares some significant properties of cellular solids such as Energy absorption which follows Rush's curve (Gibson and Ashby, 1997) and is further described at the end of section 2.5 below. Cancellous bone is found mainly in flat, irregular and short bones but it is also found in the epiphyses of long bones. The structure is light, which reduces the overall weight of a bone and allows the bone to move more readily when pulled by a skeletal muscle. Cancellous bone is the only part

in the body where red bone marrow can be found. The trabeculae of bone support and protect the marrow, as red bone marrow is the site of blood cell production (Tortora and Derrickson, 2013).

The ratio of cancellous to cortical bone will vary depending on the bone. Bones such as the ulna (forearm) contain about 8% of cancellous bone, whereas a typical vertebra (spinal column) will contain up to 38% of cancellous bone. The spaces between the structures widen with age and osteoporosis, and the overall density of the cancellous structure can decrease dramatically (Jee, 2001).

The structure of rod and plates can be classified using the structure model index (SMI), which uses the change in surface area as volume increases infinitesimally. The SMI is calculated on a scale from 0 to 4 where SMI = 0 is for plate-like structures, 3 for rod-like and 4 for solid spheres. Unfortunately the SMI is negative for concave surfaces, which are common in trabecular bone; making results difficult to interpret and therefore often unusable (Hughes, 2014) though this method is the only measure of the bone's plate-like or rod-like structure.

Figure 2-4 Desiccated bone of the Glenohumeral joint, showing cortical shells and inner cancellous bone (http://medicalpicturesinfo.com/cancellous-bone, 10/09/2011)

2.4.c. Histology

Human bone, such as is found in the femur, is subject to constant remodelling as part of growing and ageing of the body. Woven bone is replaced by lamellar bone in the infant, and this cycle continues throughout the lifecycle. Bone remodelling consists of resorption, the removal of bone, and ossification, the

production of new bone. The mean age of cortical bone is of around 20 years while cancellous bone is around 1 to 4 years (Jee, 2001).

The cells which are involved in the bone remodelling process, and as such, the cells that compose a healthy human bone can be listed below:

- Osteogenic (Osteoprogenitor) cells are located on the inner portion of the periosteum, in the endosteum and in the canals within bone that contain blood vessels. They are the only bone cell to undergo cell division in order to produce osteoblasts. They are classified as stem cells and are most active during bone growth or fracture repair. They are a derivative of the mesenchyme, the tissue from which almost all connective tissues are formed.
- Osteoblasts are single nucleus bone building cells. They synthesise and secrete collagen fibres (90%) and other organic components (non-collagenous protein – 10%) in order to build the extra-cellular matrix of bone tissue. They also initiate calcification, the mineralisation of bone by calcium and phosphate ions. The number of osteoblast cells decreases with age and this is one factor responsible for the decrease in bone density with age. As osteoblasts surround themselves with bone matrix, they may become trapped in their secretions and become osteocytes.
- Osteocytes are mature bone cells which maintain the metabolism of bone tissue, such as the exchange of nutrients and wastes with the blood. They are the most abundant form of bone cell and differentiate from osteoblasts, their original trapped function, by the loss of their organelles (sub-units of a cell).
- Osteoclasts are very large cells (20-100µm wide) derived from the fusion of as many as 50 monocytes (a type of white blood cell) and are concentrated in the endosteum. On one side, the cell releases powerful enzymes and acids that digest the protein and mineral components of the underlying bone matrix, a process called bone “resorption” (Tortora and Derrickson, 2013).

- Bone lining cells are thinly extended over bone surfaces and have flat organelles to easily cover bone without interfering with other cellular functions and are inter-connected by gap junctions. They are a relatively inactive form of osteoblast but may be activated and may secrete growth factors which trigger osteoblast progenitor proliferation, as well as be involved in the propagation of the activation signal that initiates bone resorption and bone remodelling. They may also have a role in mineral homeostasis as they act as an ion barrier between the bone fluid and interstitial fluid and maintain these (Miller et al., 1989).

Together, these cells remodel bone but over time, more cells are removed than are created, which leads to a reduction in bone density and bone width, which in turn decreases bone strength and may lead to natural osteoporosis.

2.5. Mechanical Properties of Bone

The mechanical properties of cancellous bone vary greatly due to a set of multiple factors. As a heterogeneous porous cellular solid, cancellous bone has an anisotropic behaviour. Anisotropy is when a material performs differently mechanically in its three Cartesian directions. These anisotropic properties vary depending on the porosity of the bone as well as the geometrical arrangement of specific trabeculae and plates. The geometric arrangement of the "grain" of the bone follows trajectory lines of the highest principal stresses in the bone (Figure 2-5), and the remodelling of cancellous bone will adapt according to these forces. This theory that, over time, bone adapts to the loads placed upon it is called Wolff's Law (Goodship and Cunningham, 2001; Cowin, 1986). There is some debate about the theory's origin, accuracy and exact working, but understanding this behaviour is important for the healing of bone fractures both in healing time, and minimising additional stress on the bone.

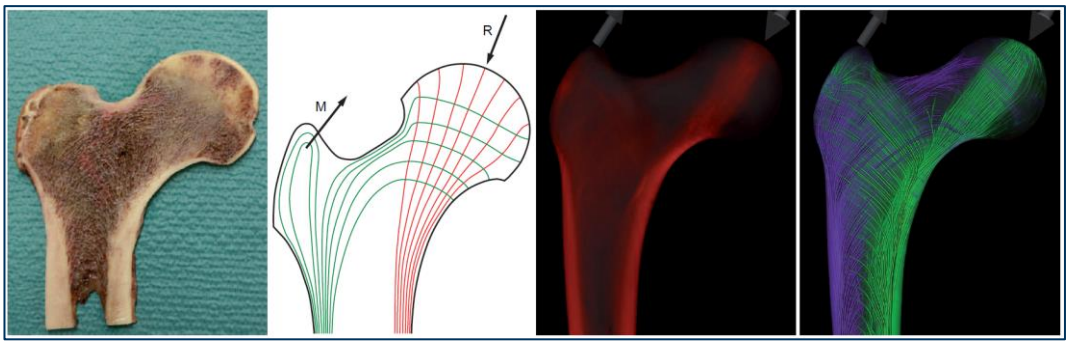

Figure 2-5: Dick *et al.* (2009) show the cross section of a human femur as well as schematics and renderings of the stresses in the femur.

Perilli *et al.* (2008) show that the microarchitecture has an important effect on the strength of bone: by studying human femoral samples, they conclude that localised minimums of BV/TV (Bone volume over total volume) are an important factor in determining ultimate stress of the material. Local minimums of BV/TV predicted ultimate stress better than average BV/TV. This work followed a study done by Nazarian *et al.* (2006) on human vertebrae bone that first concluded that the minimum value of BV/TV is a better predictor than BV/TV of the entire specimen. Failure of the samples was mainly localised within sub regions with minimum BV/TV.

Both of these studies show that the cancellous bone structure would only be as strong as its weakest element, when looking at the structure as a whole. This is very important for implant performance and to this study.

Wolff's Law also leads to an important mechanical factor of metallic implants in cancellous bone: Stress shielding. When a very stiff screw fixation carries most of the load, it causes the adjacent bone to resorb due to the lack of stimulus during remodelling (Gefen, 2002). Stress shielding is an important consideration for the long-term effect of bone implants. Through bone remodelling, the local cancellous structure will be affected by stress shielding and resorb, as an example is seen in Figure 2-6.

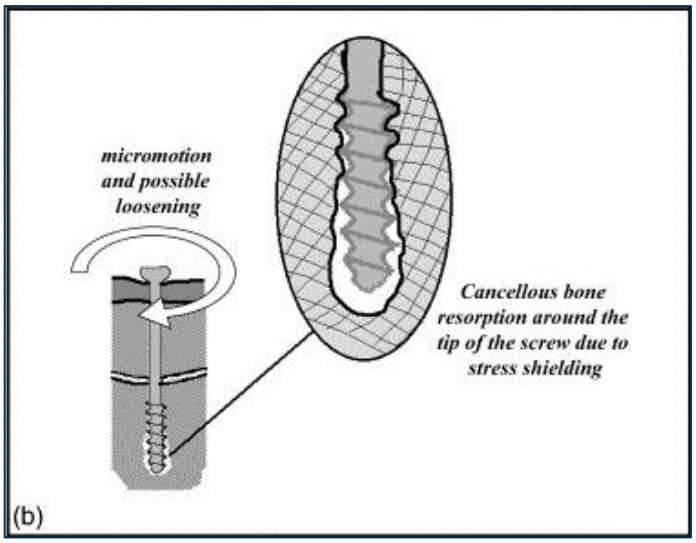

Figure 2-6: "Bone fracture fixation: (b) an illustration of the process leading to failure of the fixation as a result of lack of biomechanical compatibility between the screw and surrounding cancellous bone (Gefen, 2002)."

In addition to geometrical uncertainties, bone is also affected by its non-uniform mineral distribution. Currey (1988) shows that the stiffness of bone tissue correlates exponentially with its mineral content. As bone is remodelled, new bone tissue is mineralised over the course of a few days, where approximately 70% of the mineral is deposited but mineralisation continues slowly for several more years. In cancellous bone, the surface layer of trabeculae is frequently renewed while interstitial bone in the centre can become much older than the surface layer. Bone tissue with a high mineral content has a higher stiffness but at the same time lower failure energy (Currey, 1984). This mineral distribution might therefore be advantageous: the inner, stiffer bone is protected from cracks by an outer layer with a low mineral content, which has better mechanisms against cracks due to its low stiffness (Zioupos and Currey, 1994). The highly mineralised core of trabeculae provides high compression stiffness and when cracks start in this tissue, the lower mineral content surface layer prevents complete failure thus repair of the damage is possible and the mechanical integrity is maintained. This mineral distribution is influenced by the bone turnover rate, and can therefore be influenced by anti-resorptive treatments (Van der Linden *et al.*, 2001).

Tissue-level elastic properties of cancellous bone have been reported in numerous studies (Figure 2-7), but discrepancies in the data are common due to technical challenges and there is almost no data for failure properties at the tissue level. Bayraktar *et al.* (2004) report that high resolution finite element models derived from micro-computed tomography (μCT) with specimen-specific data at the whole specimen level are used to calibrate "effective" elastic properties of the tissue. These studies used compression testing with platens to provide calibration data, but due to the presence of end-artifacts (Jacobs *et al.*, 1999; Keaveny *et al.*, 1997), the results of calibrated effective tissue moduli are low (Hou *et al.*, 1998; Ladd *et al.*, 1998) when compared to the experimental studies done with cancellous bone that used ultrasound and nanoindentation (Turner *et al.*, 1999; Zysset *et al.*, 1999; Rho, Tsui and Pharr, 1997). Some finite element studies that used testing protocols that minimised end-artifacts at the apparent level matched the experimental data more accurately (Niebur *et al.*, 2000). Their own comparative study (Bayraktar *et al.*, 2004) provides more data matching the experimental values for bone elastic modulus (18.0±2.8 GPa) as well as some values on yield properties at the tissue level for both cancellous and cortical bone. For the cancellous tests, they used nonlinear FEA of trabecular bone specimens with apparent level experimental data, but used techniques that eliminated end-artifacts. The values obtained were similar to results found for bovine trabecular tissue using a similar technique for analysis (Niebur *et al.*, 2000).

Reference	Anatomic site	Method	Spec./indent.[a] (donors)	E_{tissue} (GPa)
Ulrich et al. (1997)	Human femoral head	Experiment-FEA	6 (6)	3.5–8.6[b]
Rho et al. (1997)	Human vertebra	Nanoindentation[c]	72 (2)	13.4±2.0
Hou et al. (1998)	Human vertebra	Experiment-FEA	28 (28)	5.7±1.6
Ladd et al. (1998)	Human vertebra	Experiment-FEA	5 (5)	6.6±1.0
Turner et al. (1999)	Human distal femur	Nanoindentation[c]	30 (1)	18.1±1.7
		Acoustic microscopy	3 (1)	17.5±1.1
Zysset et al. (1999)	Human femoral neck	Nanoindentation	N/A[d] (8)	11.4±5.6
Niebur et al. (2000)	Bovine proximal tibia	Experiment-FEA[e]	7 (7)	18.7±3.4
This study	Human femoral neck	Experiment-FEA[e]	12 (11)	18.0±2.8

See Guo (2001) for a more comprehensive review, which includes cortical bone.

[a] Number of specimens (or indentations for nanoindentation studies) and donors used in the study.

[b] Only range reported.

[c] Specimens were dehydrated.

[d] Information not available.

[e] Endcaps were used to eliminate end artifacts in the apparent-level mechanical testing.

Figure 2-7: A comparison of elastic moduli of trabecular tissue, E_{tissue} (mean7SD, in GPa), reported in the literature and in the study by Bayraktar *et al.* (2004).

Rho *et al.* (2002) did some further nanoindentation analysis to compare the elastic properties of interstitial bone and secondary osteonal bone in femoral cortical bone. Young's Modulus of the older, interstitial bone was on average 2.3GPa stiffer than the osteonal bone. There was also a significant difference in the properties of bone between the different individuals from which the samples were obtained. The modulus for interstitial cortical bone ranged between 21.5 and 25.4GPa, while osteonal bone ranged between 18.6 and 23.6GPa.

As shown by Turner et al. (1999), these values are for cortical bone in the longitudinal axis, for which they obtained results of 20.55±0.21 GPa acoustically and 23.45±0.21 GPa by nanoindentation. Due to its anisotropy which stems from the lamellar structure formed during growth, the values obtained in the transverse direction were lower: 14.91±0.52 GPa acoustically and 16.58±0.32 GPa by nanoindentation. Nanoindentation results were 10-20% higher than the results obtained by the acoustic technique. This may have been caused by the re-hydration of their samples when tested acoustically, which would explain a lower Young's modulus. This would indicate that the two techniques would give similar results if they were carried out under the same conditions (Turner *et al.*, 1999).

Another aspect of the mechanical properties of bone is density. Zioupos, Cook and Hutchinson (2008) show that apparent bone density (D_{app}) and bone material density, the tissue density (D_{mat}) have different relationships for cortical and cancellous bone. The results were obtained from mammalian bone, specifically the femur of an elephant, as the shape and properties at the bone matrix level are similar to those of a human femur, though the size of the sample is much larger. The results show that the more porous cancellous samples have denser trabeculae, which is an inverse D_{app} vs D_{mat} relationship, while in compact bone, the more porous samples show reduced material density and mineral content, as in compact bone, D_{app} and D_{mat} go hand in hand. It is assumed that two different tissue physiologies or two different tissue mechanobiology imperatives are involved. When fewer trabeculae are present, they are stiffer and denser. As such, for the same level of stress, the stiffer material would

experience smaller strain, which would mean less damage and less motivation for homeostasis. Cortical bone is the opposite, and higher strain maintains mass, which would result in the tissue experiencing less strain and reach an overall equilibrium. These are both possible explanations for strain homeostasis and damage, though the authors only suggested these methods are mentioned possibilities (Zioupos, Cook and Hutchinson, 2008).

With great variability, cancellous bone structures in compression and tension follow the non-linear behaviour of cellular solids (Gibson, 1985; Gibson and Ashby, 1982) as characterised by distinct failure mechanisms (Figure 2-8).

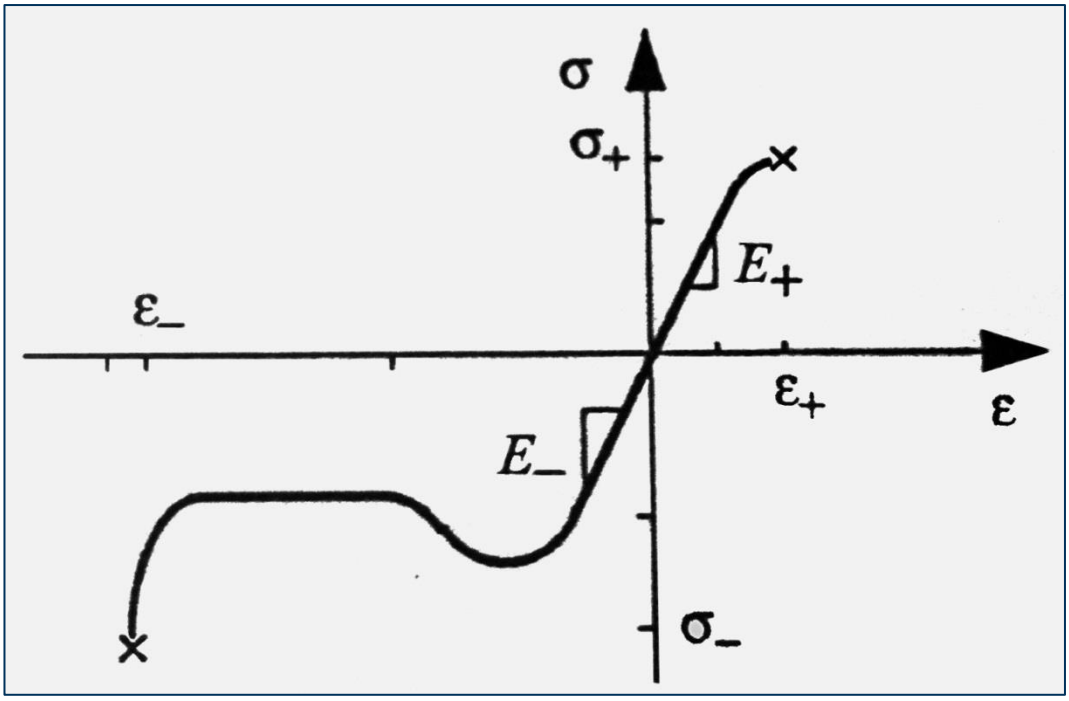

Figure 2-8: Uniaxial stress-strain curve for cellular solids. The linear stress-strain relationship is defined by the Young's elastic modulus ($E_-=E_+$), while the ultimate compressive and tensile stresses (strains) are defined by σ_- (ε_-) and σ_+ (ε_+) (Rincón Kohli, 2003).

In compression (E-) the solid begins with a linear-elastic relation as the cell wall bends or compresses axially. This then changes when the cells start to collapse and the curve softens and cells collapse at an almost constant stress. This continues until the walls meet and create a sharp rise in the stress (Gibson and Ashby, 1982). This final rise is known as densification. In tension the structure

has a linear-elastic portion followed by failure when the struts crack and break with a final destruction of the entire structure (Rincón Kohli, 2003).

2.6. Weakened Bone

2.6.a. Osteoporosis

From the Greek *"ostoun"*, bone and *"poros"*, pore, osteoporosis is a progressive bone disease in which bone density and mass are reduced due to increased osteoclast activity. It can lead to cancellous bone porosity of over 90% and cortical bone porosity of up to 12%. Osteoporosis is defined by bone mineral density (BMD) and its deviation from the mean of the young adult. A value of BMD within 1 standard deviation of the young adult reference mean is referred to as "normal" (T-score ≥ -1). A value of BMD more than 1 standard deviation below the young adult mean, but less than 2 standard deviations below this value is called "osteopenia", low bone mass (T-score < -1 and > -2.5). A value of BMD 2.5 standard deviations or more below the young adult mean is then "Osteoporosis" (T-score ≤ -2.5) (Figure 2-9)(World Health Organization, 2003).

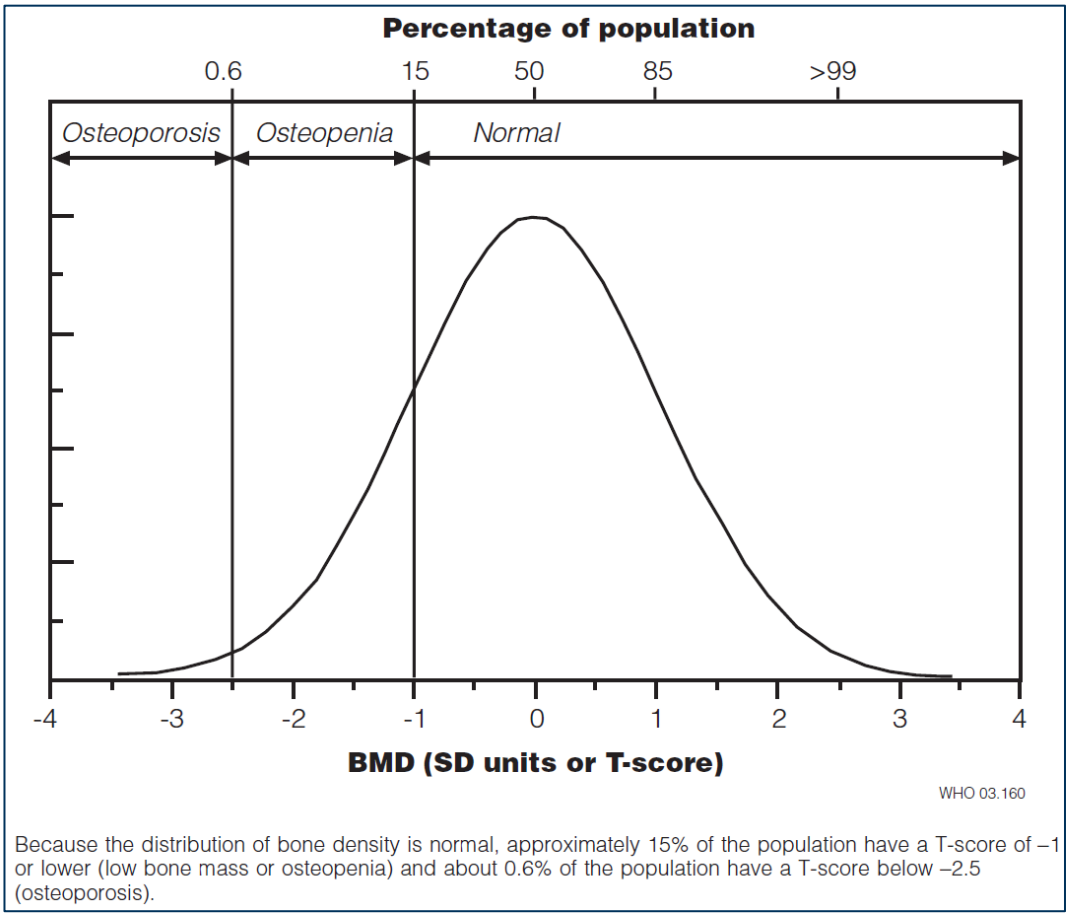

Figure 2-9: Distribution of BMD in young healthy women aged 30–40 years (World Health Organization, 2003).

Reduced bone density can stem from age, where substantial bone loss starts around age 65 years in men and 50 in women (Rizzoli and Bonjour, 1999). This is due to the expansion of the periosteal surface (outer surface) being less than the resorption at the endosteal surface, where the space occupied by bone marrow increases. As such, the bone cortex becomes thinner, and combined with increasing porosity of cortical bone and the destruction of cancellous trabeculae through thinning and perforation, accounts for age-dependent bone loss (World Health Organization, 2003).

Another main factor for BMD loss is oestrogen deficiency, as oestrogen is necessary for maximizing peak bone mass and maintaining it. Oestrogen deficiency accelerates the rate of bone turnover and appears to be the main cause of osteoporosis in women after the fifth decade and could also have an effect on men. In addition, there exist other endocrine causes for bone loss such as Thyrotoxicosis, Hyperparathyroidism, Cushing syndrome, Insulin-dependent diabetes mellitus, adrenal atrophy and Addison disease, Ectopic adrenocorticotropic hormone syndrome and Sarcoidosis (ectopic calcitriol production) (Kanis *et al.*, 1997).

Further factors that cause bone loss include nutritional factors, such as deficiencies in calcium, vitamin D, protein, Vitamin K, or a high intake of phosphate in combination with a low intake of calcium. Other trace elements and vitamins may all play a protective role in the normal metabolism of bone tissue but studies are needed to identify their respective roles in the maintenance of BMD. Physical inactivity is another factor, both from motor deficits due to neurological disorders or space flight, despite vigorous physical exercise. In opposition, physical loading and mechanical stress can increase the BMD to higher-than-average levels, as can be seen in retired adult gymnasts. Cigarette smoking and alcohol consumption can both reduce BMD, as well as a lower BMI (Body Mass Index), or a host of other diseases and disorders (World Health Organization, 2003).

Osteoporosis causes more than 2.3 million fractures annually in Europe and the USA (World Health Organization, 2003).

2.6.b. Fractures

Presently, the number of fractures sustained is gradually increasing as the population increases though this might also increase per capita as the risk increases. The main fracture single type observed is hip fractures of the femur in elderly women, but there are also extensive numbers of cases of diaphyseal fractures and wrist. In most of these cases, there is a 66% survival rate in these cases of hip fracture, where there is an overall 43.3% of home return within 30 days and 30 days mortality rate is at 8.4% (Currie *et al.,* 2011).

One of the complications which is not yet fully understood is that of cut-out of the femoral nail/dynamic hip screw in the femur head, as described in 2.6.c.

A value of BMD 2.5 standard deviations or more below the young adult mean with the presence of one or more fractures is classed as severe osteoporosis, also known as established osteoporosis (World Health Organization, 2003).

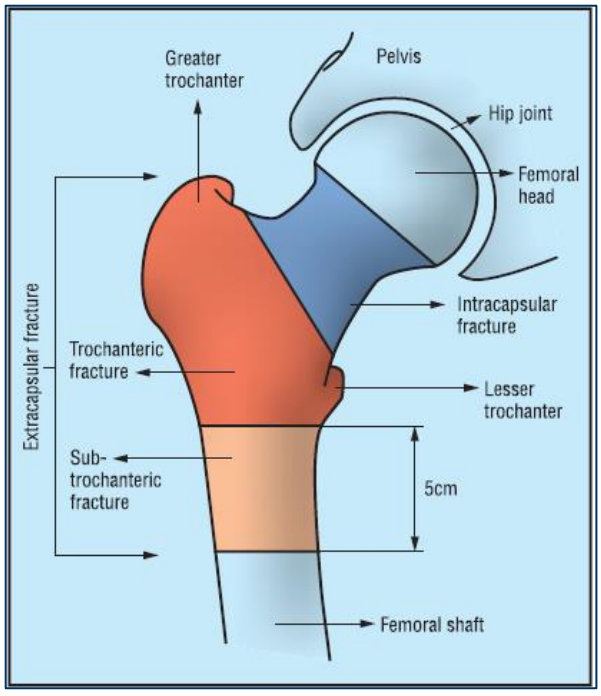

Figure 2-10: Classification of hip fractures. Fractures in the blue area are intracapsular and those in the red and orange areas are extracapsular (Parker and Johansen, 2006).

Fractures in the proximal end of the femur bone can be classified in 3 separate sections, each of which have further classifications or attributes:

- Intracapsular: These fractures are also known as neck fractures, and are most commonly classified using the Garden classification (Figure 2-11)

which are split into 4 sections: (A) Garden I fracture: incomplete and minimally displaced. The fracture shown is impacted and is in valgus misalignment. (B) Garden II fracture: complete, nondisplaced. (C) Garden III fracture: complete fracture and partially displaced. The fracture shown is in varus misalignment. (D) Garden IV fracture: completely displaced, with no engagement of the 2 principal fragments. This classification is measured by the level of displacement of the fractures (Guyton, 1998).

Femoral neck fractures account for approximately 60% of hip fractures (Currie *et al.*, 2011).

Neck fractures pose a danger to healing as they may disrupt an artery which would affect blood supply at the fracture site and femoral head. The loss of this blood supply increases the risk of non-union and the risk for avascular necrosis of the femoral head (Guyton, 1998).

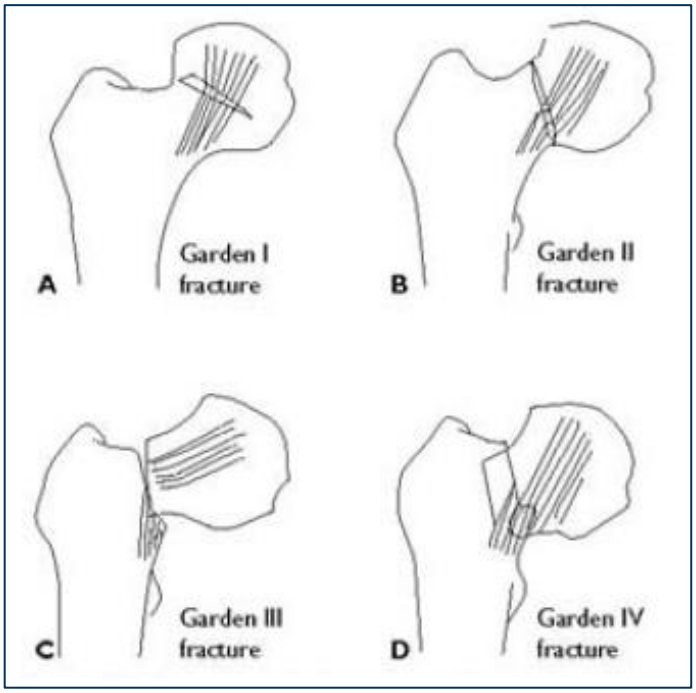

Figure 2-11: Garden classification system of femoral neck fractures (Guyton, 1998).

- Trochanteric: Trochanteric fractures or intertrochanteric fractures are usually classified using the AO/ASIF classification. It is comprised of A1 stable pertrochanteric fractures, A2 unstable pertrochanteric fractures with medial comminution and A3 unstable intertrochanteric fractures with or without medial comminution including reversed intertrochanteric

fractures and transverse intertrochanteric fractures with possible dorsolateral comminution (Schipper *et al.,* 2002).

- Sub-Trochanteric: Sub-Trochanteric fractures occur below the lesser trochanter up to the main femur shaft they are less common than intertrochanteric and Intracapsular hip fractures (Guyton, 1998).

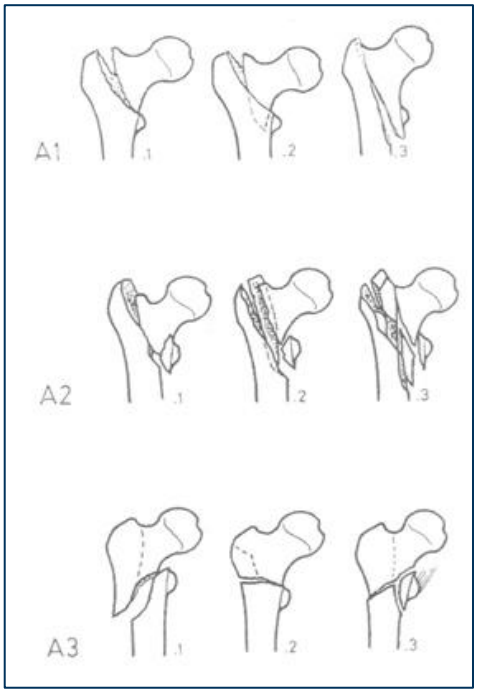

Figure 2-12: The AO/ASIF classification (Müller *et al.*, 1990).

From the National Hip Fracture Database, admissions in the UK covered: 46.3% Intracapsular displaced; 11.4% Intracapsular undisplaced; 33.8% Intertrochanteric; 5% Subtrochanteric; 2.9% Other; and 0.6% Unknown (Currie *et al.*, 2011).

Akan *et al*. (2011) also show that the presence of osteoporosis has a negative effect on clinical outcome after hip fracture. They use the Singh index to classify osteoporosis, an index based on the radiological appearance of the trabecular bone structure of the proximal femur (Singh, Nagrath and Maini, 1970).

Following fracture of the bone with damage to the endosteal, periosteal and intramedullary blood vessels, where high-energy fractures cut through the microstructural element of bone such as osteons or low-energy fractures split around such structures, a haematoma is formed at the fracture site. The healing

process falls into two type of repair depending on the mechanical stability of the fracture site: direct and indirect.

2.6.b.i. Direct fracture repair

If the fracture is kept rigid, with the bone matrix of one fragment in contact with the opposing matrix of the other, a process called “direct (Primary)” fracture repair occurs. At the points of contact any gaps present are filled with woven bone and new secondary osteons replace the damaged area and the bone heals. During this process, there is almost no formation of bone by the periosteum or endosteum and the fracture heals while keeping anatomical integrity, which is an important factor for intra-articular fractures. This process in very long however, and may take months or years to complete. The pattern of healing is called gap healing, but any motion in areas of small fracture gaps creates high strain fields which may be detrimental to the formation of bone. This is why direct bone repair may not be a common occurrence in clinical fractures (Goodship and Cunningham, 2001).

2.6.b.ii. Indirect fracture repair

The second type of bone healing involves the formation of a “callus” around the fracture site. The haematoma forms and kills all blood cells within it, but fibroblasts are present and start replicating, forming granulation tissue. In this first reactive phase, the adjacent tissue reacts and swells to provide support and protection to the bone underneath (Brighton and Hunt, 1986). The fracture haematoma undergoes a process of tissue differentiation. The granulation tissue, fibrous tissue, fibrocartilage and hyaline cartilage which, by endochondral ossification forms woven bone form the callus that remodels to the definitive disuse of lamellar bone. This process of repair is rapid, but create a bulge of callus for an extended period of time during remodelling. Evidence suggests that indirect fracture repair provides a faster return to pre-fracture values of strength and stiffness than direct repair, but is much more sensitive to biological and mechanical factors. The mechanical environment created by implants will have an effect on the mass and distribution of callus. Small changes in the mechanical

environment at the fracture site are major factor for the healing of the fracture. Two extremes exist: A very rigid fixation will result in an atrophic non-union as it supresses the formation of callus, while a fixation that is not rigid enough will cause an overproliferation of callus which has failed to bridge due to excessive movement and result in a hypertrophic non-union. Between these two extremities, one could hypothetically reach an environment that is ideal for an optimal healing rate (Goodship and Cunningham, 2001).

2.7. Bone Implants

2.7.a. Intramedullary Devices

There are two types of devices currently used by surgeons for the treatment of hip fractures fixed without arthroplasty: extramedullary devices, such as the dynamic hip screw® (DHS, Mathys Medical) or the compression hip screw® (CHS, Smith and Nephew), and intramedullary devices such as the gamma nail® (Stryker), intramedullary hip screw® (IMHS, Smith and Nephew) or proximal femoral nail (PFN, Synthes). They are composed of one large intramedullary nail section and either 1 or 2 lag screws which screw into the femur head.

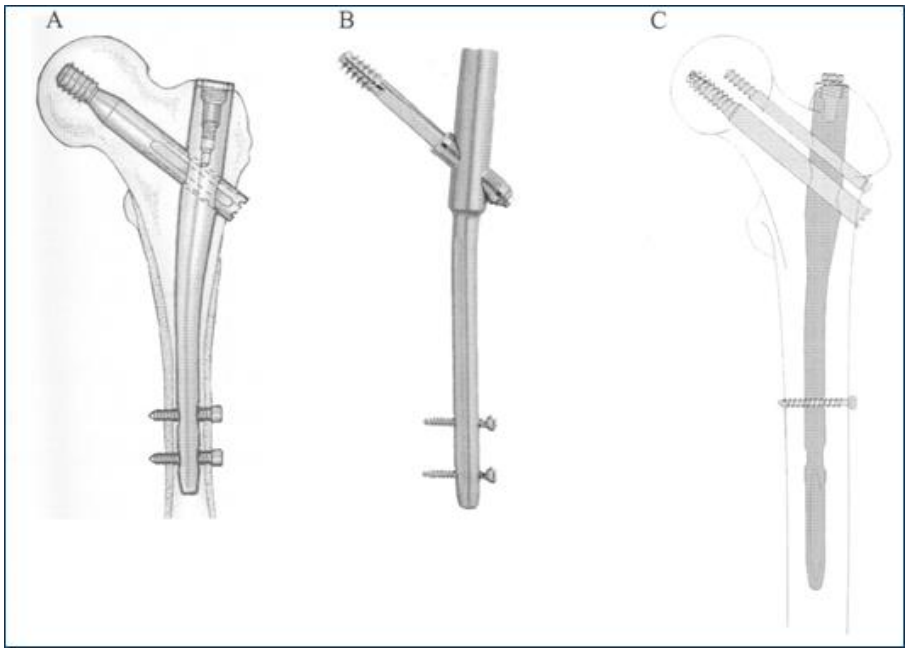

Figure 2-13: A) Gamma Nail®, B) Intramedullary Hip Screw®, C) Proximal Femoral Nail® (Schipper, Marti and van der Werken, 2004)

Unstable trochanteric fractures and femoral neck fractures in young people are often treated with intramedullary devices, as they are biomechanically superior (Schipper, Marti and van der Werken, 2004).

Schipper *et al.* (2004) have carried out a multi-centre prospective clinical study in which they compared the gamma nail and the proximal femoral nail. The conclusions of the study are that functional outcome and consolidation were equal for the Gamma Nail and PFN. They state that "the pitfalls and

complications were similar, and mainly surgeon- or fracture-related, rather than implant-related."

Cadaveric analysis of femoral head fixation failure shows that there is a 20% increased performance of the Gamma Nail compared to the DHS for screw migration. The mean force required for the gamma nails to fail by migration was 3634.3N (±978) compared to the DHS failure load of 3116.7N (±494) either by migration or bending of the screw at the fracture site. All testing was performed on central-central positioned lag screws (Haynes *et al.*, 1997).

Bridle *et al.* (1991) showed then that there was no difference in operation time, blood loss, wound complications, stay in hospital, place of eventual discharge, or the patients' mobility at final review. They state that "There was no difference in failure of proximal fixation: cut-out occurred in three cases with the DHS, and twice with the Gamma nail." But a 3 to 2 ratio shows that the Gamma nail may have a lower cut-out rate as Haynes *et al.* (1997) showed.

These results are echoed in the supracondylar fractures of the femur (distal end of the femur), where the comparison of the condylar screw fixation and the closed retrograde intramedullary nailing by Christodoulou *et al.* (2005) showed that the retrograde intramedullary nailing is preferable to the condylar screw fixation in terms of blood loss, operative time and hospital stay, but the time to bony reunion and clinical results have statistically insignificant differences.

Lucke *et al.* (2010) report 2 cases of primary medial migration of the lag screw of a Gamma 3 Nail (Stryker®). They believe that complete disengagement is a matter of implant design. The PFN-a consists of a gliding spiral blade that features a positive stop (widening) at its lateral end, thus making disengagement impossible as the bulge does not fit through the gliding hole. They suggest that primary medial migration might be higher than assumed and that failure of osteosynthesis could be misinterpreted as a cut-out phenomenon when medial migration could have been the reason for clinical failure. The proposed solution

is simply close follow-up of patients with highly unstable fractures, difficult reduction and poor bone quality in order to detect migration as early as possible.

2.7.b. Screw Fixation

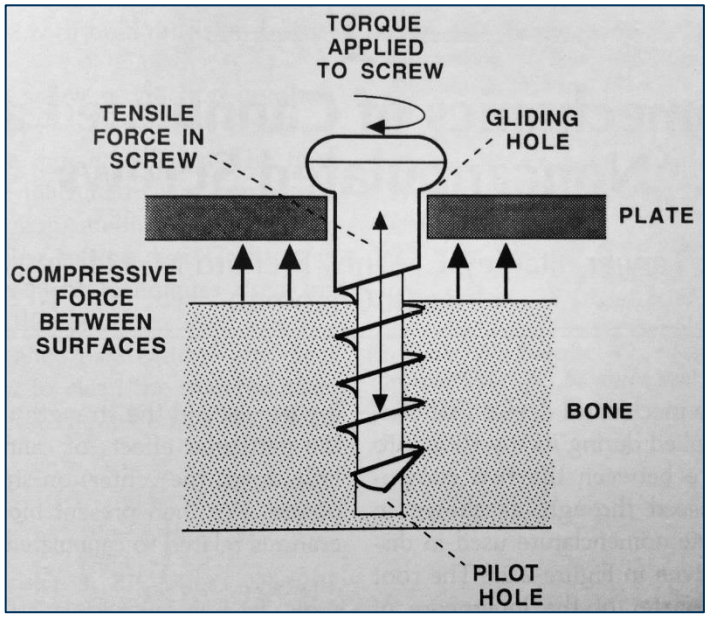

Figure 2-14: "The function of a Screw" (Asnis *et al.*, 1996)

Figure 2-14 shows the basic function of screw in bone, where the type of bone (cortical or cancellous) would dictate the type of screw (cortical or cancellous) used. The use of screws in fracture fixation dates back to 1894 and William Arbuthnot Lane (1856-1943) (Lane, 1894). The first internal implant used and made popular by Lorenz Bohler was a metal rod called Steinman pin or Kirschner wire (now known as the K-wire). In 1939 Gerhard Kuntscher first used an intramedullary nail to treat long bone fractures during the war, were developed during the Second World War.

A decade later the introduction of titanium alloys in implants and the first ACL reconstruction happened in 1960 when John Charnley pioneered the use of a cemented polyethene cup to replace a worn socket.

The ultimate holding power of the tensile force marked in Figure 2-14 is called the pull-out force, and used as a measure for screw stability. The pull-out strength of screws is the most commonly assessed as a predictor for implant failure and thus the most valid to consider. In order to predict the failure force of a screw, the widely accepted failure is by shearing of the bone at the bone-screw

interface (Chapman *et al.*, 1996), and this was defined in an equation derived from the equation given by Oberg *et al*. (1987):

$$(1) \quad F_s = S \times A_s = \left(S \times L \times \pi \times D_{major}\right) \times \{0.5 + 0.57735[d/p]\}$$

Where:

$$F_s = Predicted\ shear\ failure\ force\ (N)$$
$$S = Material\ ultimate\ shear\ stress\ (MPa)$$
$$A_s = Thread\ shear\ area\ (mm^2)$$
$$L = Length\ of\ thread\ engagement\ (mm)$$
$$D_{major} = Major\ diameter\ (mm)$$
$$d = Thread\ depth\ (mm)$$
$$p = Thread\ pitch\ (mm)$$
$$0.57735\ is\ a\ constant\ derived\ for\ this\ equation$$

Parker and Ali (2010) did not find any difference in outcome between short and long thread cannulated cancellous screws for intracapsular hip fractures in a clinical trials environment. They alluded to the lower pull-out strength and fracture compressing occurring from using the shorter screws. The potential disadvantage of the longer thread would be that by crossing the fracture line the screw would impede consolidation and fracture union.

The biomechanical compatibility of orthopaedic screws is an important factor in screw fixation. Metallic screw fixation carries most of the load, causing the adjacent bone to resorb, an effect called 'stress shielding'. (Gefen, 2002) has identified a method using dimensionless stress transfer parameters (STP) to optimize screw design. The parameters provided a rating for biomechanical compatibility by evaluating the stress transfer between the screw and surrounding bone. There were 2 stress transfer parameters used, one for the first thread of the screw and the second for the remaining threads. For all of the screw designs tested, the results showed that the first thread of the screw was the peak stress region of their models. They also show that the length of the screws, as well as the number of threads modify this stress concentration. A

higher number of threads and longer screw reduce stress concentration. The stress transfer parameters were used to identify new screw designs that would reduce stress shielding and concluded that graded-stiffness composite screws an active-compression screws would be more biomechanically compatible.

Stress transfer parameters were used in a bone continuum model, but peri-implant bone trabeculae and discrete modelling are critical for implant anchorage. Gabet et al. (2010) performed *in-vitro* testing on animal bone (Sprague-Dawley rats) in order to differentiate the effects of osseointegration and peri-implant trabecular bone on anchorage. The tests were performed using 2 types of implants in order to differentiate osseointegration, and the animal bone was split into 3 groups in order to differentiate peri-implant trabecular bone. The results confirmed a lessening of the pull-out strength in low-density bone. This reduction was not due to an impaired osseointegration but primarily due to structural changes in the peri-implant trabecular bone. Trabeculae thickness (Tb.Th) and the number of trabeculae, which leads to a change in the bone volume, both influence toughness but Tb.Th is the main factor in influencing the initial linear and yield behaviours of the implant. This experimental evidence suggests that failure of implants occurs in the bone where anchorage failure involves buckling and ultimately breakdown of the weakest trabecular struts followed by failure of the stronger trabeculae. It is shown that anchorage is critically dependant on the peri-implant bone.

Wirth, Müller and Van Lenthe (2012) have done important work on bone models using super-computers (1024 cores of a CRAY XT5^{tm}) which show the importance of the discrete modelling of the bone area close to the screw rather than using a continuum to simulate bone. The study found clear distinctions in mechanical behaviours between continuum and discrete modelling, with a variability of the bone-implant stiffness of more than 100%. The models were solved using bonded interfaces between the bone and the implant, simplifying the solution process.

They were, however, computationally massive with 12 million and 24 million elements in the discrete models, and 96 million elements in the continuum model. The discrete models were created from micro-computed tomography (µCT) scans of bone using a direct voxel-to-element conversion (van Rietbergen *et al.*, 1995).

Wirth *et al.* (2011) have also shown the importance of the local bone microstructure quality, comparing 300 local virtual biopsies from 12 µCT Scans of femoral cancellous bone (25 screw positions) using FE modelling and using k_{SB}, the resulting stiffness in the direction opposed to the pull-out force, to compare results. They confirm their hypothesis that implant stiffness is governed by the bone quality of trabecular bone directly in the vicinity of the implant.

Zdero and Schemitsch (2009) have shown that a direct pull-out at a constant rate of loading resulted in an increasing failure force, failure stress and resistance force when the pull-out rate was increased. This test was made with cancellous bone screws in synthetic cancellous bone. This study shows the importance of the rate of loading of models in physical testing and though this might not have an effect on computational rate of static loading, it might affect transient models.

2.8. Cut-out

When repairing fractures with implants, one of the complications that might arise is cut-out. This is when the implant "cuts out" through the bone it is finding purchase in and meant to repair. The phenomenon of lag screw cut-out is not to date fully understood. Some of the questions still troubling surgeons and researchers include: "What initiates cut-out?", "How does cut-out occur?", or "Why is cut-out initiated?"

2.8.a. Previous work and surrounding analyses

Banan *et al*. (2002) reported an 8.7% cut-out rate in their first 60 cases of treatment of unstable, extracapsular hip fractures. This data is dated February 2002.

Parker (1992) shows that on antero-posterior and lateral radiographs positions, the position of the Lag screw may influence cut-out. He compared the position of the Lag screws which cut-out from 25 patients with the positions of 200 cases where there was radiographic evidence of bony union without cut-out. The conclusion of the comparison showed that cut-out happens more frequently when screws were placed superiorly or posteriorly.

This superior, posterior position of the lag screw is shown to have increased cut-out by multiple studies. Pervez, Parker and Vowler (2004) concluded a superior, anterior position increases the chance of cut-out; Gundle, Gargan and Simpson (1995) concluded a superior, posterior position increases the chance of cut-out; Davis *et al.* (1990) concluded a posterior position increases the chance of cut-out; and Mainds and Newman (1989) concluded a superior position increases the chance of cut-out (Parmar *et al.*, 2005). These studies show a clear detrimental effect of a superior position of the lag screw.

Konstantinidis *et al.* (2013) performed tests on cadaveric femurs and confirm that biomechanical superiority is found in and inferior positioning of the lag screw on antero-posterior radiographs, but concluded that the incidence of cut-out is unaffected by the position of the implant.

Schipper *et al.* (2002) hypothesized that a reduction of load on the hip pin of a PFN (®Mathys Medical, Bettlach, Switzerland) would reduce the risk of implant cut-out, but the cadaver study did not conclude if the reduction of load led to prevention of implant cut-out. The study did however show a significant reduction of load on the hip pin when using a modified PFN where the proximal hole in the intramedullary nail for the hip pin was made oval.

Kawaguchi, Sawada and Nabeta (1998) provide an analysis of 75 intertrochanteric fractures of the femur treated with the Asiatic gamma nail (Gamma AP Locking Nail System, Howmedica) where the cut-out of the lag screw occurred in six cases. They conclude that the degree of osteoporosis, the type of fracture and the degree of reduction did not contribute to cutting-out, but that the location of the lag screw in the femoral head was a crucial factor. They conclude that a shallow insertion of the lag screw as seen from the antero-posterior radiograph and an antero-posterior deviation from the central position were significantly related to the incidence of cut-out.

Nishiura, Nozawa and Morio (2009) have devised a technique to obtain a correct lag screw placement within tolerances of ±5° from the recommended position. Being able to place the lag screw exactly in the centre of the femoral head on the true lateral view means that it can be set forward as closest to articular surfaces as possible and thus reduce tip-apex distance to below 20mm as has been recommended by Baumgaertner *et al.* (1995). They have also composed a summary of studies and their recommended positions in Table 1.

Table 1: "The optimal position of the lag screw in the femoral head (Nishiura, Nozawa and Morio, 2009)."

	Recommended position		Inadequate position	
	AP view	Lateral view	AP view	Lateral view
(Mulholland and Gunn, 1972)	Central	Central		
(Kyle, Gustilo and Premer, 1979)	Central	Posterior	Superior	
(Laskin, Gruber and		Posterior		Anterior

Zimmerman, 1979)				
(Larsson, Friberg and Hansson, 1990)	Inferior half	Central	Superior	Anterior
(Mainds and Newman, 1989)	Inferior half		Superior	
(Davis *et al.*, 1990)	Central	Central		Posterior
(Den Hartog, Bartal and Cooke, 1991)	Central	Central		Posterior
(Leung *et al.*, 1992)	Inferior half	Central		
(Parker, 1992)	Inferior half	Central	Superior	Posterior
(Baumgaertner *et al.*, 1995)	Central	Central		
(Wu *et al.*, 1996)	Inferior half	Central	Superior	
(Kawaguchi, Sawada and Nabeta, 1998)	Central	Central		

Kane *et al.* (2014) have done recent mechanical testing which challenges the accepted principles of optimal placement in that a low position on the AP radiograph showed equal, if not superior stability than a central position with tip apex distance of less than 25mm. Their results show that a lag screw in the inferior half of the AP view is the primary factor, as has been previously suggested (Wu *et al.*, 1996; Parker, 1992; Laskin, Gruber and Zimmerman, 1979).

Wu and Tai (2010) report 18 cases of fixation failure using SCS (Sliding compression screw) fixations in a group of 591 patients. Failure was attributed to cut-out of the lag screw for 13 cases, telescoping and more than 2cm shortening of the femur for 3 cases, one acetabulum penetration and one case where the plate loosened and the cortical screws were broken. They report that the 13 cases concerning cut-out of the lag screw occurred significantly earlier than the other 5 cases, and that the positioning of the lag screw was in the central-central area ($p<0.001$) in opposition to the 5 cases they called “Group 2” where the position was inferior 1/3-central ($p<0.01$). The tip-apex distance of the screw was also longer in group 2 patients (30mm – 19mm for group 1).

These findings are also agreed to by Kuzyk *et al.* (2012) who tested 30 synthetic femurs in simulated peritrochanteric fractures fixed with Long Gamma 3 Nails (Stryker®). Their findings conclude that an inferior lag screw position on the AP view produced the highest axial and torsional stiffness while suggesting the smallest tip-apex distance as could be achieved.

2.9. Bone peri-implant augmentation

The use of adhesives or cement into the bone where screws find purchase should increase pull-out forces. Polymethylmetharcrylate (PMMA) provides a quick setting stability and was first proposed by Mueller in 1962 (Bartucci *et al.*, 1985). Whilst PMMA is considered useful cement for augmentation, it comes with two drawbacks induced by the cement material: thermal necrosis and impaired fracture healing due to exothermic reaction. This means it is often considered as having poor bio-compatibility (Lindner *et al.*, 2009). Recent studies show that PMMA increases the implant stability in intertrochanteric fractures both *in vivo* (Dall'Oca *et al.*, 2010) and *in vitro* (Fensky *et al.*, 2013; Stoffel *et al.*, 2008). Calcium phosphate (CaP) cement is also used to augment bone and due to its good bio-compatibility and strength it has seen increasing use.

Eriksson, Mattsson and Larsson (2002) did an *in vitro* study using foam blocks to investigate the effect of both cements in relation to pull-out forces. Their conclusions are in agreement with the common acceptance that PMMA cement augmentation around implants will increase the holding power significantly when compared to the fixation strength of the metal devices alone. Augmentation with CaP cement on the other hand might reduce the strength of fixations due to the need of pre-drilling when using the cement in the case of high density bone. They do show however, that in low-density bone, CaP cement will increase the holding power of the devices compared to un-augmented cases. This difference, they explain, is at least in part due to the weakness of CaP cement in shear (Goodman *et al.*, 1998) while PMMA has much higher shear strength when compared to CaP cement and artificial bone(Eriksson, Mattsson and Larsson, 2002).

3) Chapter 3 – Modelling Technique

"Compared to the experiment models, mathematical models can offer the ideal opportunity from the point of view of control. They are characterized by absolute repeatability, with the additional advantage that any parameter can be varied in the desired degree (Zhang, Tan and Chou, 2004)."

This chapter will describe the software used to create the models and all the parameters and conditions set on the models, as well as the methodology followed. The relevant literature and previous research pertaining to the models will also be investigated. One of the main factors in the choices of modelling techniques and settings was computing power, chosen to be 2 HPC (High Performance Computing) licences for a 2 x Intel ® Xenon® E5620 @ 2.40GHz CPU and a 2 x Intel ® Xenon® E5630 @ 2.53GHz CPU machine, both with 48Gb of RAM and NVidia® Quadro FX580 cards. This was selected instead of the Brunel University cluster in order to have full and unrestricted access.

3.1. Previous work

3.1.a. Direct Contribution

The choice of modelling medium and boundary conditions for the work performed in this thesis is strongly influenced by the previous successful work performed by Hughes (2014) and Bennani Kamane (2012).

Hughes (2014) undertook a methodical comparison between continuum, lattice and CT (Computed Tomography) models and concluded CT models are created following the technique described in section 3.2.a from CT scans. These CT scans are obtained using x-ray technology and described in-depth by Monahan (1996). Continuum models are the most simple to implement and straightforward to solve, and as such, useful for quick studies and providing a basic evaluation of different loading applications or designs. Once these are compared to CT models however, the differences become apparent. For two identically loaded models, one in a continuum of the same dimensions as another of a CT model, the results were significantly different. The locations of deformation were not the same and

displacement in the CT model was five times larger than for the continuum model (Figure 3-1). This significant difference between continuum and CT models was also shown by Wirth, Müller and Van Lenthe (2012).

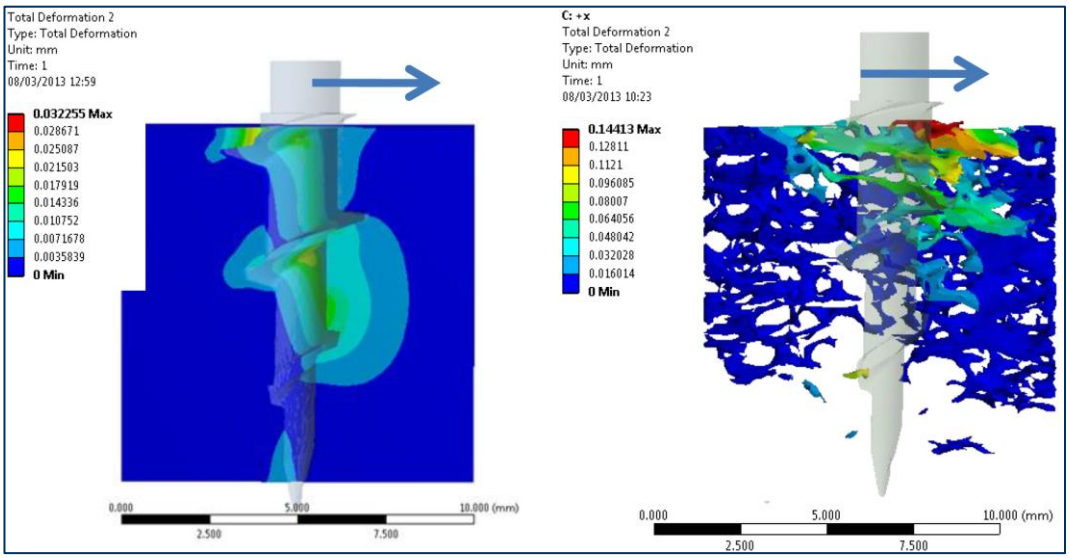

Figure 3-1: "Contrast of a continuum and CT model, arrows show the direction of loading: 0.02mm displacement (Hughes, 2014) ."

The use of lattice modelling is aimed at replicating some of the bulk mechanical properties of cancellous bone, primarily bulk elastic moduli but also volume and the mechanical effects observed, such as variation in pull-out (Procter *et al.*, 2015). They use repeating shapes to form a framework, such as cubes, rods, diamonds, spheres and many other combinations. As they use such geometries, they may be set to represent certain values for BV/TV, such as the thickness or spacing of the rods in a rod lattice (Figure 3-2).

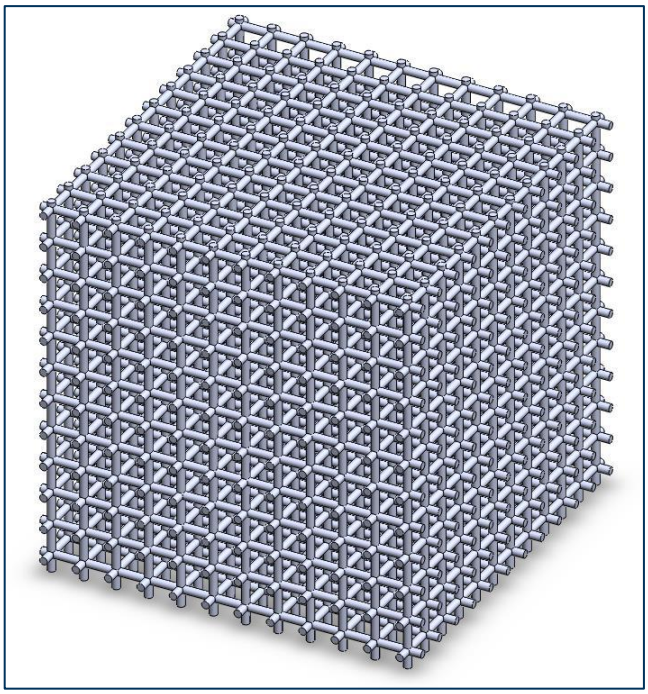

Figure 3-2: Rod lattice model of 10x10x10mm^3 with a BV/TV of 11.6% (Hughes, 2014)

The modification of thickness and spacing would modify the bulk modulus, but the bulk modulus can also be modified in a continuum model. The variability across the sample is low and predictable for such a model and any deviation in pull-out force is will be repetitively identical, which is not something found in cancellous bone as the later can be unpredictable across a single sample and even more so across a population. The production of lattice models is faster than creating models from CT scans but it was concluded that solve times in FEA for lattice models are no faster than that of CT models. The similar solve times were likely due to the similar complexity in contact areas i.e. there were many different contact points, as opposed to a single contact surface for a continuum model. Validation of the models was reported to be very difficult, and as such, lattice models could be said to be less relevant than continuum models (Hughes, 2014).

Bennani Kamane (2012) investigated a set of lattice models: a rod model, a model with cylinders cut in the 3 principal directions and lastly a model with spherical holes 1mm in diameter, 0.8mm apart. A variation of the diameter provides a simple variation in BV/TV. This was a preliminary study to

approximate the CT scan model which was obtained in his collaboration with the Laboratory of Biomechanical Orthopaedics of EPFL, Switzerland. FE results were compared to a mechanical test of the scanned bone piece in order to provide validation of the FE model.

Noting the above conclusions, the selection of modelling real bone from CT scans was the preferred option to best represent the implant to bone interface and the analysis of its effects.

Bennani Kamane (2012) looked into the boundary condition necessary for these models, and Figure 3-3 shows an investigation performed in order to assess the best loading condition in comparison with mechanical testing.

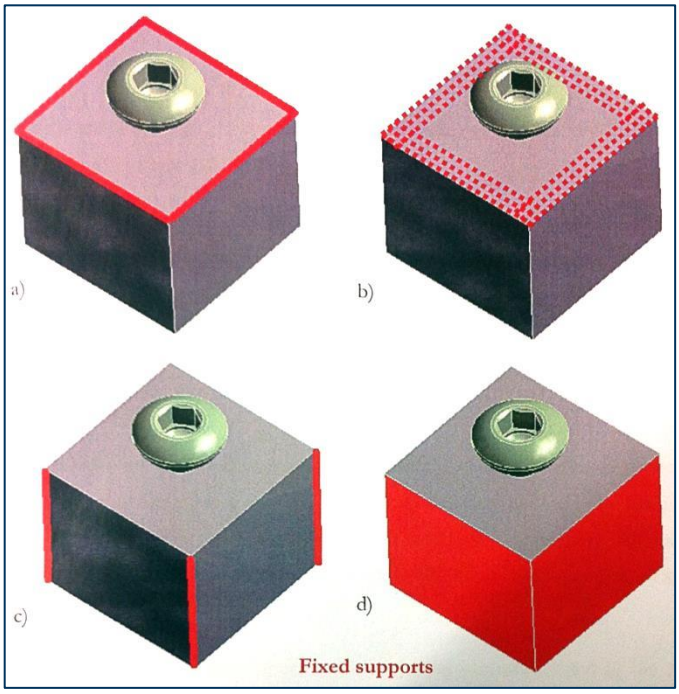

Figure 3-3: "Boundary conditions tested. Fixed supports in red: a) top edges. b) points from the top surface, c) lateral edges, d) lateral faces (Bennani Kamane, 2012)"

The last boundary condition where all sides were fixed (d) was selected as the closest approximation. The screw pull-out was noted as nearly twice stiffer as the original discrete model but the pull-out for was of similar strength The models investigated here were continuum. Further analysis of the CT scan model showed that a minimum depth of 4mm and approximately 10mm of width were required to approximate the full structure (Bennani Kamane, 2012).

These findings provided a base for the creation of the models used in the current analysis. The boundary conditions and model size were both inspired from this data, and the CT data used was also obtained from the µCT40 scan performed in the above research.

3.1.b. Lattice investigation

One of the lattices investigated was that of the 'Gyroid'. The gyroid is a triply periodic minimal surface, created by solving for the equation:

$$(2) \quad \sin x \times \cos y + \sin y \times \cos z + \sin z \times \cos x = 0$$

It is infinitely connected and was discovered by Alan Schoen (Karcher, 1989; Schoen, 1970). Große-Brauckmann and Meinhard (1996) proved that it is embedded. The gyroid separates space into two identical passages, as seen in Figure 3-4 ('A') but if a constant is added to the left side of equation (2), then the gyroid can be asymmetric in volume, thus creating a solid approximating cancellous bone. Due to its sinusoidal nature, the gyroid derivate (Figure 3-4, 'B' & 'C') appears to be very strong structurally.

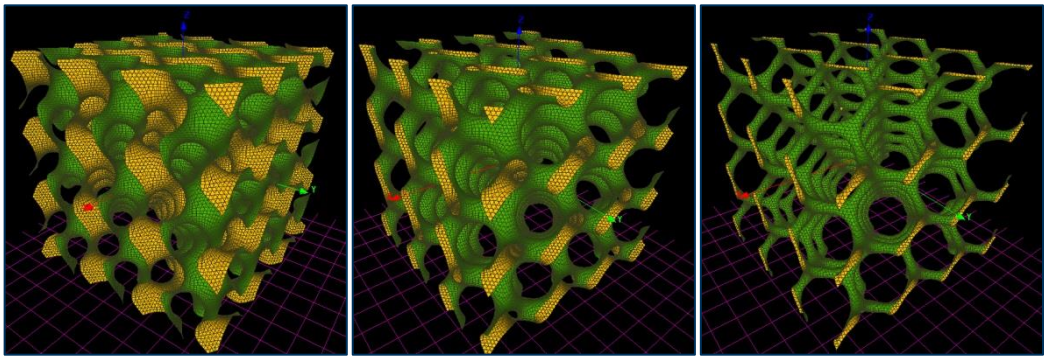

Figure 3-4: A) Standard Gyroid construct. B) ±0.8 Gyroid. C) ±1.3 Gyroid

As a program to visualize and manipulate mathematical models was used ('K3DSurf') to represent the above models, the creation of a gyroid model proved difficult and was not achieved in the current research, as the largest imported model contained 10 by 10 by 4 cells, which was not enough to comparatively analyse with either CT or continuum models.

3.1.c. Indirect Influences

A lot of research has been done on implants in bone investigation by finite element models and the interactions of both solids as well as the importance or acceptable simplification of the models.

Zhang, Tan and Chou (2004) researched the failure behaviour of cancellous bone during screw pull-out using finite element models. Although they used a homogenous and isotropic continuum model of cancellous bone, they reached the conclusion that the failure of the model was related to the surface area of the cylinder which is determined by the major diameter of the screw and purchase length, which agrees to results from previous physical studies (Chapman *et al.*, 1996). They also confirm that the major diameter of the cancellous screw has a more significant effect on pull-out than the minor diameter and pitch of the screw.

McDonnell *et al.* (2010) investigated the mechanical interaction between a trabecular core and an external approximated cortical shell using FE analysis validated with RP models in turn compared to testing of the original specimen in compression. An experimentally determined correction factor was applied to the RP model results to account for the difference in strength of real bone tissue and RP material. A video recording of both (RP and real bone) compression tests also confirmed that the failure locations and mechanisms were qualitatively similar for many of the specimens tested. Although the specimens tested were ovine trabecular bone with a high BV/TV of 17-45% compared to the elderly trabecular bone from human spine values of 4-12% (Mosekilde, 1990), the results showed that the ultimate strength reinforcing effect of the shell increased as the bone volume fraction decreased. They conclude that the ultimate strength and stiffness of the structure obtained from the interaction between the shell and the trabecular core cannot be accounted for by the components in isolation.

Noor *et al.* (2013) use their own custom-written code to model dynamic analyses to recreate falls by applying forces directly side-ways, obliquely forwards or

backwards at 45° onto the greater trochanter. They note limitations in the internal cancellous bone representation for their models, and their limited understanding of the nature of muscle forces acting on the femur during gait, simplifying the load to 392N, 23% of the 1705N load estimated by Bergmann *et al.* (2001) about 12 years prior to the analysis. In the dynamic simulation of falls, their results show common fracture patterns to those seen in clinical practice and thus validate their FEA model.

Huiskes *et al.* (1987) were the first to perform computational studies of peri-prosthetic bone remodelling using an axisymmetric finite element model of an intramedullary implant. They use the Strain Energy Density as a feed-back control variable to determine shape or bone density adaptations in order to investigate the relation between stress shielding and bone resorption in the femoral cortex in accordance with Wolff's Law. This research is then followed by Prendergast and Taylor (1992; 1990) who simulated remodelling around an intramedullary implant using damage-adaptive remodelling and analyse the stresses found in the femur after total hip replacement with finite element models. Using the experimental work by Lee, Staines and Taylor (2002) which associated micro cracking with bone adaptation and further theoretical work by McNamara and Prendergast (2007) which incorporates both strain and micro damage as stimuli for bone remodelling, they have created a bone remodelling algorithm (Mulvihill and Prendergast, 2010; Mulvihill and Prendergast, 2008) that was partly corroborated against 3D simulations around non-cemented total hip replacements (Scannell and Prendergast, 2009). They came to conclusions that computational pre-clinical testing of medical devices is a valuable opportunity, representing a population of cases as opposed to an idealised 'average' patient simulation (Prendergast *et al.*, 2011).

3.2. Modelling

3.2.a. Strategy

From the CT scans of a human femur, 3-dimentional analysis models can be created. The process used in this thesis follows the processes used by Hughes (2014) and Bennani Kamane (2012) which can be summarised in 5 steps:

- Imaging

-Volume creation

-Meshing

-Model creation

-Analysis

At the end of these 5 steps, results will be obtained and form the core of this thesis. The 5 steps above are described in depth and use 3 major software packages: Solidworks® produced by Dassault Systems®, Workbench® which is developed by ANSYS®, and Mimics® & 3-Matic® developed by Materialise®.

3.2.a.i. Imaging

Two processes exist to obtain micro-imaging data from cancellous bone samples: CT (Computed Tomography) and MRI (Magnetic Resonance Imaging). Computed Tomography is usually the preferred option for bone as it provides greater detail in denser material and offers a better resolution, currently as low as 0.4 µm (SkyScan® [1272], Belgium, 2014). µMRI is better suited for soft tissue and has a lower resolution of approximately 25 µm in high strength magnetic fields (MicroMRI Inc., USA, 2014). The issue with CT scans is that a patient will receive a high radioactive dose which results in the frequencies of CT scans performed annually per person being limited. Most samples scanned with µCT are in vitro samples as higher radiation doses are required for higher resolution, but in comparison to MRI and µMRI scans, the latter also requiring higher energy emissions, CT scans are less expensive and can be completed in seconds rather than minutes. In order to scan cancellous bone with sufficient resolution, a micro-CT (µ-CT) scanner must be used where a typical pixel size would be 0.02

mm x 0.02 mm with a 0.02 mm distance between image "slices". In order to obtain a 20 mm x 20 mm x 20 mm volume using the numbers given, each slice would be containing around a million pixels and the whole image set would contain one thousand million pixels: one giga-pixel (Hughes, 2014). This resolution results in approximately 50 slices per trabecular strut which is more than is required. The current data uses a resolution of 12µm (Bennani Kamane, 2012).

Once scanned, the image slices are imported into Mimics® and the tissue being studied has to be selected from the corresponding Hounsfield (grey) scale. This process is called "thresholding". Bone is a comparatively straight forward tissue to threshold as it is a relatively dense tissue that gives clear boundaries to be selected (Figure 3-6). Figure 3-5 shows the work by Kim *et al.* (2007) who have reviewed three principal techniques used to improve thresholding: adaptive threshold, global threshold, and matched global threshold. The first image (a) is a "*Histogram of a typical 16-bit 3D CT image of bovine trabecular bone. The left peak represents background voxels, whereas the right peak represents bone voxels. The voxels in between these two peaks are ambiguous as they may represent bone or background voxels*." While (b) shows the three techniques used on the same histogram: "*Histogram of the same 16-bit 3D CT image of bovine trabecular bone after three types of thresholding: global, matched global, and adaptive. Depending on the choice of thresholding technique, identical voxels may be assigned to bone or background* (Kim *et al*., 2007)."

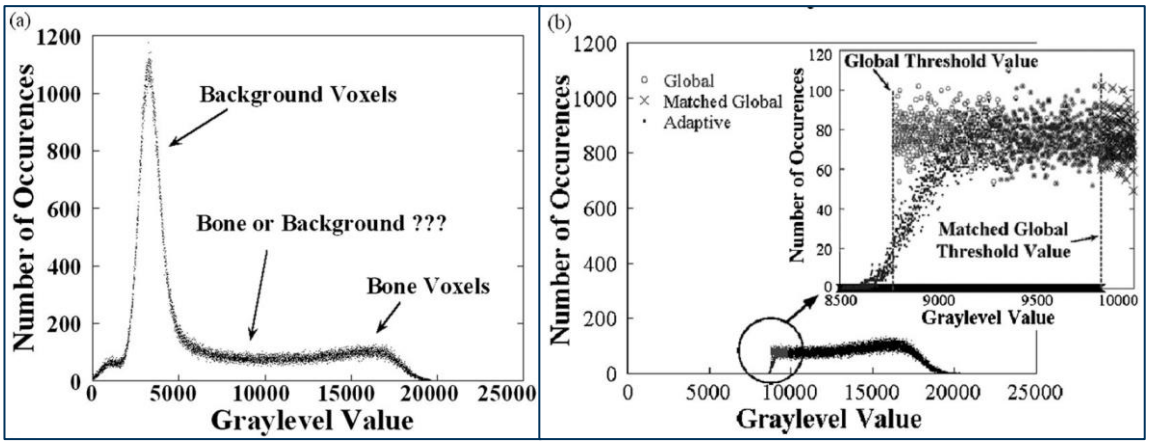

Figure 3-5: Thresholding as shown in Greyscale occurrence graphs (Kim *et al.*, 2007).

Figure 3-5 (b) shows the application of all 3 techniques: Adaptive thresholding obtains thresholds for local volumes using the grayscale value of surrounding voxels. The final threshold value for each voxel is the average of three local threshold values obtained from grayscale values for each row of voxels in all three directions.

The global threshold is a unique threshold value selected as the minimum valley between bone and background. Any voxel with a grayscale value above this selection was considered bone but any voxel of equal or lower grayscale value was reset to zero.

Matched global thresholding is the same as global but the value chosen is selected so that the bone volume fraction matched the BV/TV obtained through physical density measurements.

It is concluded that although there were some differences in architecture, the BV/TV values were relatively consistent with the apparent modulus (Kim *et al.*, 2007).

Coleman and Colbert (2007) compare a fourth technique, the half maximum height, to visually adjusting thresholding protocols. HMH calculates the threshold value as the mean of the maximum and minimum grey scale along a row of pixels that spans the boundary transition, and is an older method developed by (Ullrich

et al., 1980). It was concluded that the half maximum height technique was much more accurate than visually selected boundaries.

Finally, Scherf and Tilgner (2009) propose a fifth technique: a new segmentation method called the “Ray Casting Algorythm”. This method uses the gradient found at the boundary transition known as Sobel filtering and combines this with a ray casting filter with anti-aliasing corrections. The Ray Casting Algorythm is demonstrated to overcome several problems encountered by a single threshold technique. It operates in three dimensions, is immune to grey value fluctuations and is sensitive to fine scale structures at a critical frequency of two voxels. As such, it is said to overcome some described problems found when using the half maximum height protocol or adaptive iterative thresholding.

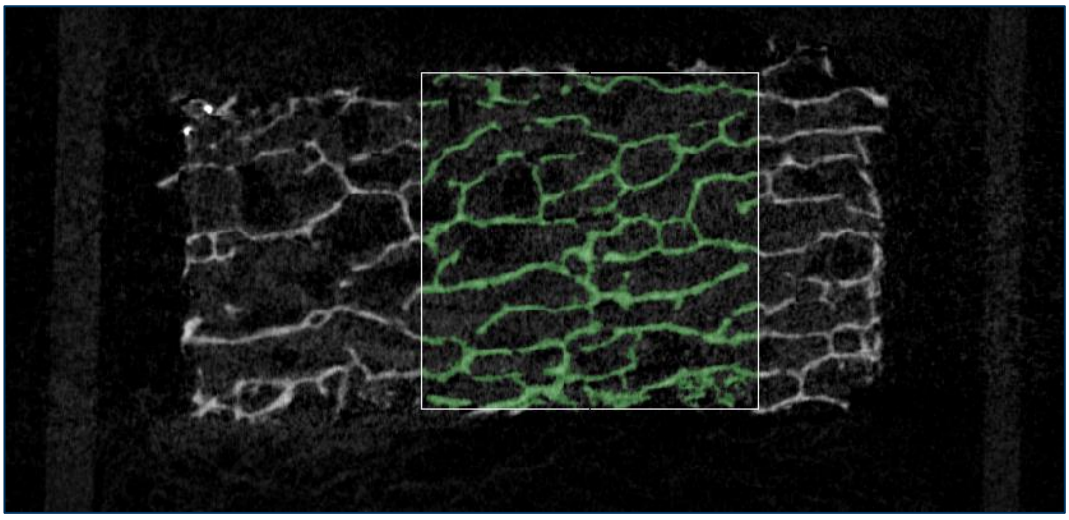

Figure 3-6: Pixels used for a cancellous model highlighted in green, also known as a "mask".

Thresholding (Figure 3-6) can be verified through comparing the BV/TV of the model obtained with the BV/TV calculated in physical tests. A common method of obtaining BV/TV is by measuring the apparent density by dividing the wet weight by the specimen apparent volume while obtaining the bone tissue density by using Archimedes’ principle. The BV/TV is then calculated by dividing the apparent density by the bone tissue density (Kim *et al.*, 2007).

The thresholding options in mimics are pre-defined values for bone which might not match the global threshold. As such, a global threshold must be selected and

verified against the real bone sample if the same BV/TV is to be obtained. In the models used for this thesis, threshold values are selected arbitrarily in order to create BV/TV values for analysis, as if further described in Section 5.2.

3.2.a.ii. Volume creation

The creation of the volume mask is carried out using Mimics®, using the image slices to create voxels. The feature has multiple options of quality, such as matrix reduction levels and triangle reduction. The 'optimal' value creates an element for each voxel while 'low' is smoothing and inflating the object. When compared to thresholding and the issues described for it earlier, these options have a much more important effect: the same threshold mask in each slice in 2D is converted to a 3D volume by the program, at different resolutions, and this may provide very different results. An optimum setting of this volume creation is shown in Figure 3-7. At this stage, smoothing options are also available, in order to reduce element count in the next stage and reduce model distortion produced by the square profile of the pixels. Over-smoothing can de-feature the model, thus smoothing must be used with consideration of this issue.

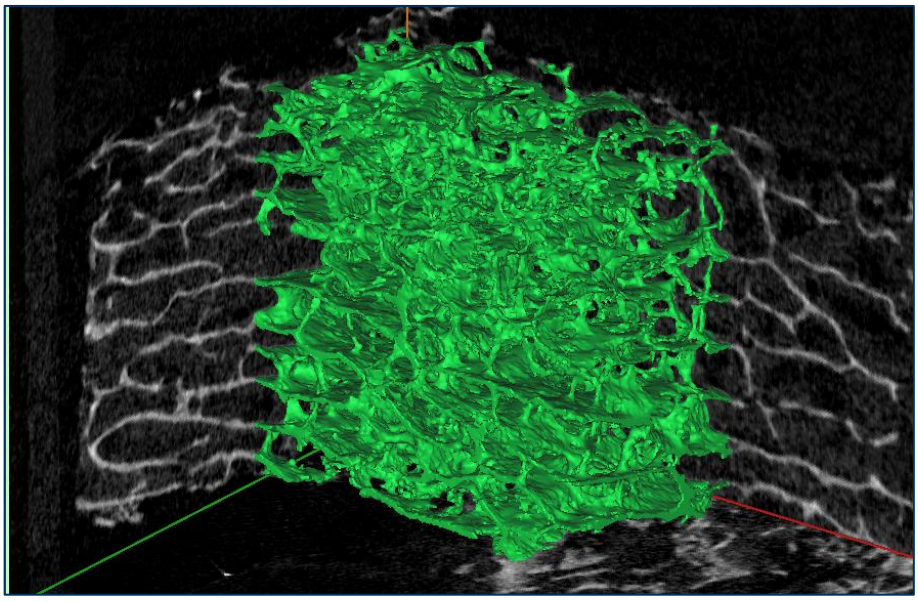

Figure 3-7: Volume mask

3.2.a.iii. Meshing

The 3D mask is then tessellated into a surface mesh made up of shell elements, and is opened in the 3-Matic® software, which is part of Mimics® and Materialise®.

In 3-Matic®, this surface mesh is then re-meshed and streamlined for FE software using the method described in appendix A. As described in the method, the re-meshing process requires manual meshing which is very time consuming as it often involves individually deleting intersecting and duplicate elements. These areas must then be re-meshed by individual addition of elements and these must resemble the original geometry as close as can be achieved, but as such, they are prone to user errors. Unfortunately these cannot be avoided, though reduced in occurrence with correct automatic parameters, and are a necessary process to produce a successful mesh. The occurrence of such detailed manual re-meshing was a major factor in the selection of automatic meshing options and element size, as finer meshes would result in a disproportionate number of manual operations that could take several weeks to implement.

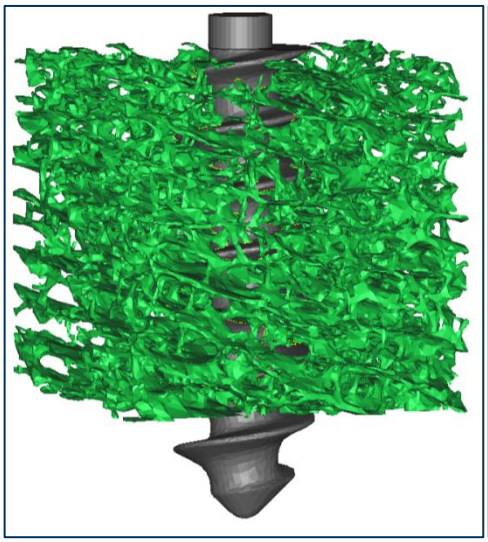

Figure 3-8: Surface mesh with implant

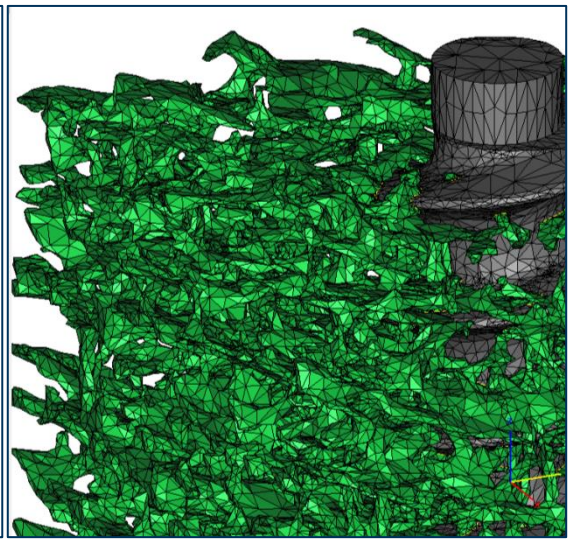

Figure 3-9: Surface mesh and interface boundary

At this stage, the implant is imported into Mimics as an '.stl' file and placed in the desired position and an assembly is created. A Boolean operation is performed to insert the implant, and although in practice the bone is pre-drilled or tapped, this

step can be omitted as the screw's inner diameter would end up overlapping the pre-insertion volume.

Manual meshing is then required a second time for the resulting model, but this time it has to adapt to 3 surface shells and an intersection boundary where the implant is joined to the bone. This would have to be repeated for every change in the geometry of the implant or the bone and would also lead to greater uncertainty about the representation of the geometry. The result can be seen in Figure 3-8, and finally (Figure 3-9) once all intersecting or overlapping elements have been removed, a volume mesh of the assembly can be created for export into FEA software.

During the re-meshing process, some decisions need to be made on the level of acceptable de-featuring of the mesh. Figure 3-10 shows the visual difference between four meshes at a tenfold step decrease from right to left. The first image on the left is almost unrecognisable while the second image is discernible as a person. The third image starts discerning important features on the model, whilst the final image on the far right is the clearest image. In comparison, however, the very last image shows very little gain for a tenfold increase in the number of elements, and thus required computing power for an analysis. Similarly, though a significant visual change can be seen between the second and third image, they will be mechanically similar in analysis.

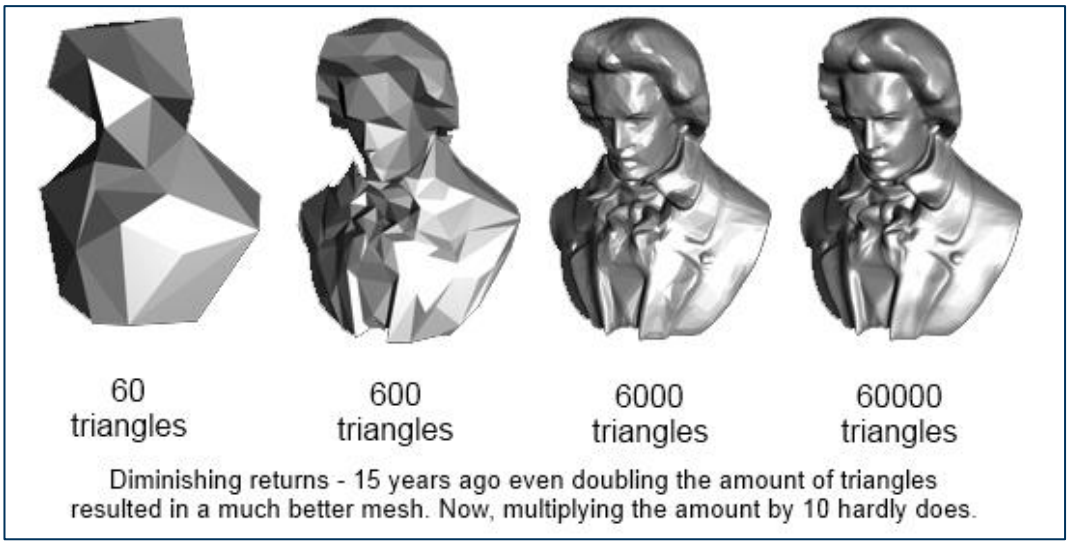

Figure 3-10: Element count comparison. Same model, with a tenfold increase in elements from left to right. (http://cdn.overclock.net/a/a4/a4a47b78_ChsSwUE.png)

In addition to visual checks, stress or displacement convergence should be investigated, but this can prove to be rather complex for cancellous bone, as approximately one million volume elements are used for a piece of healthy cancellous bone occupying a bulk volume of 1100 mm^3 (just over 10mm x 10mm x 10mm), and each of these models can take significant time (of the order of days) to load and solve. The number of elements used lead to computational requirements that are close to the limit of computational availability and significant refinement would not be achievable without a large reduction in the size of the bone around the screw. Similarly, a coarser mesh would not be acceptable as the mesh was graded to give adequate geometric definition of the screw/bone interface, and larger elements may lead to a failure to produce a solution (Hughes, 2014). This is why multi-scale modelling has been chosen as an option for the creation of the models, and explained in section 3.2.b.

In order to ensure consistency through analyses, re-meshing settings remained constant throughout the process, and the following settings were used:

- *Shape quality threshold*: 0.3 – this sets the desired quality of triangles, the value is the maximum ratio of triangle height to base. In this case no triangle had a base: height value less than 0.3. In some manual work, this

was set at 0.4 so that any further re-meshing would not modify the amended area, now of a higher quality.

- *Maximum geometrical error*: 0.01 – this is the maximum deviation between the part's surface before and after automatic re-meshing. In some manual work, this was kept at 0.005 to ensure the model geometry was not changed.

3.2.a.iv. Model creation

Once the surface mesh has been corrected of all erroneous elements and the volume mesh created in 3-Matic®, it is exported in this case to an ANSYS® recognisable '.cdb' file and imported as such into ANSYS®. Although simple, the import into ANSYS® is time consuming. Once imported, the model can be created as a static or transient structural analysis. The material properties are defined and the contact parameters, described in 3.3, are set.

3.2.a.v. Analysis

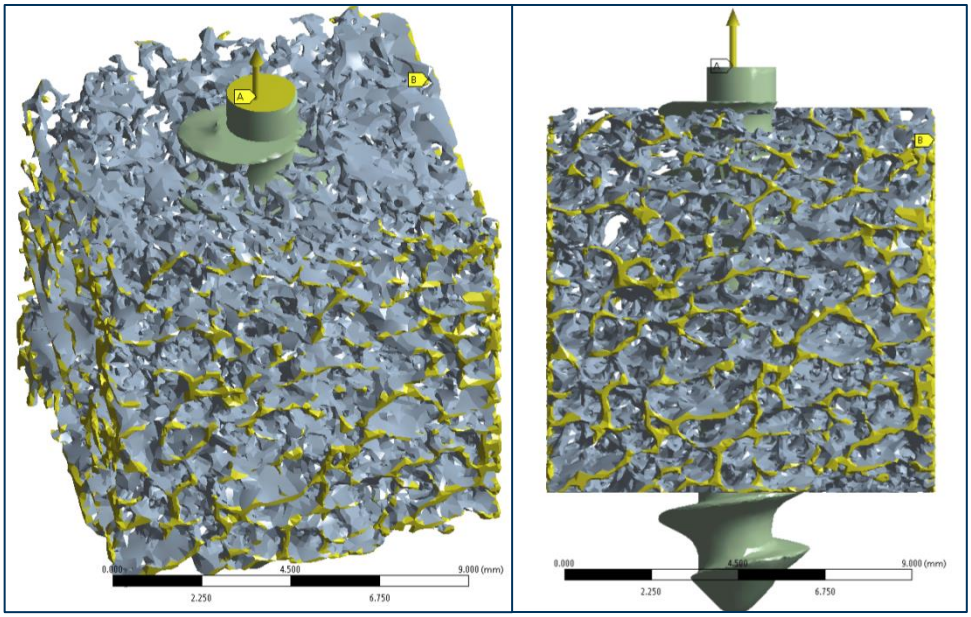

Figure 3-11: Loading conditions for most of the models

Figure 3-11 shows the boundary conditions used for most of the analysis, although alternative loading conditions would be described in their relevant sections. The cancellous bone is fully restrained on the four vertical sides in all

Cartesian directions (Label 'B'). Although the base of the bone could be restrained, some models contained very little material for this to apply, and in addition, the bottom of the screw would be assumed to also be in bone. The limitations of the model size here limit this loading condition, which is the opposite of the loading conditions used by Wirth, Müller and Van Lenthe (2012).

The screw has a vertical displacement applied on the top surface in line with the screw's principal axis, which was simplified to represent a pull-out test. The top surface was also a geometrical cut operation on the screw, applied at the same set distance for comparison of results.

3.2.b. Multi-scale modelling

Multiscale modelling refers to a style of modelling in which multiple models at different scales are used simultaneously to describe a system (Weinan, 2011). In the present study, this means that cancellous bone can be modelled in a small volume around the screw in order to correctly model the bone-implant interface, while most of the remainder of the model can be modelled as a continuum which requires fewer elements but can represent a much larger model and sustain all the relevant loading conditions.

3.3. Contact Parameters

An important aspect of the model creation and analysis is the choice of contact options, as these are important to the bone-implant interface. A recent review of literature (Taylor and Prendergast, 2014) suggests that there is only a rudimentary understanding of how the interference at the bone interface develops. At present, frictional models where only the variation of the coefficient of friction is used, but there is potential to use more sophisticated methods or algorithms such as cohesive zone elements. As such, contact parameters may be the second most important configuration stage after loading boundary conditions for simulations based on primary stability and the analysis of it. Most of the literature simplifies the contact options to a bonded model (Taylor and Prendergast, 2014; Wirth, Müller and van Lenthe, 2012) as it solves with fewer

iterations. Figure 3-12 shows how penetration is modelled. Only elements which are in contact may transmit compressive normal forces and tangential friction forces, but if the penetration is too high, bodies may pass through each other.

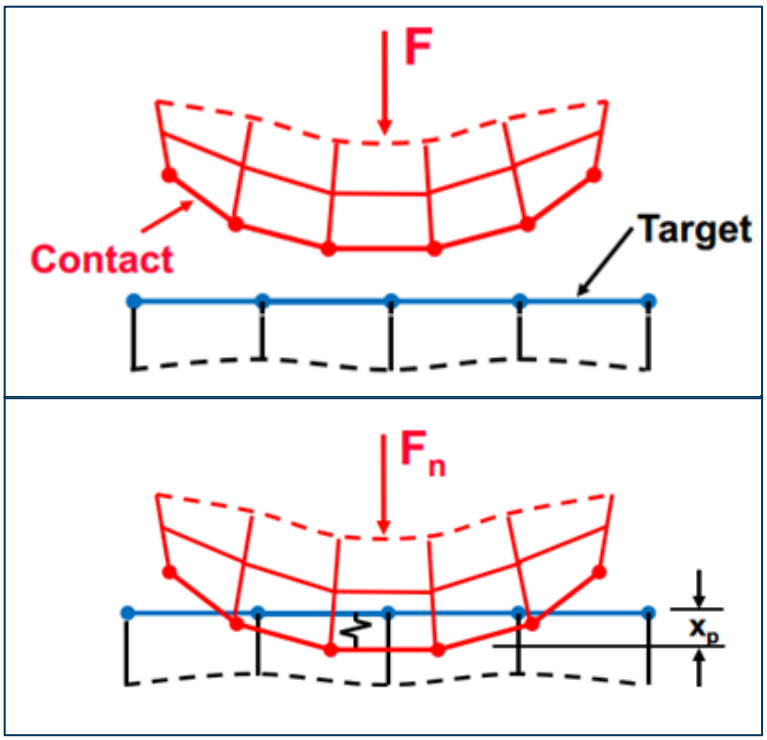

Figure 3-12: Penetration of target (Ansys® Mechanical Structural Nonlinearities Notes)

$$(3) \quad Pure\ Penalty\text{:}\ F_{normal} = k_{normal} x_{penetration}$$

$$(4) \quad Augmented\ Lagrange\text{:}\ F_{normal} = k_{normal} x_{penetration} + \lambda$$

$$Where\ \lambda\ is\ an\ internally\ calculated\ term\ that\ augments\ the\ calculation.$$

The Pure Penalty contact formulation was used for all of the models in this analysis, though it is quite sensitive to contact stiffness settings. The Augmented Lagrange formulation can also be used for non-linear problems, but Pure Penalty is more likely to converge, or converge with fewer iterations, and thus was the preferred method selected. The contact settings were also set to asymmetric behaviour, in order to represent the stiffer titanium implant which could bite into the softer bone. (Figure 3-13)

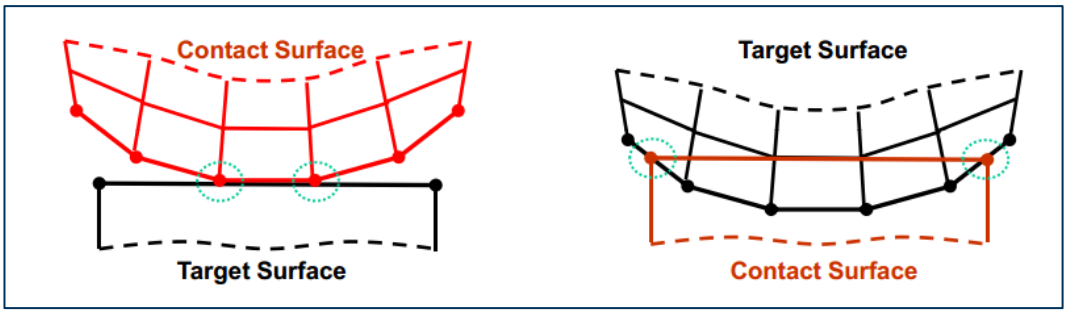

Figure 3-13: Asymmetric behaviour (Ansys® Mechanical Structural Nonlinearities Notes)

The stiffer material was always set as the target mesh, while the softer material, such as bone, was set as the contact surface. This ensured that only the titanium implant was allowed to penetrate the bone or the cement.

3.3.a. Friction and stiffness

A frictional contact allows for sliding between bodies and for the bodies to come in and out of contact. It also importantly allows for shear forces to develop between the two bodies. As such, a frictional contact was chosen for the analysis of screw implant to bone interface, as there is no evidence that this interface is bonded. Previous work has suggested a friction coefficient of 0.3 (Chen, Lung and Cheng, 2009) and this was the value used for the early analysis and simplified models. In the more complex discrete models, the conclusions by Hughes (2014) that a friction coefficient of 0.6 was more appropriate were used. This results from an analysis that was done on bone anchors which shows that there was a very large increase in pull-out forces between coefficients of 0.32 and 0.35 (Figure 3-14) but a smaller increase after 0.35. Bennani Kamane (2012) compared three coefficients of 0.1, 0.3 and 0.5 and found no significant change for a screw model, a similar model to the current study of screws. The chosen frictional coefficient value of 0.6 is also consistent with the literature.

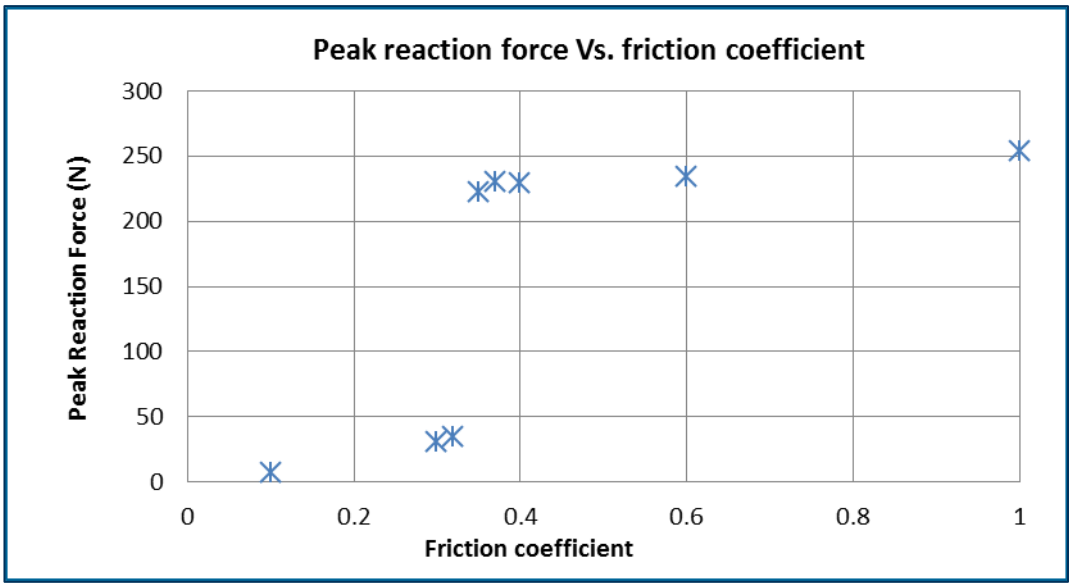

Figure 3-14: "Plot of peak reaction force of an anchor in a CT model vs. friction coefficient, 1 represents bonded"(Hughes, 2014)

The contact stiffness was updated with each iteration and contact stiffness was set at 0.01 for the more complex discrete models. Although this was a relatively low value allowing greater penetration, it was a necessary step in order to achieve solution convergence. Although a contact stiffness of '1' would be recommended for accuracy, some short studies by Hughes (2014) showed the peak stress to be less than 2% different.

4) Chapter 4 – Intramedullary implants and cut-out

This chapter will cover the investigations of the bone-implant interface with a focus on the issue of cut-out of femoral nails from the bone as simplified finite element models. The objective of the work was to investigate stress concentrations and possible cut-out features in proximal femoral nails as very simplified models. These also helped to develop better models which were used to investigate the specific effect of the lag screw of a Gamma nail in a more detailed model of the femur head. Gamma nails and proximal femoral nails (PFN) have similar geometries and have been shown to have no difference between the results of treatment (Schipper *et al.*, 2004). A further study was also made on the effect of the position of the lag screw on outcomes and compared with existing medical surveys (Parker, 1992).

4.1. Simple Bone Models

4.1.a. First case

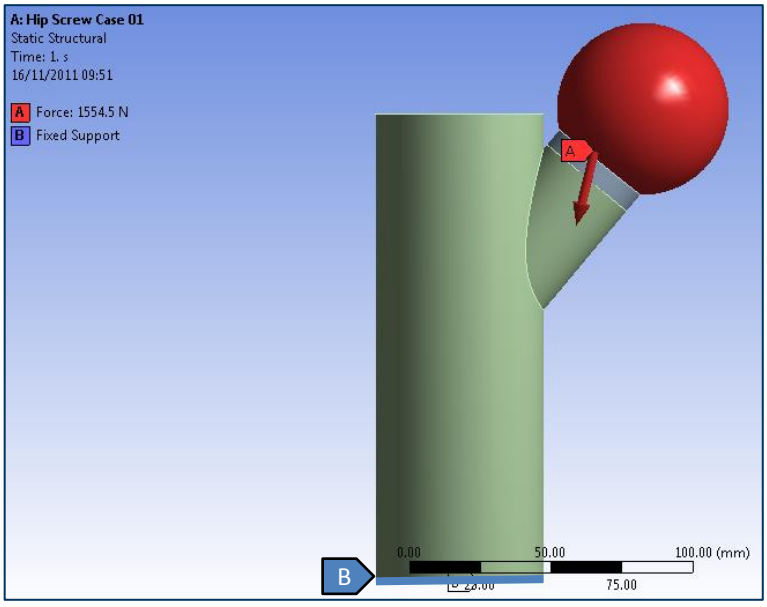

Figure 4-1: Simplified femur loading conditions

The models used for the initial study were very simplified approximations of a femur proximal section with trochanteric section, neck and head. Static load was initially used in order to investigate stress concentrations in the PFN. The static loading was provided at different time steps by Bergmann *et al.* (2001) where

each static step was solved using one step of the tabular data. This was placed on the model approximation of the femur head, while a fixed support was used at the base of the shaft (Figure 4-1). The shaft and trochanteric region are modelled as a simple cylinder of 60mm diameter and 165mm length. The neck of the femur is a second cylinder 35mm in diameter linking the trochanteric region and the femur head, a 30mm radius sphere. These measurements were very crude approximations of a femoral proximal section. The cylinder which models the neck of the femur was cut to approximate a Garden II or reduced Garden III-IV fracture (Guyton, 1998).

The proximal femoral nail was modelled as a 14mm diameter cylinder with a reduction to 11mm on the shaft end. Two lag screws were cut from the main section, the lower being 9mm in diameter with an 11mm locking diameter, while the top one is 4.5mm in diameter with a 6.5mm locking diameter. They are both angled at 140° from the vertical (Figure 4-2).

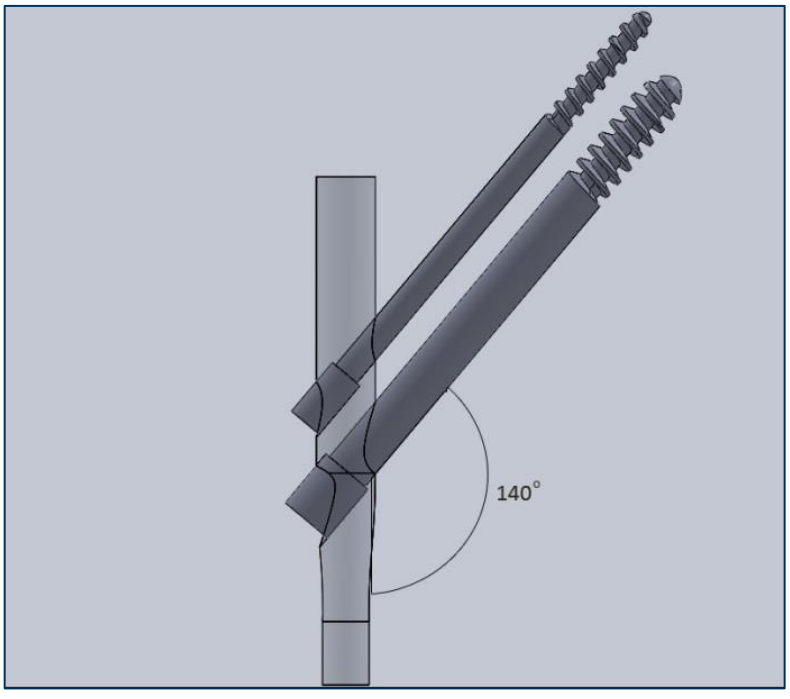

Figure 4-2: Proximal Femoral Nail model

ANSYS® (Workbench version 13.0) was used to implement the F.E. analyses. The implant uses the Titanium alloy material pre-set, which has a Young's Modulus of 96GPa, Poisson's Ratio of 0.36, C/T Yield Strength of 930MPa and Tensile

Ultimate Strength of 1.09GPa. The bone modelled was defined as having a Young's Modulus of 300MPa and a Poisson's ratio of 0.3, the apparent density properties of cancellous bone when modelled as a continuum (Wirth, Müller and van Lenthe, 2012; Currey, 2002). The bone model was homogenous and linear isotropic. The contact between both lag screws and the head was set as frictional with an auto-asymmetric behaviour, a friction coefficient of 0.35 and a Pure Penalty formulation. The stiffness was also updated at each iteration (Hughes, 2014). The contact between the two bones had the same settings but a frictional coefficient of 0 (frictionless).

4.1.b. Results

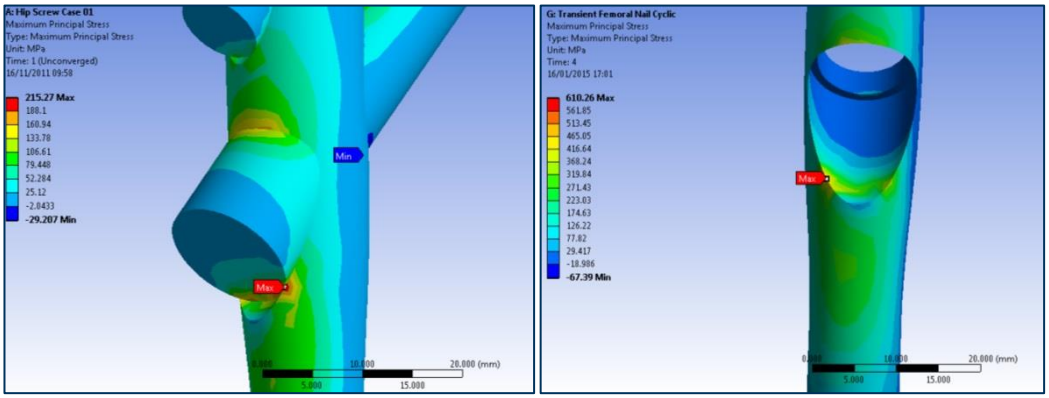

Figure 4-3: PFN Maximum principal stresses

The results of the static test at the highest load (t=4 model), shown above (Figure 4-3) match previous research by Wang *et al.* (1998) which showed that the highest concentrations of stresses occur at the insertion holes for the lag screws (Figure 4-3).

The Figure 4-4 and Figure 4-5 showing results obtained from the contact tool for penetration and frictional stress of the screws can be seen.

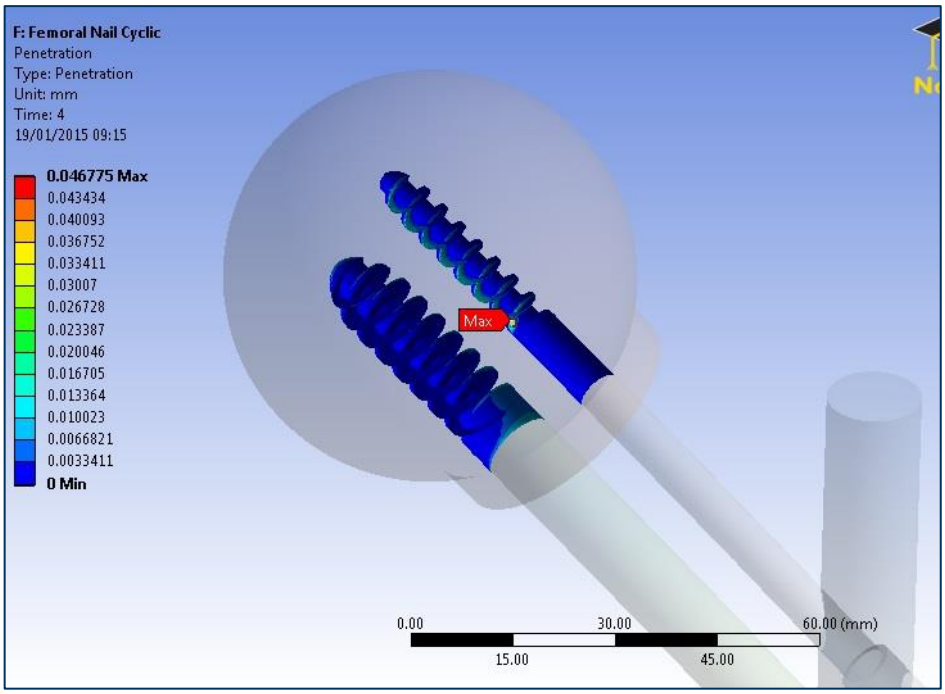

Figure 4-4: Penetration reading from the bone volume (mm)

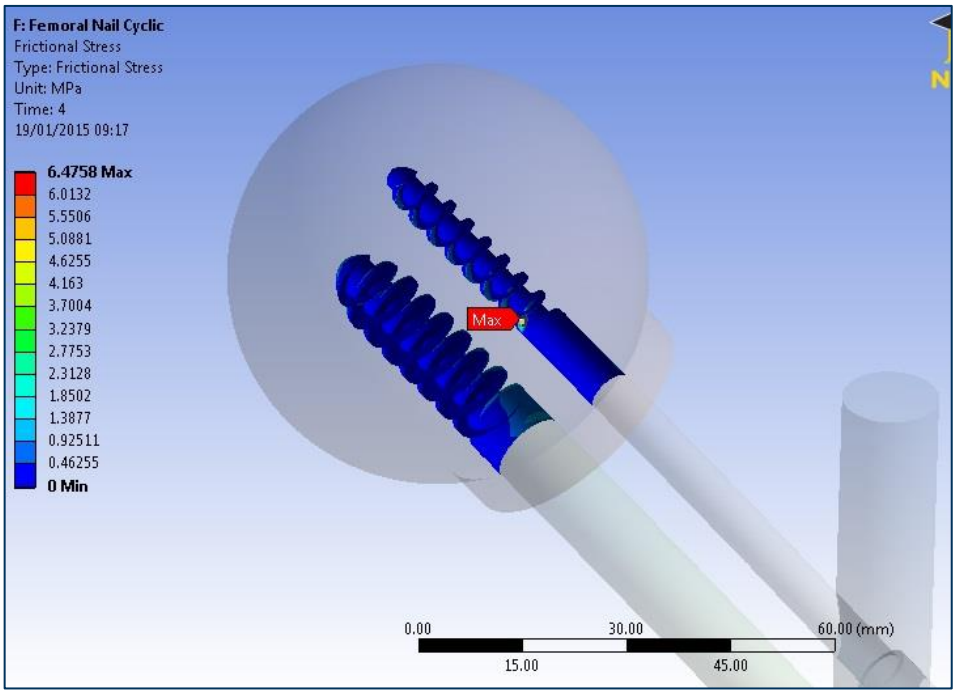

Figure 4-5: Contact frictional Stress (MPa)

The highest penetration of 0.05mm occurs at the base of the thread of the top small lag screw, and corresponds to the location of the highest contact frictional stress. The intensity of the frictional stress matches the intensity of the loading, and is identically related in each load model. The penetration is at maximum at

the second load step until the 14th step, the second step is when the lateral (in line with the 2 lag screws) component of the load is at its maximum.

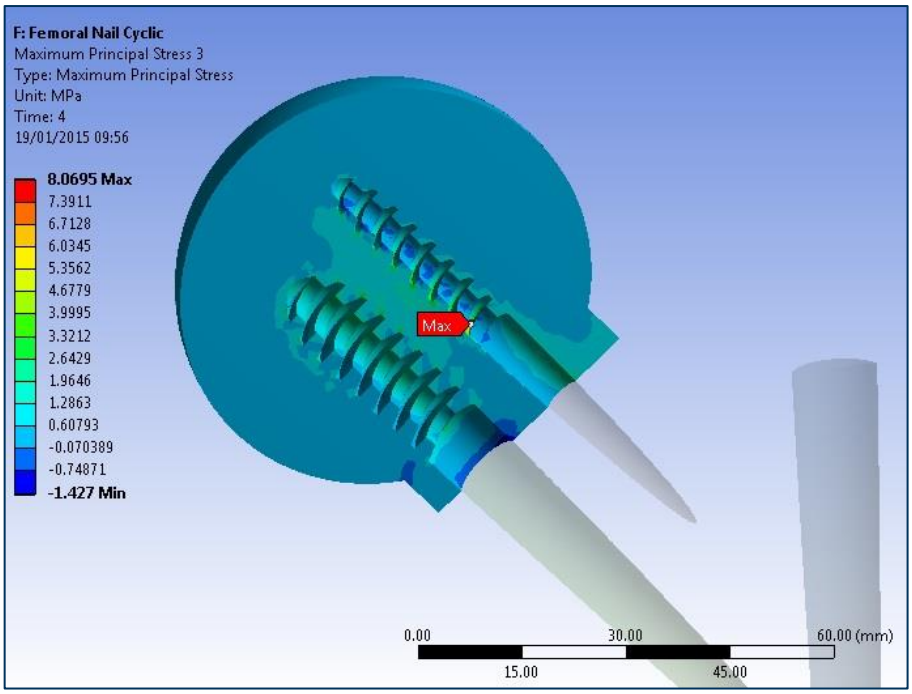

Figure 4-6: Maximum principal stress within the bone (MPa)

The maximum principal stress in the bone is the same as the contact frictional stress in location and the loading in intensity for each of the load steps, reaching a maximum of 8MPa (Figure 4-6).

4.1.c. Discussion

The results shown are in agreement with previous work on femoral nails with two lag screws (Schipper *et al.*, 2002; Wang *et al.*, 1998). The load is shared between the two screws and high stresses are found at their nail insertion holes. As these models are run in a static structural system, each load configuration point is resolved as a single entity. In the cases where the resultant load is high, such as time points 4 and 13, the maximum principal stress is also at its peak. Starting from load case 2 until load case 15 the penetration peaks at 0.05mm. This is a result of the Pure Penalty asymmetric contact option, limiting the allowed penetration of the screw by its stiffness constant k_{normal}. The location of the penetration is explained by a scissoring of the two screws, as the stiffer lower screw will withstand more deformation than the thinner upper screw. This can

be seen in a deformation result of 2.7 times the true scale, with modified scale to focus on the lag screws as shown in Figure 4-7. These results might give an indication to the initiation site of lag screw cut-out, but a more in-depth investigation would be needed as too little is known of specific cut-out conditions.

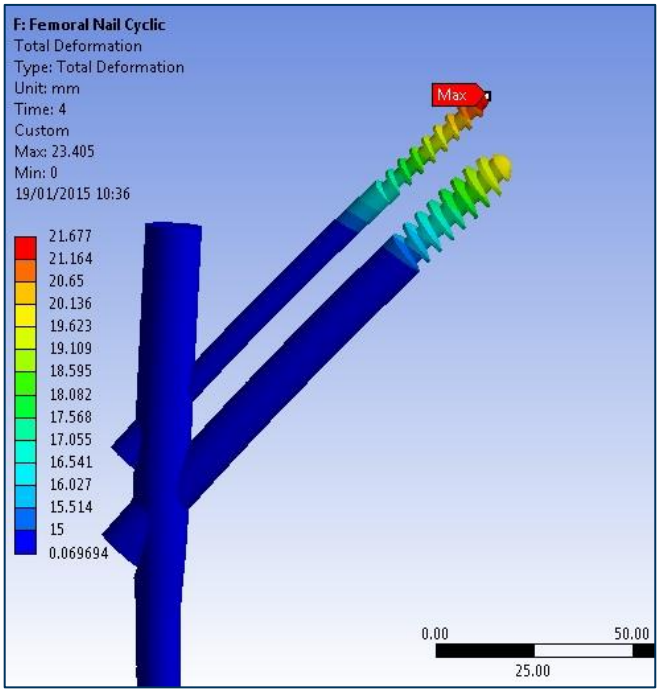

Figure 4-7: Total deformation of the Lag screws (adapted scale - mm)

This model has shown how a simplified model can provide results approaching *in vivo* situations, requiring very little computational power to ascertain general design features of femur augmentation implants. The results from this model show, however, that a transient model and improved femur geometry are needed in order to ascertain the likelihood of cut-out more accurately.

4.1.d. Second Case

The model was improved in order to investigate the effect of cyclic loading by using the Transient system and the load cycle obtained by (Bergmann *et al.*, 2001) for standard gait loading. The loading was repeated four times, which would represent four steps in gait. For this investigation, the fracture was modelled as a 1mm gap between the head and trochanteric region (Figure 4-8).

4.1.e. Results

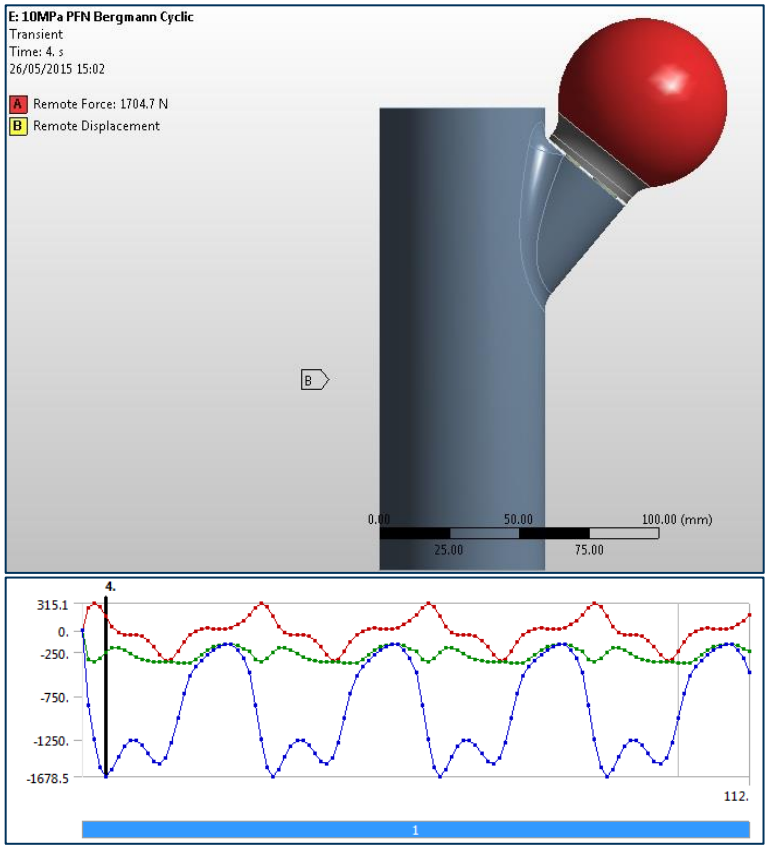

Figure 4-8: Cyclic transient loading model

The results for this model do not show the scissoring effect, as can be seen in the depth of penetration in Figure 4-9, however this is replaced by a displacement in the X direction, as can be seen in Figure 4-10. This displacement also results in much higher stress levels (1.23GPa) in the top neck screw which overshadows the highest concentrations of stresses that occur at the insertion holes for the lag screws.

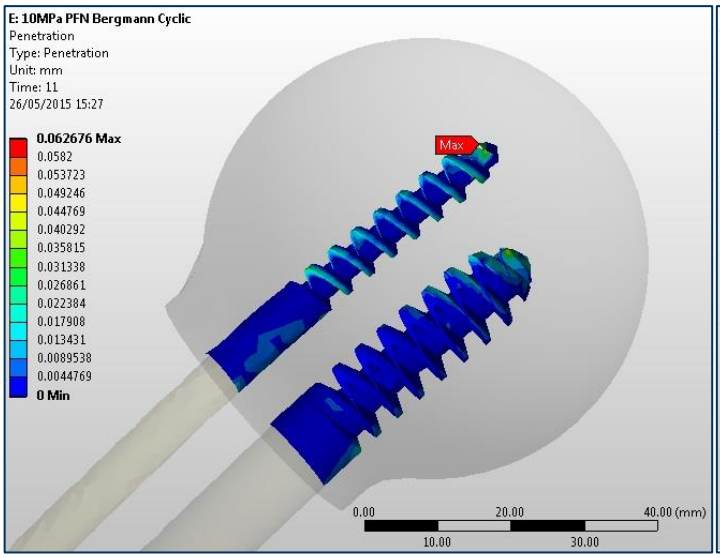

Figure 4-9: Highest penetration result (mm)

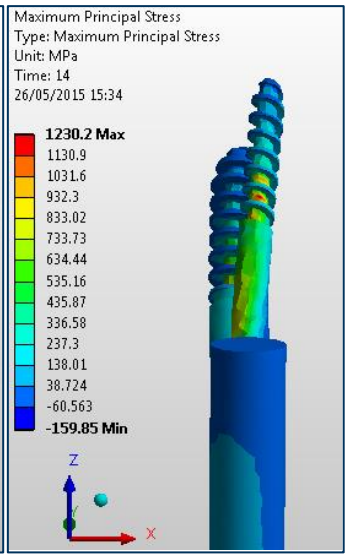

Figure 4-10: Maximum principal stress (MPa)

The depth of penetration is also increased to 0.06mm and no longer under the top lag screw but on the top of the tip, in the opposite X direction from displacement (Peak depth on the posterior side of the head). This means that the static model's scissoring effect of the two lag screws no longer exists, or is lessened in the transient model.

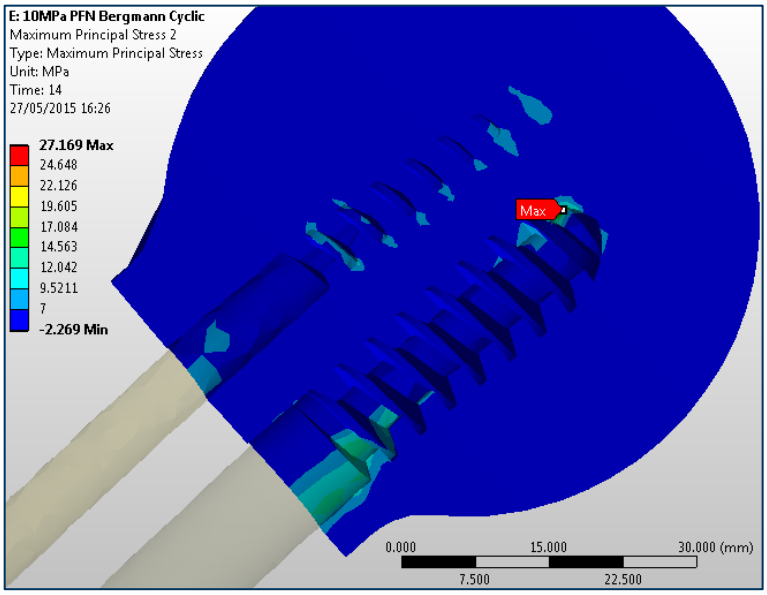

Figure 4-11: Bone maximum principal stress

As can be seen in Figure 4-11, the stress in the bone is much lower and matched a cantilever pattern: The peak stress in the bone is at the top of the tip of the lower lag screw while an opposing stress can be noted at the bottom of the bone at both lag screw locations.

4.1.f. Discussion

As was discussed for the previous model, the amount of penetration is limited by its stiffness constant k_{normal}. However, for the transient study, the load applied to the model is not re-iterated for each time step. It is conserved through each step and thus increases the effects of a load of the same magnitude for each analysis step in comparison with the static modelling. This also becomes apparent when comparing principal stresses for the bone head and the femoral nail with the deformation at each time step (Figure 4-12): although the deformation and load (a total 1705N at step 4, but a 1601N force at step 13) are reduced on the second peak, the maximum principal stress found in the femoral nail is increased by about 24% from 995MPa at step 4, to 1230MPa at step 14, which is also one time point after the second load peak. The maximum principal stress in the bone does not peak until the maximum principal stress in the nail peaks, at step 14. It is also of note that it does not recede at the same time as the load and deformation, but retains intensity until both have become quite low (step 20 & 472MPa in the Nail). This means that although the femoral nail sustains both gait load peaks, only the second load peak creates a high peak of stress in both the bone and the implant.

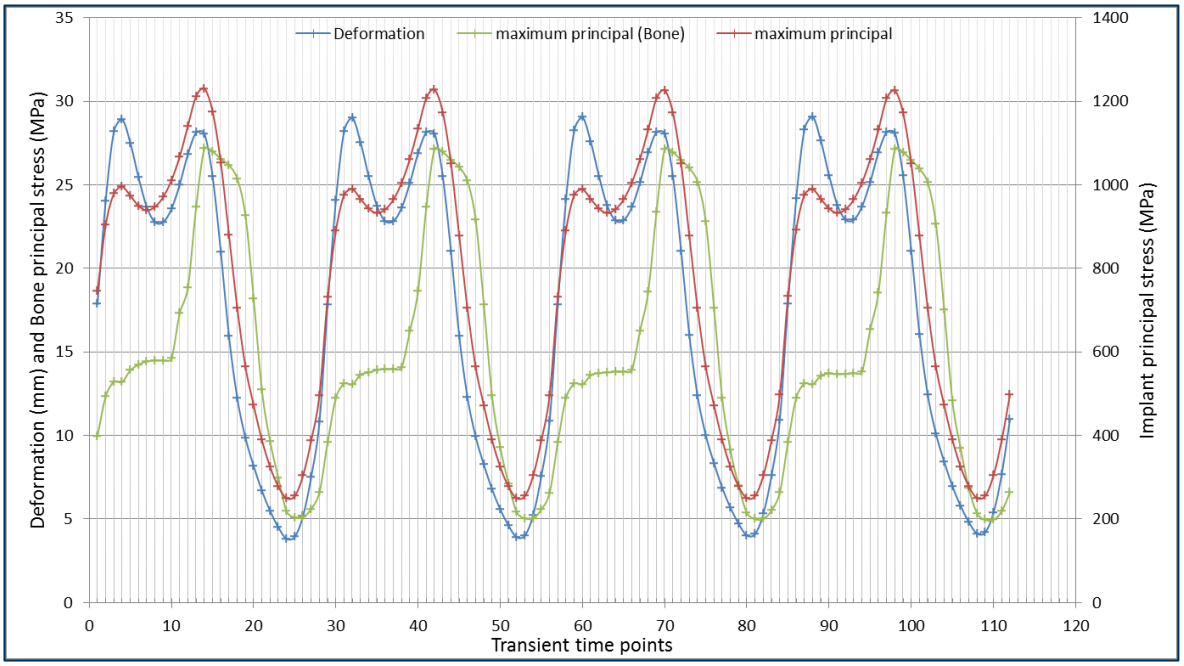

Figure 4-12: Deformation and maximum principal stress (mm & MPa)

Another interesting point not wholly apparent in Figure 4-12 is the reduction of stress and deformation over the course of the simulation. As mentioned above, the maximum principal stress in the nail peaks at 1230.2MPa in the first loading cycle, and time step 14. However this peak then becomes 1228MPa (-0.18%) on the second cycle, step 42, 1226.4MPa (-0.13%) on the third cycle, step 70, and 1225.5MPa (-0.07%) on the fourth cycle, step 98.

In conclusion, this study shows the importance of transient loading for the investigation of femoral implants by FE analysis, as the load was twice the intensity and of a very different nature when the model was loaded in a transient format. Both studies also show that FE models provide solutions that may act very similarly to in vivo results, such as the scissoring of the two lag screws in the femoral nail, the stress distribution across the nail or the reduction of stress over load cycles.

4.2. Gamma Nail

The previous models studied above were very simplified models. In order to further the analyses, the design of a *Gamma3 Locking Nail*® was kindly provided by Stryker®. The model was implanted into a more accurate femur model, obtained from available Mimics® files. The resulting model can be seen in Figure 4-13 and was a shorter approximation of the system as only the Lag screw model was provided. As the purpose of the study is the lag screw to bone interface, this was an acceptable assumption as the entire Gamma nail or the shaft of the femur were not under investigation, though proved to follow previous results in literature in section 4.1.

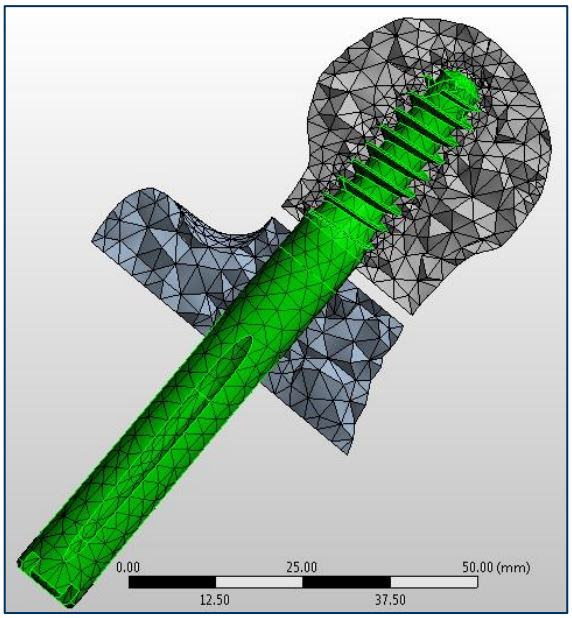

Figure 4-13: *Gamma3 Locking Nail*® model

For this model, the complex geometry was meshed and converged in a short study. Once the appropriate mesh was ascertained, an analysis was performed following a comparative study the results previously obtained with the PFN in section 4.1. Some minor changes include the boundary conditions: the fixed support is much closer and constrains the lag screw in this study due to the reduced geometry, and the force loading was only applied to multiple surface sections on an estimation of the acetabular cap loading condition (Figure 4-14). Contact frictional options remained identical (0.35 coefficient, Asymmetric, PP)

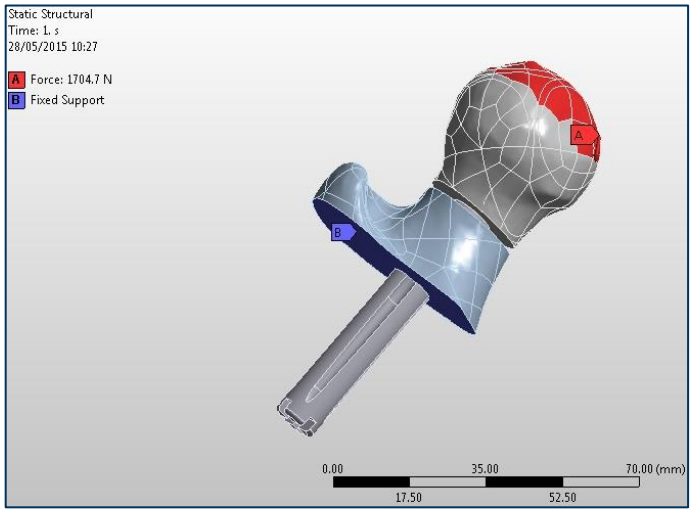

Figure 4-14: Gamma model loading conditions

4.2.a. Results

Both static structural and transient analyses were run using this model, and the results (Figure 4-15 & Figure 4-16) for the contact penetration and maximum principal stress follow the same differences as was found for the PFN although the altered model meant that exact values cannot be used for an acceptable comparative study. Some issues were still present with the remote displacement at [B] but minimally changing deformation results only.

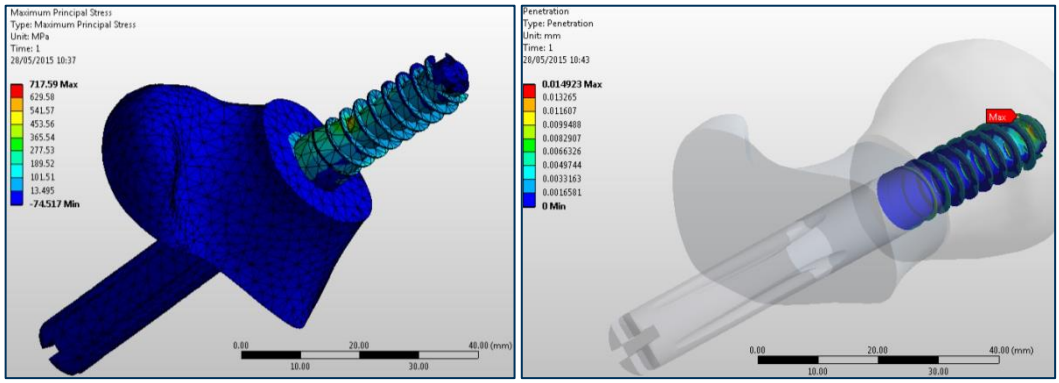

Figure 4-15: maximum principal stress (MPa) & penetration (mm) in the static model: peak load condition

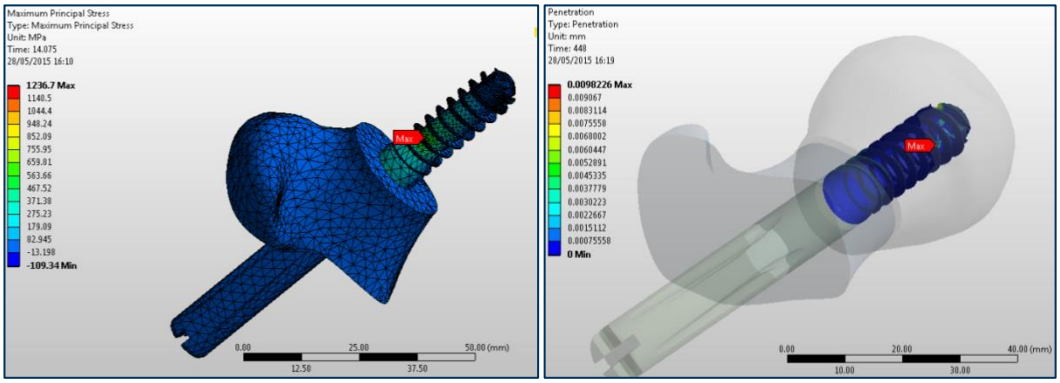

Figure 4-16: maximum principal stress (MPa) & penetration (mm) in the transient model

The maximum principal stress for the single load case was 717.6MPa in the lag screw, penetration limited to 0.015mm while the maximum principal stress of the bone was 13.3MPa. In comparison, the transient case had a maximum principal stress of 1237MPa in the lag screw, a penetration of 0.014mm and a maximum principal stress of 29.6MPa in the bone. The transient model was also cycled 16 times, which showed the reduction of stress and deformation over the course of the simulation.

4.2.b. Discussion

The discussion of these results can draw resemblance to the proximal femoral nail results, as the results for maximum principal stress were of the same order of magnitude, around 600-700MPa for the static model, and 1230MPa for the transient case, but this is a comparison of two very different models. Although this is the case for the exact magnitude of results, a comparative analysis can be made for the nature of the results: 1) A transient model is needed to represent a precise analysis of the forces affecting a hip fracture implant during motion as a static, single-loaded case is insufficient for a stress analysis of the implant to bone interface during gait. A single-load model will however be an adequate assumption for short-term modelling, as the 16-cycle model, as simple though it seems, took more than 2 weeks to reach a converged solution. 2) It is clear from both models that the implant will perform the majority of the load bearing, to a few orders of magnitude (1237MPa > 27MPa) higher than the bone. Stemming from this, the level of penetration and contact friction at the top (proximal) side of the lag screw is high, but migrates anteriorly as the gait loading moves posteriorly (Figure 4-17). The limitations of both models however restrict the analysis of these results to explain their involvement in cut-out. 3) Although the simplified PFN model showed interesting results at the lag screw insertion holes, it can be concluded that only the head of the femur, contact definition, and implant are needed in these simple models where the muscle loads on the trochanters are not applied. The base of the femur acts as a simple constraining mechanism, unless the two bone sections are modelled in contact.

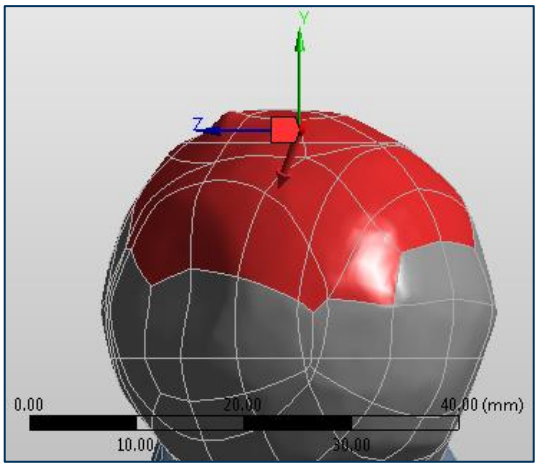

Figure 4-17: larger Z component in the model load at the 28th step

4.3. Positional Study

The femur and Gamma3 nail model was then amended to perform a positional study to assess the results by (Parker, 1992) on a FE model. The hypothesis proposed here is that simply translating the lag screw on the fracture plane would provide different results and that an inferior position on the antero-posterior radiograph, represented in this case by the X-Y plane, would show an ideal, or at least different, case. The model is presented in Figure 4-18 and shows 5 of the 9 positions studied: the original, central case; ±Y positions; and ±Z positions. Not represented here are the 4 ±Y±Z cases. The lag screws were placed 4.5mm from each other (3.18mm from the central screw) and at the same depth: The tip-apex distance was largest for the central case while the tip-fractures distance was identical for all the cases.

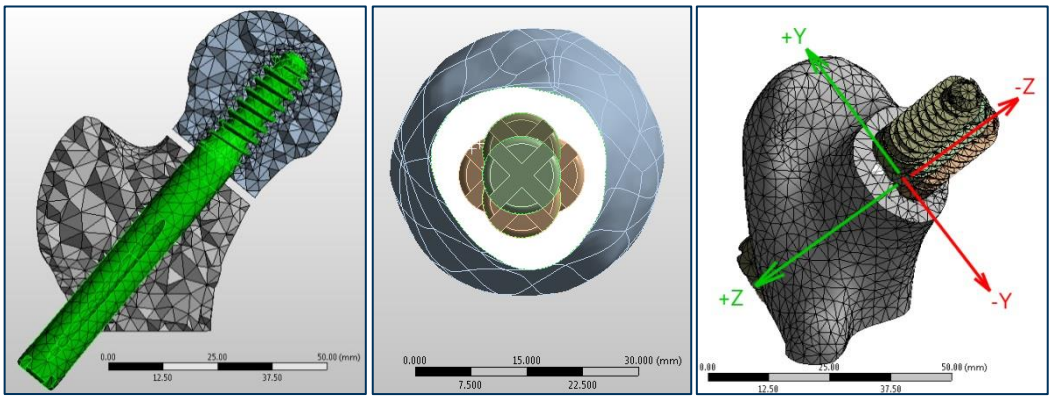

Figure 4-18: Gamma3 model and lag screw positioning (±Y and ±Z)

The contact settings were kept from the previous models (fc=0.35, Asymmetric, Pure Penalty) as were the load conditions and material properties. For the purpose of this study and obtaining results of penetration for the thread edge, a set of result paths were created, and can be seen represented in Figure 4-19.

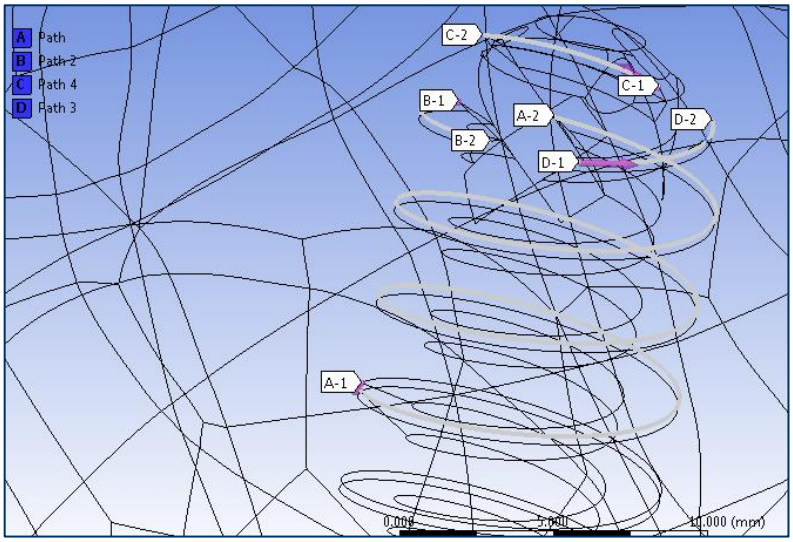

Figure 4-19: Path function on the Gamma3 model

This was done in an attempt to quantify any effect of the screw on the surrounding continuum of cancellous bone. These paths were placed on the bone circumference, not the edge of the screw.

4.3.a. Results

The results of this study have been compiled in Figure 4-20, showing both the penetration and equivalent (Von Mises) stress in the bone at the screw interface.

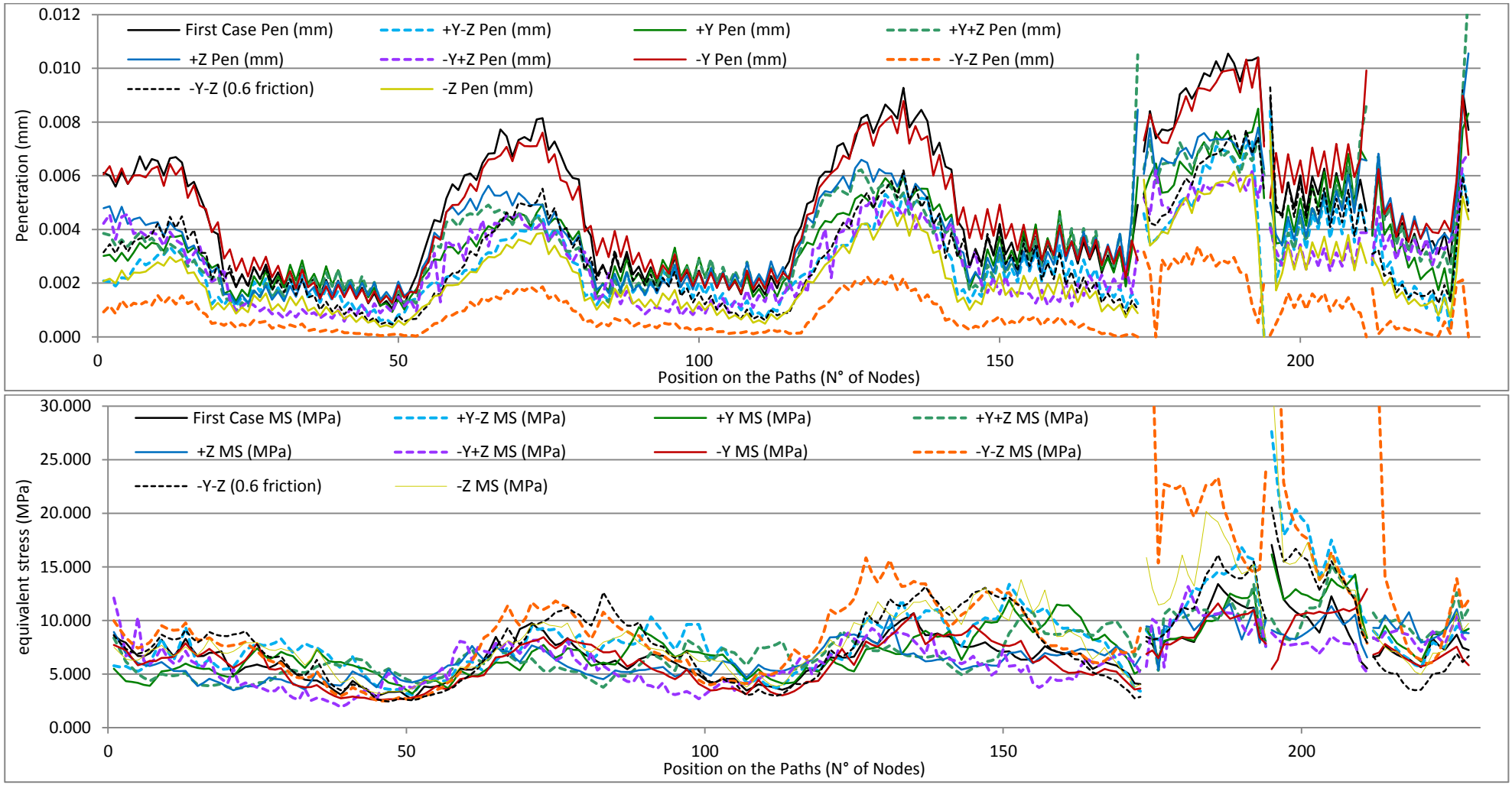

Figure 4-20: Penetration and equivalent (Von Mises) stress along the screw thread edge (mm & MPa)

In both graphs above, the results of the model where the lag screw was positioned in the inferior-anterior (-Z-Y model) were of some concern and checked. The results for that model showed a rotation of the head section around the lag screw which reduced the amount of penetration but increased the stress in the bone by a significant amount, especially at the cutting tip of the screw.

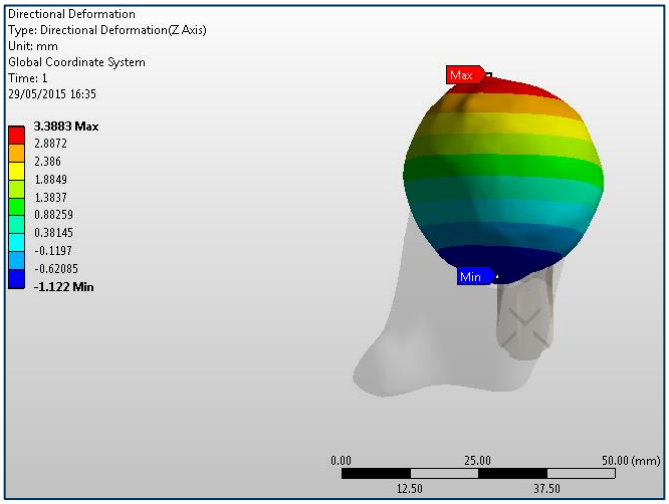

Figure 4-21: -Y-Z model deformation in the Z axis (mm)

As such, a 10th model was run in this simulation, identical to the –Y-Z model in all but the coefficient of friction, which was modified to 0.6 in order to increase friction and remove the potential for rotation.

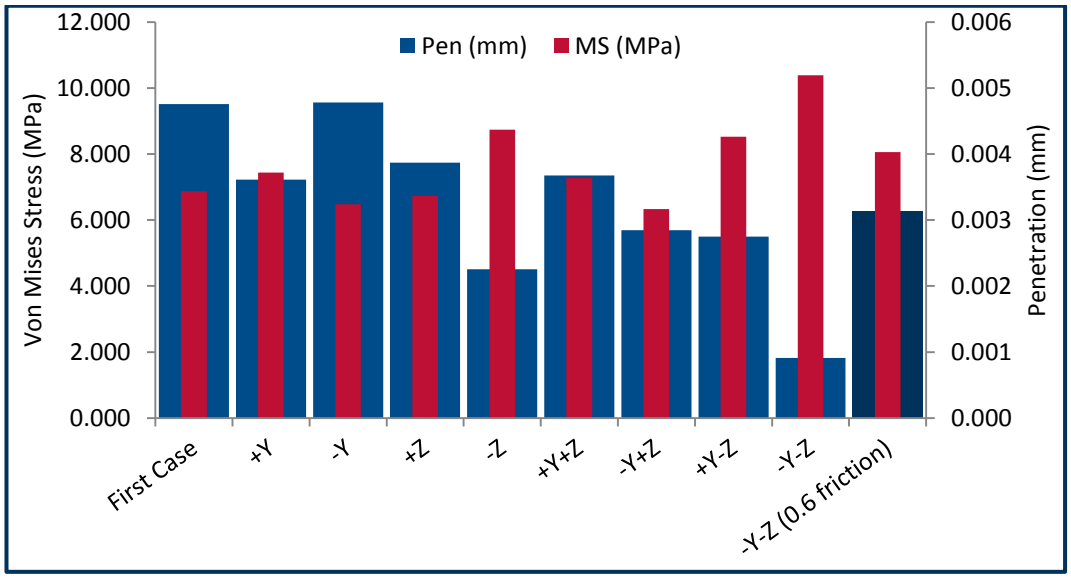

Figure 4-22: Average penetration and equivalent stress along the screw thread edge (mm & MPa)

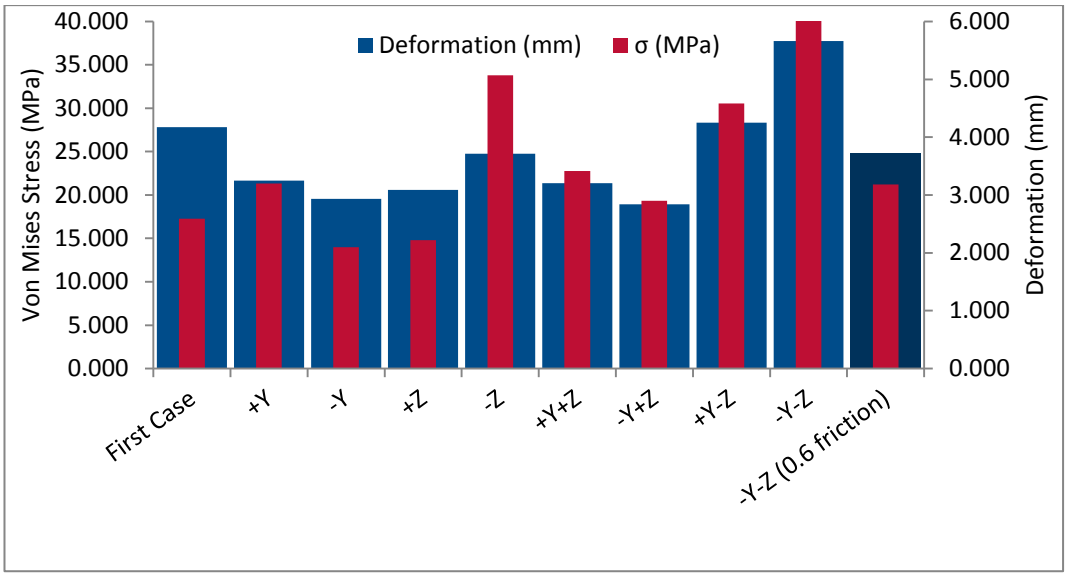

Figure 4-23: Deformation and equivalent stress maximum of the bone (mm & MPa)

Figure 4-22 above shows the average penetration & equivalent stress around the screw and Figure 4-23 the maximum deformation and maximum principal stress in the bone.

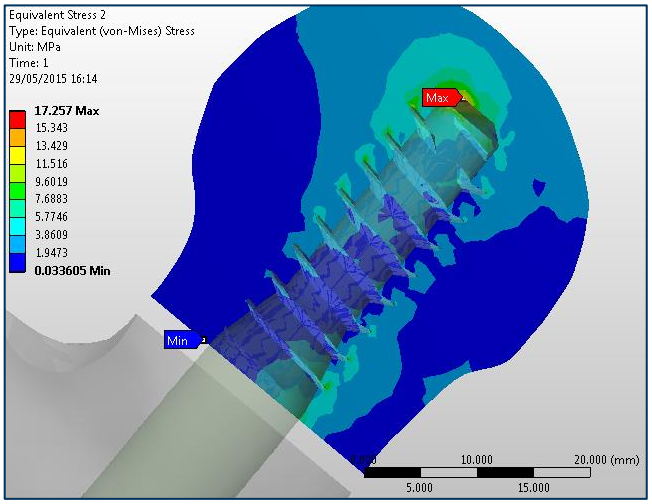

Figure 4-24: Equivalent (von-Mises) stress on the central-central lag screw (MPa)

A typical stress representation (first case) can be seen in Figure 4-24 acting in the same way as the simplified models: in a cantilever pattern with peak stress at the tip of the lag screw. The 3 models where the lag screw was placed in the anterior position (-Z; -Y-Z; +Y-Z) also showed higher stresses on the posterior cutting edge of the screw (Figure 4-22).

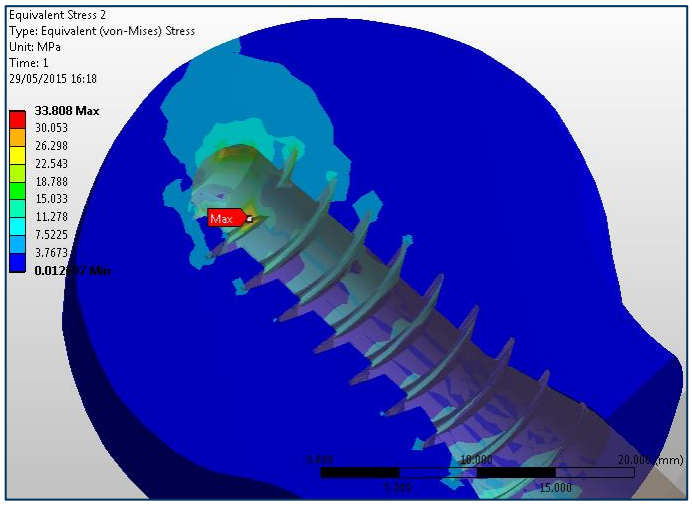

Figure 4-25: Equivalent stress in the central-anterior lag screw (MPa)

These models show the highest levels of stress, both at the screw edge and within the bone, in comparison to the other models, while showing a lower penetration depth.

4.3.b. Discussion

The first point of discussion of these results is to accept a good representation of positional literature regarding cut-out: The best cases in terms of equivalent stress in the bone are the central-central (first case) and inferior-central (-Y case) models. The posterior cases (+Z; -Y+Z) also show reduced stress and deformation, while anterior cases and especially the superior-anterior (+Y-Z) and inferior-anterior (-Y-Z) cases show the highest stresses and deformation, although in the inferior-anterior case, the higher friction model reduces these, which are a result of the rotation of the model. This is in line with the conclusions by Laskin, Gruber and Zimmerman (1979) though they were healing intertrochanteric fractures, and other studies (Parker, 1992; Den Hartog, Bartal and Cooke, 1991; Davis *et al.*, 1990) agree the anterior position to be preferable. The general consensus that an inferior-central position is preferred is reflected in Figure 4-23, as both the maximum stress and deformation are the lowest values out of all the cases investigated. From these results, it would seem that the posterior case is also a good candidate, but as can be seen with the rotation of the inferior-anterior case, many factors may not be accounted for, such as the effect of muscle loads on the trochanters or the strength of a reduced fracture,

as the current model simplified this to a 1mm gap. Another point of note is that the contact penetration has an inverse relation to the contact stress and bone equivalent maximum stress, the latter two having a close relationship. As such, from the results one would read a higher penetration of the contact to be a favourable factor, and a lower penetration, such as can be seen in the inferior-anterior case to be avoided. In this instance, both central-central and inferior-central cases yet again come out on top, while the posterior case is closer to the superior and posterior-superior cases, and not such a favourable position. An important note is that this study does not include any data on the tip-apex distance, known to be of importance (Baumgaertner *et al.*, 1995). The central-central case in this study has a much larger tip-apex value than the surrounding cases, and this might be one factor for the results.

4.3.c. Conclusion

In conclusion, this study shows that an approximate FE model of the femur will be consistent with in vivo result studies and agrees that the inferior-central case is the preferred position for a Gamma3 lag screw, if only mechanically to reduce stresses and deformation. Unfortunately, the study does not show good reasoning for the effect of cut-out, as penetration is inversely proportional and equivalent stress might only give an indication to a general area of weakness. In order to properly investigate cut-out, a multi-scale model must be used, as a continuum model does not provide adequate data.

4.4. Multi-scale Modelling, Associated Issues (Discussion)

The next step of the investigation of cut-out would have been a multi-scale model which includes both the correct general geometry of the Gamma3 screw and femur bone in addition to the correct discrete geometry of cancellous bone. The resulting model can be seen in Figure 4-26 as an incomplete surface mesh model. This section of the chapter exists to explain the shortcomings, both in the hardware but mainly in the software used, in order for further studies to expect difficulty in this area and adapt research accordingly. Hardware issue are simply the advancement of computing power; the fact that when these models were

run (2012-13), the machines used (described in Chapter 3 – Modelling Technique) were on the higher end of available resources, while upon publish of this thesis (2015),better hardware would be chosen if a new analysis were to be made.

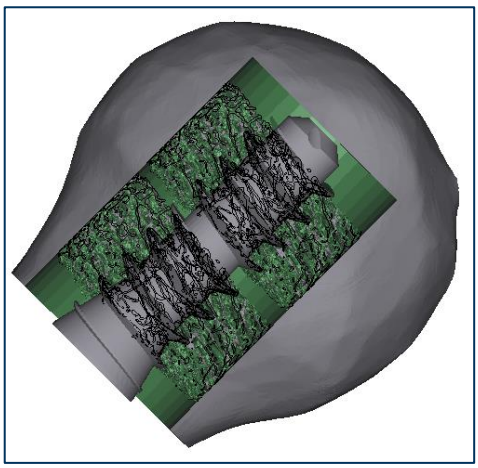

Figure 4-26: Gamma3 multi-scale model (surface shell)

The software issues are mainly related to the coding of the 3-Matic® software by Materialise®. Though very appropriate for its purpose, and possibly still the software of choice to convert CT scans into FE models, it encounters issues in the re-meshing and meshing improvement algorithms.

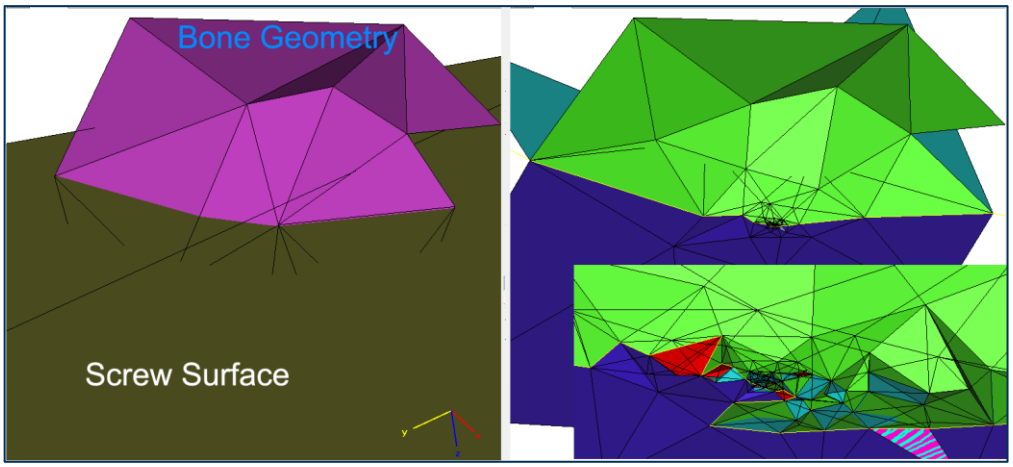

Figure 4-27: 3-Matic meshing issues encountered

An example of this is shown in Figure 4-27 where a relatively simple surface mesh for the bone is intersected with a screw mesh, and the resulting re-meshing process generates a very complex mesh with numerous intersecting and duplicate elements. This was a relatively common occurrence in all of the models

re-meshed in 3-matic, and the principal cause of the extended manual work needed to obtain appropriate FE models. When the number of concerned areas was low, the manual correction could be completed daily or over the course of a few days, but in the case of the Gamma3 multi-scale model, these were numbered in amounts that would have not been feasible to correct manually (Figure 4-28). An automatic resolution would be needed, but none was available and thus this model could not have been completed.

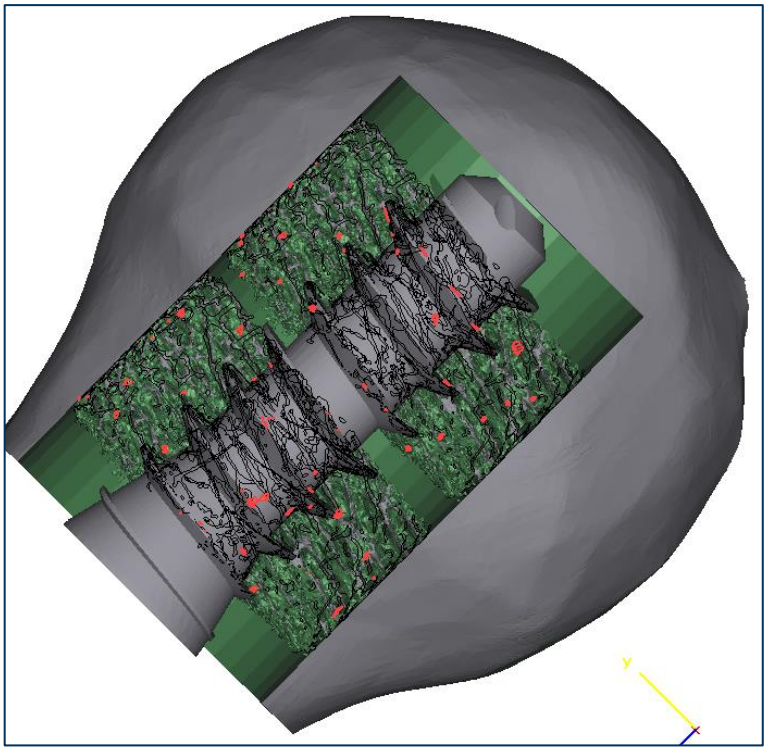

Figure 4-28: manual corrections required marked in red

Recommendations for further work on this subject include:

- A meeting was held with the Materialise® software team and they mentioned being aware that the re-meshing algorithms needed some improvements, and as such, later versions of the software might not encounter these issue, or might contain automatic resolution methods if the re-meshing process still results in complications.
- The multi-scale modelling involved intersecting 4 to 5 different solids (cancellous bone; screw; continuum bone geometry). Obtaining a CT scan of the entire bone, such as the whole femur head with cancellous bone

interior, and only then modelling the lag screw inside the structure might reduce the generation of the complications described.

- In a similar fashion to the previous recommendation, a scan of the bone and implant as one might remove these complications entirely, though some materials can cause image diffraction (Sullivan, Smith and Rozzelle, 1994). Shot-peened titanium alloy is known for this interference effect.

5) Chapter 5 – Parametric Analysis of a Cancellous Screw

As the multi-scale modelling route was not available for further research, the investigation of the bone-implant interface followed a different route of investigation: a continuation of the cancellous screw modelling by Bennani Kamane (2012), but using larger models in order to investigate the interaction between the screw and the discrete cancellous bone structure more accurately. The latter part of his work investigates the resulting change in pull-out stiffness from to the effect of some parameters such as screw type, pilot hole presence or screw angles. According to Tencer et al. (1996), a good holding power when a large force is needed to 'pull out' the screw in porous materials such as cancellous bone is dependent on six factors, three of which are related to the geometrical design: *Outer diameter; length of engagement in bone; thread geometry (length and pitch)* as well as three related to the bone and its preparation: *bone shear strength; pilot hole size; tapping*. This chapter will investigate some of the screw parameters in more depth and find out which parameters might have the greater effect. Each set of parameters studied will be separated into a section.

5.1. Introduction

In this study, two out of the above 6 factors were studied. As part of the *thread geometry (length and pitch)* and *bone shear strength* factors, three groups of parameters were studied as 3 analyses:

- Bone volume fraction (BV/TV): This set of models made use of thresholding to obtain 9 different BV/TV values of the same piece of bone, which was thus eroded (Kim *et al.*, 2007; Hara *et al.*, 2002).
- Pitch and inner diameter: These are two major components of the cancellous screws; these two parameters were investigated without any modification in the outer diameter of the screw, as this is known to have a very large effect (Gausepohl *et al.*, 2001; Wittenberg *et al.*, 1993).

- Proximal half angle: (Wang *et al.*, 2009) performed recent testing which showed this parameter to be of significant influence. These results will also be used to validate modelling data.

The models used for this analysis were created using the method described in Chapter 3 – Modelling Technique. The CT scans were obtained from the femoral condyles of a cadaver (adult female) and the method described above was used to create FE models with the geometry of the cancellous screw obtained from Stryker® (Bennani Kamane, 2012).

The models created were submitted to a vertical linearly ramped displacement of 0.2mm applied to the top of the screw geometry ([A]), and fully restrained on the four vertical sides (i.e. the outer surfaces lying in the Z-X and Z-Y planes), marked on Figure 5-1 as [B], though the front and back face are not marked.

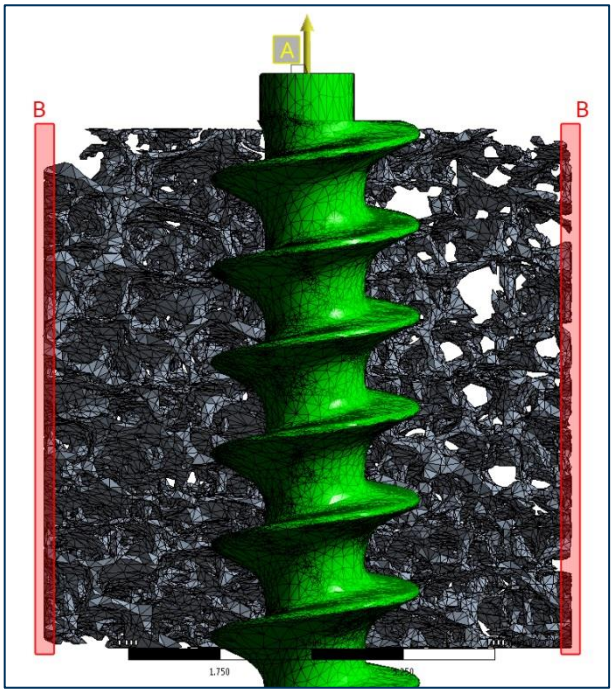

Figure 5-1: Loading of the discrete model (0.2mm displacement)

The reaction forces of the model against the 0.2mm displacement are the forces given as 'pull-out' for the analysis. The values of 0.2mm was the largest mean trabecular thickness of the original bone model (Hughes, 2014) though the lower threshold models would have a mean trabecular thickness closer to 0.1mm. As such, displacement values above 0.2mm would likely create large deflections in

the trabecular struts and create complex contacting mechanisms. Due to the bone model being linear isotropic, failure of trabecular struts is not resolved as it would be in a plastic model. The 'pull-out force', denoted as the ultimate force required to remove the screw from the bone, is therefore quantified as the reaction force of the model to the 0.2mm displacement. Rice, Cowin and Bowman (1988) also conclude that Elastic modulus and strength of cancellous bone are linearly proportional, and has been experimentally demonstrated. The contact definition is described in Chapter 3 – Modelling Technique and the interface between the bone and the screw is a frictional contact with frictional coefficient of 0.6, asymmetric behaviour, and contact stiffness updated for each iteration. The bone elements have the following properties:

Density, ρ = 1180kg/m^3

Young's modulus, E = 17GPa

Poisson's ratio, ν = 0.3

Yield strength, σ = 100MPa

Ultimate strength, σ = 110MPa

These values are chosen to fall within measured values in literature (Bayraktar *et al.,* 2004; Jee, 2001) for 'normal' bone. The titanium screw elements were set as the defined "*Titanium alloy*" by ANSYS®: ρ = 4620kg/m^3, E = 96GPa, ν = 0.3, Yield σ = 930MPa, Ultimate σ = 1070MPa.

The aim of the study is to identify the effect of parameters and ascertain which would increase pull-out strength in cancellous bone.

5.2. Varying Volume Fraction

The first analysis performed investigated the effect of varying bone volume fraction (BV/TV) on pull-out. In order to vary BV/TV, multiple lower threshold cut-off points of the Hounsfield greyscale were selected in a linearly increasing pattern to give different volume geometries. This created a set of models, from

the highest 20.7% BV/TV model, in steps of approximately 2.5% to the highest threshold which resulted in a model of 6.16% BV/TV. In order to keep these models fully consistent, mesh refinement and corrections were applied simultaneously to all 7 models in Mimics as these can select multiple items to run in a single batch, thus resulting in simultaneous modifications of the models. The Mimics pre-defined bone threshold would generate a model of 16.8% BV/TV. As such, the two largest models have a larger volume than the original model: 20.72% BV/TV and 18.00% BV/TV, while the smallest models have been eroded: 15.73% BV/TV; 13.21% BV/TV; 11.12% BV/TV, and finally two models would be below the WHO BV/TV threshold of 11% (Legrand *et al.*, 2000) and would be classed as osteoporotic bone, though 11.12% could be classed as osteoporotic in some circumstances. The yield stress and ultimate strength properties listed in 5.1 Introduction were not defined for this analysis.

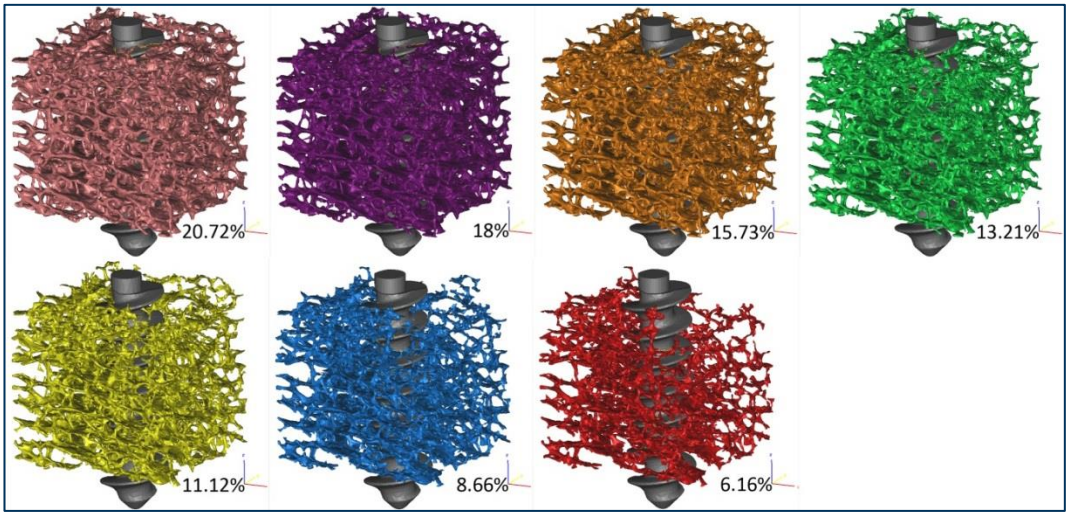

Figure 5-2: Bone Volume Fraction models

The 7 resulting models are shown in Figure 5-2 with the bone volume percentage displayed on the right of each model. The decreasing volume of bone also signifies a decreasing contact area, and though not directly related to pull-out strength (Bennani Kamane, 2012), there is strong evidence that higher apparent density gives higher contact area and therefore provides increased pull-out force (Asnis and Kyle, 1996).

Figure 5-3: Contact area for each model

The highest BV/TV model had a total contact area of 31.3mm^2. In decreasing BV/TV, the following models had contact areas of 27.3, 23.4, 19.3, 15.9, 12.8, and finally 8.41mm^2 for the 6.16% BV/TV model (Figure 5-3).

The pull-out force is given as the peak reaction force for a screw displacement of 0.2mm. The pull-out strength for the different densities is shown in Figure 5-4 with the added 0-0 point (No bone = no reaction force). The results show a clear difference between each of the models, where 6.16% BV/TV provides only 78.6N, but 8.66% provides a 230N reaction force and 20.72% reaches 2035N, a significant 2489% increase from the lowest volume fraction.

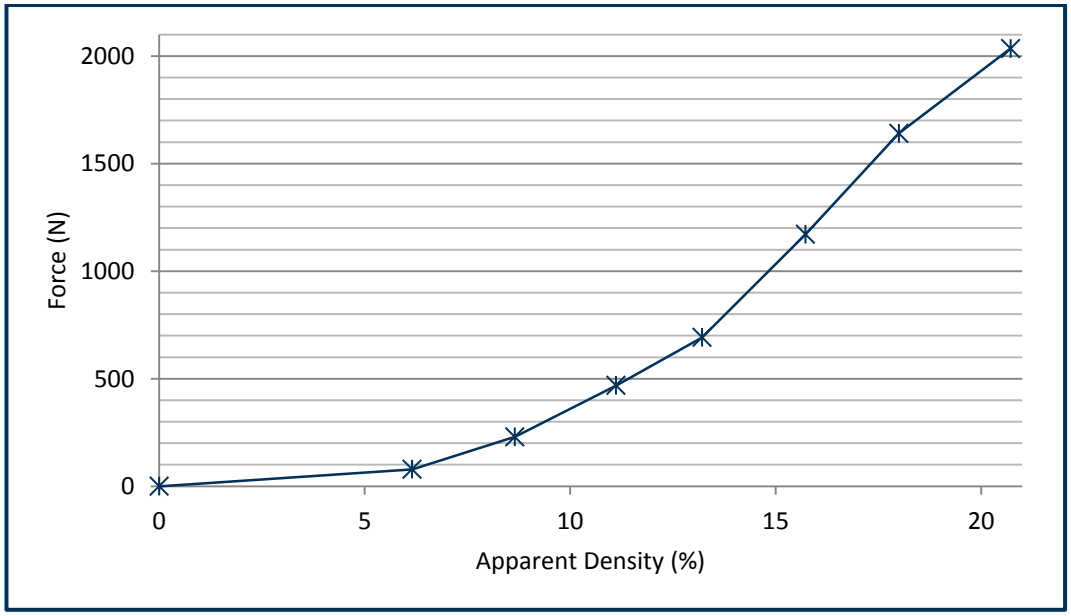

Figure 5-4: Screw pull-out comparison of different bone volume fractions

The clear relationship between reaction force and bone volume fraction was matches the data observed by Morgan and Keaveny (2001) when they related yield stress to apparent density in tension or compression. Both relationships show that a small variation in volume fraction for the same bone geometry can significantly alter pull-out strength. The effect of BV/TV on pull-out strength is known from physical testing (Tencer *et al.*, 1996), and confirmed via this FE modelling study.

5.2.a. Volume Fraction and Screw Pitch

Another aspect of the volume fraction analysis was to compare this effect to the variation of another parameter. In this case, the screw pitch was chosen as one of the principal factors affecting pull-out strength (Tencer *et al.*, 1996). The same parameters were used for the contact options and boundary conditions as for the previous 7 models in order to allow for exact comparison. The resulting reaction forces are compiled in Figure 5-5 with the additional 0-0 point. The original 1.75mm pitch of the cancellous screw is displayed in blue while the second set of models based on the 2mm pitch screw are displayed in red:

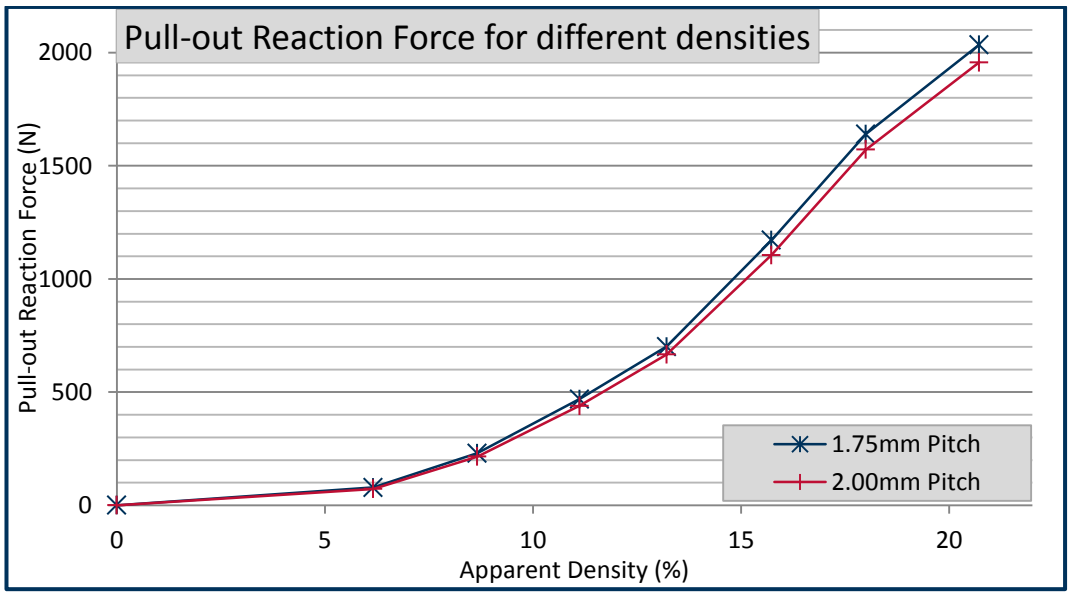

Figure 5-5: Screw pull-out comparison of different bone volume fractions at 2 different Screw Pitches

The results show a decreasing reduction of an average 5.5% in the reaction force of the 2mm pitch screw, with 8% at 6.16% BV/TV, 6.5% at 8.66% BV/TV, 5% at 13.21% BV/TV, and 3.8% at 20.72% BV/TV. As such, the effect of varying the pitch of a screw has almost no influence on pull-out, in comparison with the varying volume fraction. It is worth noting that the 6.16% BV/TV decreased by 8% to 72.3N and this points to a proportionately larger effect of the screw pitch on lower BV/TV bone, which is supported by previous studies (Asnis *et al.*, 1996). This lead to the selection of the lowest apparent density model for the following analysis in the influence of pitch and inner diameter of the screw, as these parameters would not have had such a large effect in higher density bone.

5.2.b. Volume Fraction and Contact Area

Using the contact areas of each model as seen in Figure 5-3 which were obtained from the Mimics® program which provides the surface area data of each surface mesh, the reaction force in relation to the contact area can be calculated for each model, and results can be seen in Figure 5-6.

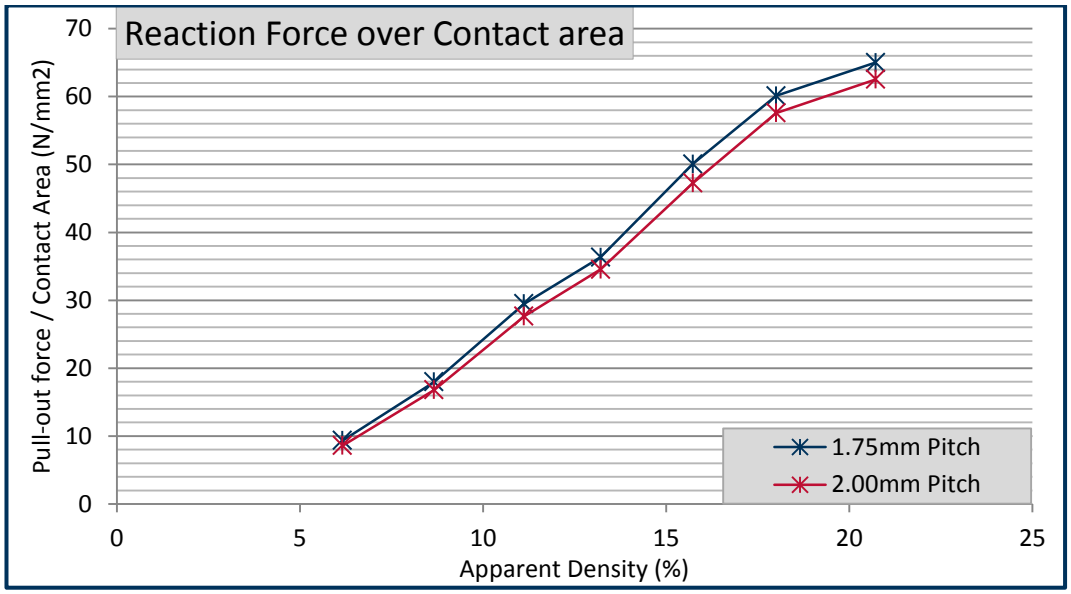

Figure 5-6: Screw pull-out according to contact area of different BV/TV

The results show an S-shaped curve while the data would be expected to be a linear relation, as a plot of contact area against apparent density is linear. This suggests that in a higher density model the apparent cancellous structure is stiffer than the lower density structure, but this change does not follow a linear trend.

5.3. Pitch and Inner Diameter Relevance

The study's second analysis performed investigated the effects of varying the pitch and inner diameter (ID) of the cancellous screws. The outer diameter of the screw is known to be an important, if not the most important factor, in pull-out strength (Gausepohl *et al.*, 2001; Chapman *et al.*, 1996; Asnis *et al.*, 1996) and will not be investigated in this study. Chapman et al. (1996) propose a shear failure force formula that includes a thread shape factor 'TSF', which was highly correlated to their experimental pull-out forces (slope = 1.05, R^2 = 0.947) and is defined in Chapter 2 – Review of Literature:

$$(5) \qquad F_s = S \times A_s = \left(S \times L \times \pi \times D_{major}\right) \times TSF$$

$$Where\ TSF = \left\{0.5 + 0.57735\left[\frac{D_{major} - D_{minor}}{2}/p\right]\right\}$$

The models all used the same section of 6.16% volume density bone and the implant was modified using the dimensions for the screw shown in Figure 5-7. The length and angle of the thread flank angles were kept constant where possible (blue construction lines), and minimally modified when required, such as in models with low pitch and small inner diameter.

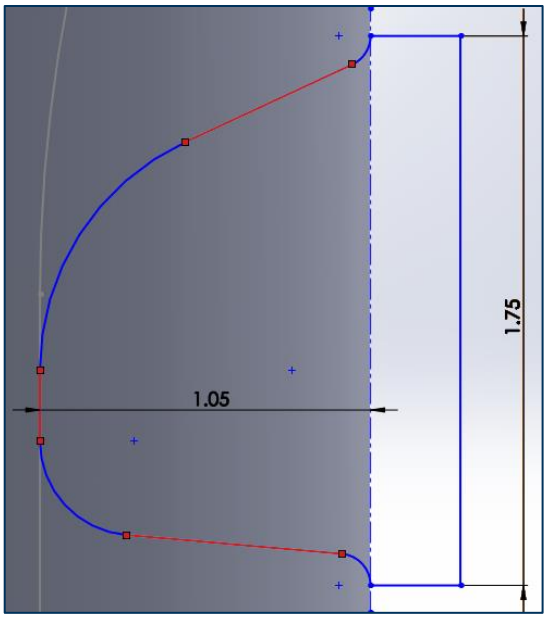

Figure 5-7: Modified Screw geometry (dimensions in mm)

The four values used for pitch were 1.55, 1.75, 2.00 and 2.50mm, where the original screw pitch was 1.75mm. Similarly, the four values used for the inner diameter (I.D.) were: 0.8, 1.2, 1.9 and 2.6mm. The original inner diameter was 1.9mm, with ±7mm while 0.8mm was used to investigate a minimal inner diameter. A few models are shown in Figure 5-8 to indicate the range studied.

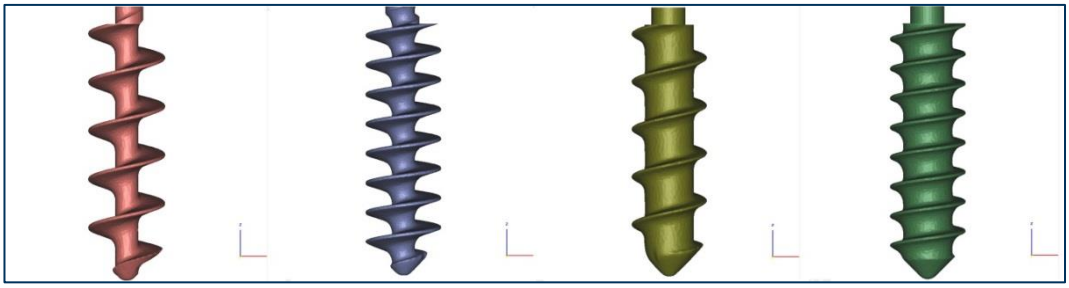

Figure 5-8: Varying Screw TSF, from left to right: 1.2mm I.D. with 2.5mm pitch, with 1.55mm pitch, then 2.6mm I.D. with 2.5mm pitch, and 1.55mm pitch.

Table 2 shows the collection of models created and the resulting TSF calculated using the standard outer diameter of 4mm and the inner diameter and pitch marked.

Table 2: Thread shape factor.

	Inner Diameter			
Pitch	0.8	1.2	1.9	2.6
1.55	1.096	1.022	0.891	0.761
1.75	1.028	0.962	0.846	0.731
2	0.962	0.904	0.803	0.702
2.5	0.870	0.823	0.743	0.662

The lowest BV/TV (6.16%) was selected as the apparent density at most influenced by screw geometry. It also represents osteoporotic bone density and qualifies as the principal candidate for improvement. Once the models were assembled and imported they were subjected to the same load conditions as were used in the last analysis (5.2 Varying Volume Fraction). All of the properties described in section 5.1 for cancellous bone were used. The manual work performed in the creation of the models is still a major factor in this analysis

where a very small change in supporting geometry could cause more significant changes in the results.

5.3.a. Results

The results obtained have been compiled into Table 3 and Figure 5-9 below, where all results are in Newtons for the table and the Z-axis of the 3D surface graph.

Table 3: Pull-out reaction force (N).

	Inner Diameter			
Pitch	0.8	1.2	1.9	2.6
1.55	64.376	66.166	78.202	74.56
1.75	69.486	67.731	78.611	71.374
2	46.434	47.001	72.275	69.613
2.5	58.946	58.371	65.621	68.243

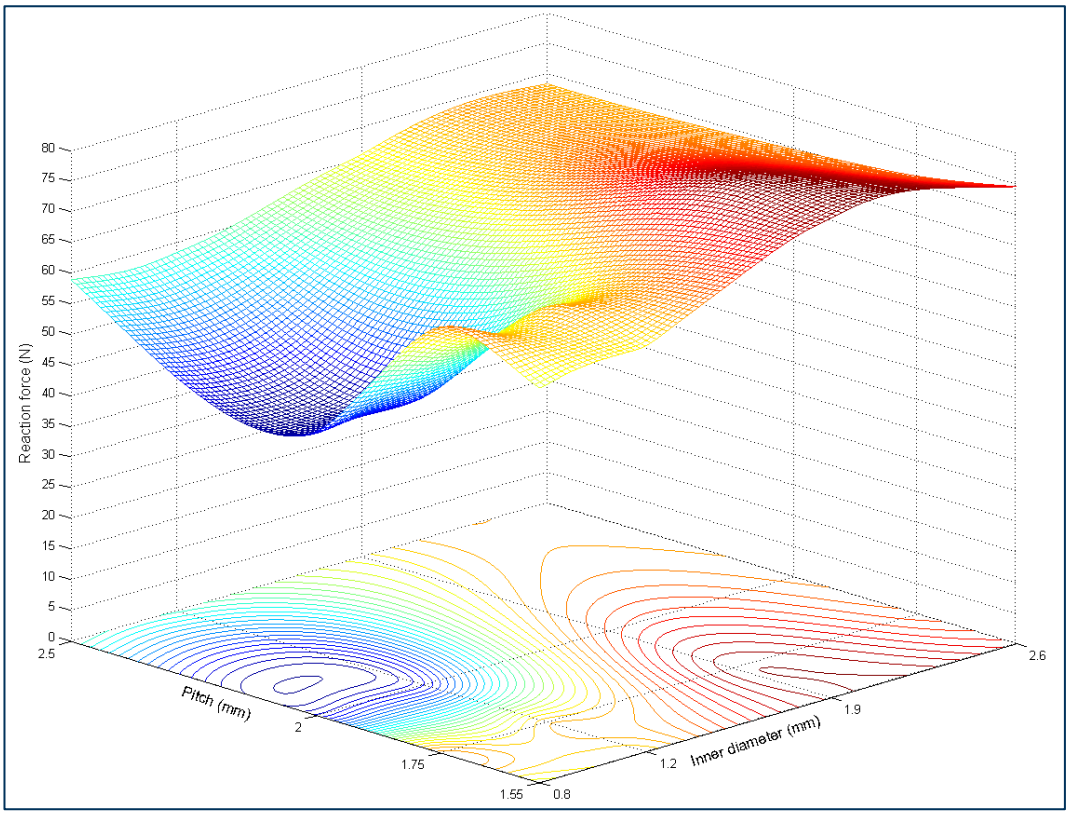

Figure 5-9: Screw 0.2mm pull-out reaction force at different TSF

The graph in Figure 5-9 was plotted using Matlab® from the data in Table 3. Each of the contours on the X-Y plane represents a step of 1N and the smooth surface plot was generated using the 'griddata', 'v4' function of Matlab® in order to give

a visual representation of the pull-out forces obtained. The original screw parameters, 1.75mm pitch & 1.9mm diameter provide the highest pull-out force at 78.6N. Inner diameter and pitch had some effect on pull-out, a 60% reduction in diameter or a 40% increase in pitch decreased the reaction force by approximately 25%. An exception to this is two results at a pitch of 2mm, with an ID of 1.2 and 0.8mm which showed a 40% decrease in pull-out force. To investigate the result further, all of the 0.8 & 1.2mm implants were rotated in the model by 180° around the screw's vertical axis and the results of these can be seen in Figure 5-10.

Table 4: Pull-out reaction force (N), rotated screw.

	Inner Diameter			
Pitch	0.8	1.2	1.9	2.6
1.55	67.113	69.168	78.202	74.56
1.75	63.693	62.286	78.611	71.374
2	61.561	63.461	72.275	69.613
2.5	58.265	60.812	65.621	68.243

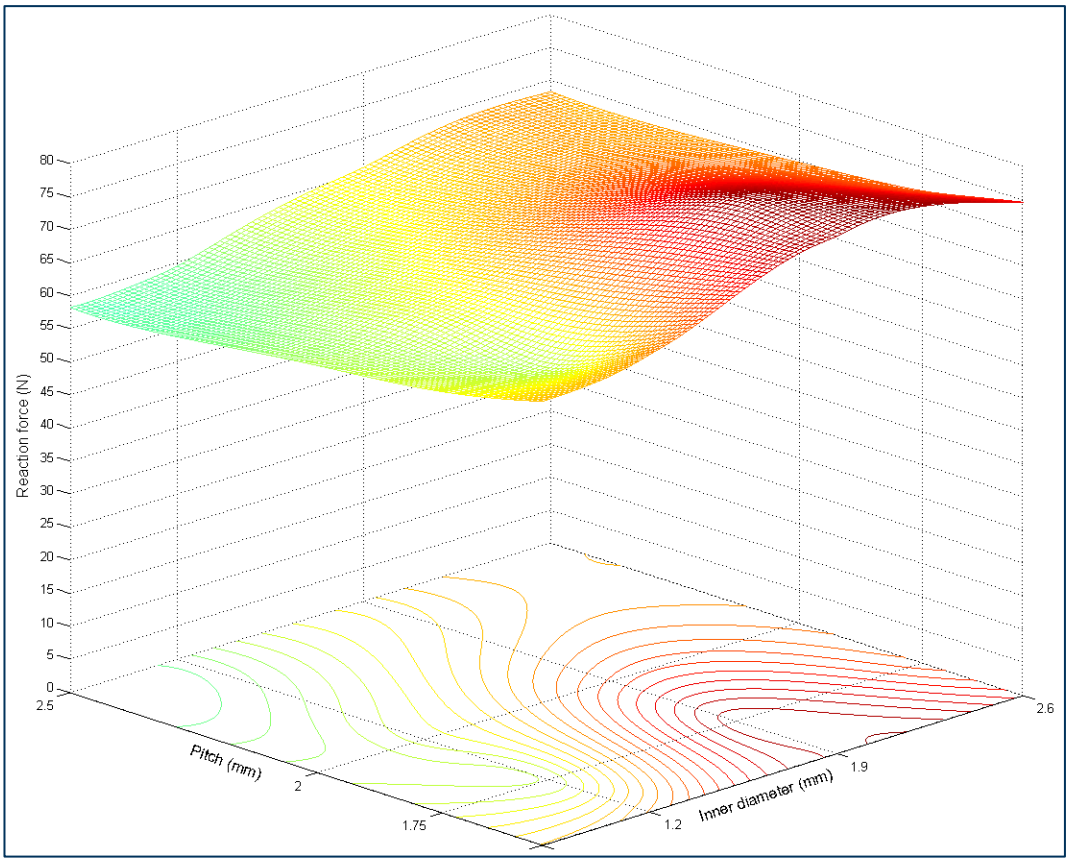

Figure 5-10: Screw 0.2mm pull-out reaction force at different TSF, rotated Screw

The effects of a 180° rotation of the screw in its longitudinal (vertical) axis were significant and no results were below 25% of the original pull-out force. The scale of the colour representation for both graphs was identical, with a minimum of 40N and a maximum of 80N. The contours on the second graph were also in 1N steps.

Further analysis of these two 'low' results is needed to understand which phenomenon might be at play. An additional set of three models was produced with parameters for pitch and ID close to the results concerned. Two models at an ID of 1.2mm but a pitch of 1.9 and 2.2mm, and a model at a pitch of 2mm but an ID of 1.4 were created. These can be seen added to the previous study in Table 5 (Green tinted results) and Figure 5-11.

Table 5: Additional pull-out reaction force models

	Inner Diameter				
Pitch	0.8	1.2	1.4	1.9	2.6
1.55	64.376	66.166		78.202	74.56

1.75	69.486	67.731	77.482	78.611	71.374
1.9		45.328			
2	46.434	47.001	49.311	72.275	69.613
2.2		64.584			
2.5	58.946	58.371		65.621	68.243

Further geometrical analysis was required to explain this 'low' data. An assumption was made that certain parts of the model under investigation, such as a face, trabeculae or thread were causing a drop in the stiffness of the model. This assumption is based on the previous work by (Procter *et al.*, 2015) which shows the high variability of pull-out strength in cancellous bone.

The "right" and "left" views of the model when used below are defined by the orientation of the model in Mimics®.

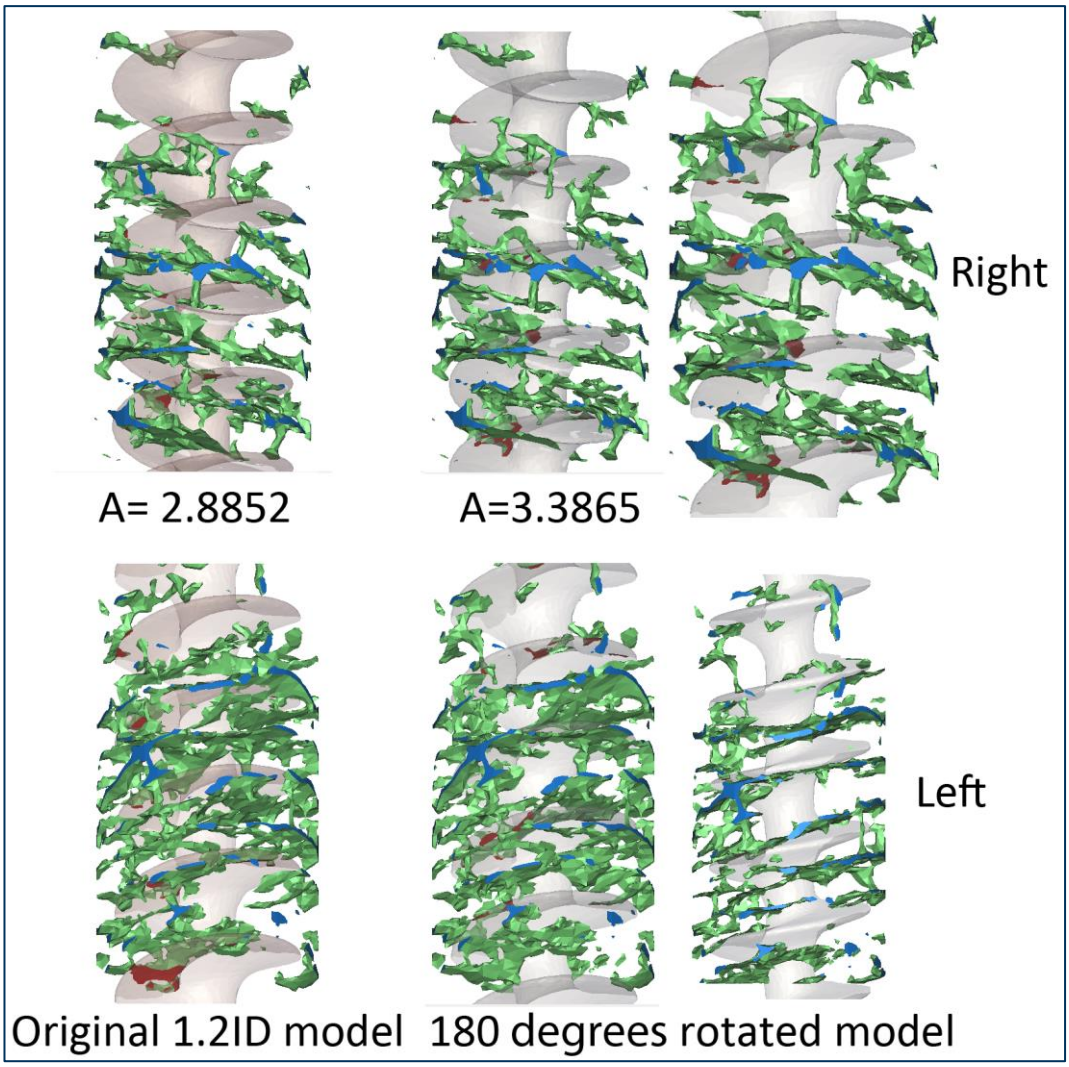

Figure 5-11: geometrical variability upon 180 rotation of the implant

On the left side of the model, the bone plate structure is aligned with the geometry of the screw thread (Figure 5-11) and this is the case for both models. As can be seen in Figure 5-12, the left side of both models would provide similar structural strength. The right side of the model, where the bone plates intersect the screw at much higher angles, they provide the strongest structure and would be the first struts to yield. On this right side, both models differ in geometry and contact area (Figure 5-11, A=2.8852 against A=3.3865). In this case, contact area gives an indication to the volume of principal holding struts, in opposition to the right side which contains very large contact areas providing low stiffness, as seen in Figure 5-12. The contact area on the left side is 17% higher in the rotated model.

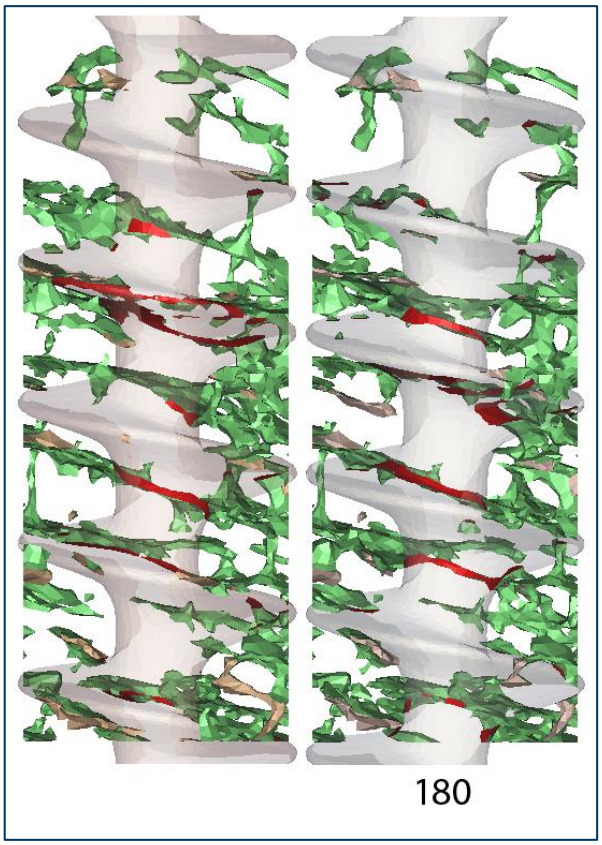

Figure 5-12: Left side view of the screw contact

This unique geometry effect is also seen across models of the same pitch and position. As Figure 5-13 shows, a section of cancellous bone of high strength (2.a) has become a very weak structure (1.b) although conserving a high contact area (1.a). This geometry is unique to each discrete trabecular section modelled as was described by Bennani Kamane (2012) or when they are used in physical tests (Procter *et al.*, 2015). Though a simple rotation of the cancellous screw stabilised the 'low' results (Figure 5-10) and providing expected results, it had no effect, or little effect on the other models at 1.75mm pitch, that were decreased by approximately 5.5% or the 2.5mm pitch models that only increased by 2.44% (ID = 1.2mm) or decreases by 0.68% (ID = 0.8mm).

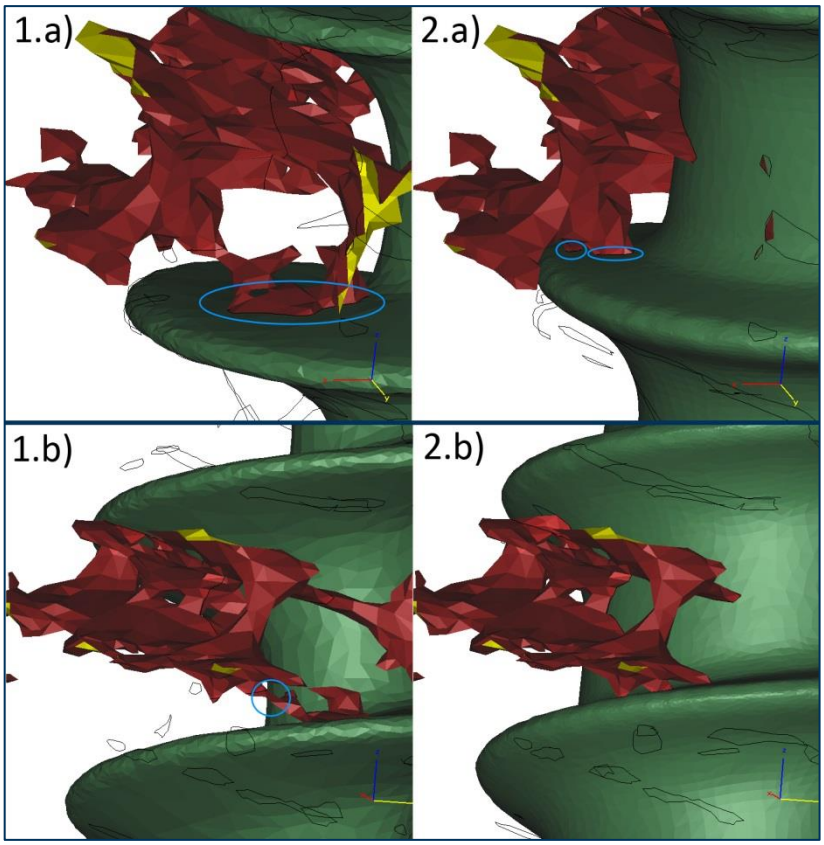

Figure 5-13: 'a' and 'b' views of 1) 1.2 inner diameter 2) 2.6 inner diameter

5.4. Proximal half angle: a critical design variable?

The third analysis was performed after a conclusion by Wang et al. (2009) that a proximal half angle of around 30° provided the highest pull-out strength when compared to 0° and 60°. The proximal half angle is the angle between the screw Head side thread surface and the vertical, on a side view. The proximal half angle on the original model is 5° and is marked, together with the modified 30° angle on Figure 5-14 below.

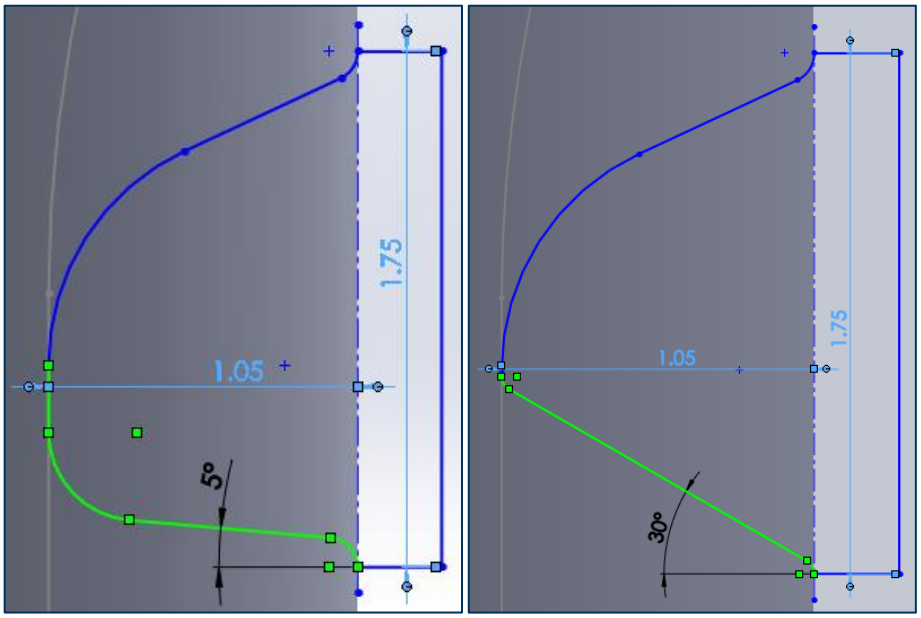

Figure 5-14: Screw proximal half angle (degrees)

Only the length of the two adjacent arcs and the length of the inner and lower edge were modified, seen coloured in Figure 5-14. Though Wang et al. (2009) performed a study on 0° and 60° the current analysis compared the original dataset of 5° and a modified model of 30°. Six models where analysed in this study: Low pitch, high pitch, low/high inner diameter, the original screw model, and the lower value model. The results of the models are given in Table 5 and showed that the alteration of the proximal half angle from 5° to 30° increases the reaction force by an average of 8.4%, where the two models with a higher pitch of 2.5mm contribute to a 0.6% and 1.2% increase for inner diameters of 1.2 and 2.6mm respectively. The original screw design, when modified, increases by 8.2% from a reaction force of 78.6N to 85.1N and the low value model was increased by 28.6% from the original low value of 47N to 60.4N

Table 6: % difference (and reaction force) between the original screw geometry and the 30° top angle models

	Inner Diameter			
Pitch	0.8	1.2	1.9	2.6
1.55		17.3% (77.6N)		14.5% (85.39N)
1.75			8.2% (85.06N)	
2		28.6% (60.45N)		
2.5		0.6% (58.71N)		1.2% (69.06N)

5.5. Discussion

This study explored the effects of different parameters of the screw and cancellous bone in a computational approximation of the bone-implant system of screw implantation. The model was idealised from a human femur CT scan in order to closely approach an in-vitro mechanical simulation. Assorted assumptions were made about the contact mechanics and boundary conditions, where the first relies heavily on a fully intact peri-implant structure and the second is linearised as the 10x10x10mm study area. As the study compared the effect of parameters on the model and compared results between the original case and the different variants, using the same conditions for all, the comparison can be made correctly.

The results obtained in section 5.4 show that the model used here supports and agrees with to the results obtained by Wang *et al.* (2009) in low density bone where an increase in the proximal half angle will increase the pull-out strength of the screw. The lower percentage increase from the current work is due to 2 factors affecting the model. The first factor is the 5° proximal half angle of the original screw. The 16% increase in pull-out they obtained was by modifying the angle from 0° but in the case of the present model, the original angle would already positively affect the pull-out force. The second factor is assumed to be the higher pitch of the screws modelled which would in turn decrease how much the pull-out can be improved. The low pitch of 1.55mm has an average increase of 16%, which matches the predicted results, even though the comparison is made between 5° and 30°.

The BV/TV is the largest influence on pull-out strength. The results here show that the same bone structure, when modelled at different apparent density, can give results that vary hugely from a very weak 80N to a 2100N reaction force. This confirms the very large effect that osteoporosis has on bone structure, as the lower 6.16% and 8.66% apparent density might represent something approximating to an osteoporotic bone structure, while 18% and 20.72% are modelled and might be representative of standard, healthy bone. The pitch of

the screws used has little effect in comparison. This means that screw development and improvement is always eclipsed by an improvement of the peri-implant structure and bone density.

This analysis of the pitch and inner diameter of the screw shows that varying both of these parameters is not of a large influence on pull-out strength. However a lower pitch value and higher inner diameter value seem to re-enforce pull-out strength while a higher pitch and smaller inner diameter seem adverse. This matches previous studies by Asnis *et al.* (1996) and Gausepohl *et al.* (2001). Two models at a pitch of 2mm and ID of 0.8 and 1.2mm are significantly lower than the others and required further analysis. The results obtained in Table 5 support the view that the low value obtained is a special case, specifically at 1.9mm pitch, where the screw thread aligns on one half of the screw with the bone plate structure (Figure 5-11) and provides very little support on the other. This confirms the thought that bone augmentation is composed of random events, often unpredictable, that are produced when a form of alignment is present within the model's geometry. This could easily happen in-vitro or in-vivo and explain certain phenomena (Procter *et al.*, 2015). The models with the exact same screw geometry, but an insertion position rotated by 180° (Figure 5-10) confirmed that this was due to the cancellous bone geometry as the modified model resulted in similar pull-out forces to the surrounding parameters values. The interaction between specific bone geometry and its interaction with specific screw geometry of 2mm pitch created a unique model.

Another point of note is that the results obtained (Table 3) do not follow a linear relation as was proposed by Chapman *et al.* (1996) and shown prior to analysis in Table 2. The linear relation proposed contains the value for the outer diameter; a parameter not studied here which has been shown to be the driving factor for pull-out strength (Hou *et al.*, 2004; Asnis *et al.*, 1996). The results show that, as predicted by Chapman *et al.* (1996), decreasing the pitch increases pull-out. However increasing the thread depth does not necessarily increase pull-out: The increasing of the outer diameter might have a significant effect while, as seen

from this study, reducing the inner diameter would have an adverse effect. As such, the simple assumption that increasing thread depth will increase pull-out must be avoided and the choice of which diameter (inner or outer) is being modified must be specified.

The validation of this model has been done previously by Bennani Kamane (2012) where he compares the CT scan model and physical testing of the same sample. He concludes that the model gives realistic results as the stiffness of the model was less than 4% different to that of the mechanical test performed and satisfactory within the modelling constraints applied. The same sample is used in the current discrete analyses. In addition, validation can also be performed by using the physical testing results obtained by Wang *et al.* (2009) and comparing the effect of such a simple geometrical modification to the same modification on FE models, which confirmed physical principles. The effect of the higher proximal half angle on pull-out is also a parameter which could have been a significant factor in the analysis by Gausepohl *et al.* (2001) as the fine machine screws have a high proximal half angle but this is not reported.

6) Chapter 6 – Screw Augmentation

The results from Chapter 5 – Parametric Analysis of a Cancellous Screw show that modifying the parameters of the screw, such as pitch and inner diameter, do not have a significant effect on pull-out. This should be compared to the possibility of cement augmentation, as there has been clinical evidence for cement augmentation in a recent meta-analysis by Namdari *et al.* (2013) who concluded that augmentation of intertrochanteric fractures may provide complication rate and radiographic parameter benefits.

This study is split into two analyses, both simplifications of modelled cement augmentation. Both Bennani Kamane (2012) and Hughes (2014) reported limitations in modelling 3 solids in a three-way contact arrangement in Mimics® 3matic®. Upon assembly of the 3rd solid in contact with two others, already in contact, the surface mesh erroneously disfeatures. The only method to obtain these models is via extensive manual work, which is both very time consuming and prone to errors in modelling. The simplification used by both for analysis of cement augmentation is the integration of the cement layer and cancellous bone structure into a unique solid. Both assumptions were based on the elastic modulus of both the cement and the bone being close and the rigid contact between the two, approximated in the current analysis as bonded, to be represented as a single solid.

The first analysis will investigate the separation of the trabecular bone around the implant: a chosen diameter of the bone structure will be split but fully bonded to the remainder of the bone, which will thus enable an increase of the material's elastic modulus. This model would both represent the stiffening of bone when surrounded by cement, but would also represent the possible modification of bone properties using chemical compounds, though this is currently used to affect the bone in its entirety (Schilcher, Michaëlsson and Aspenberg, 2011) and has not been targeted to implant sites. Two diameters were used for this study: 3.5mm and 4.75mm. 3.5mm was chosen to represent augmentation within the screw thread while 4.75mm represents augmentation

around the entire implant. Though multiple models could be made between the 4mm outer diameter and the largest inner diameter of 2.6mm, any diameter below 3.5mm would not affect a significant part of the bone on these models and a comparative study would not discern differences in a substantial way.

The second analysis used the manual method mentioned previously as the only way to obtain models via extensive manual work, which is both very time consuming and prone to errors in modelling. This was a suggested work-around by materialise® where the model's multiple surfaces, obtained after the intersection of two sets of surfaces (e.g. the screw and the bone), had to be intersected with the third surface (e.g. the cement) individually. These had to then be re-joined separately in 3-Matic® and the whole model had to be re-meshed in order to both ensure a model of complete surface shells with no open gaps and confirm the absence of duplicate or intersecting elements. A simplification was still required in order for the models to work in ANSYS®: the trabeculae found within the cement had to be removed, which consequently reduced the strength of the model as the cement properties were weaker than those used for the cancellous bone. Two diameters were also used in these models, matching the previous analysis: 3.5 and 4.75mm.

It has to be noted that both methods required integration of the new methods, which meant re-meshing, modification and further manual correction of the models. This resulted in erroneous disfeaturing, even though effort was made to conserve the geometry as close to the original as could be attained.

6.1. Multiple Bone Properties

The cancellous bone section was spilt as seen in Figure 6-1 for the 4.75mm model. Most parameters and boundary conditions are identical to those used in Chapter 5 – Parametric Analysis of a Cancellous Screw: The models were submitted to a vertical linearly ramped displacement of 0.2mm applied to the top of the screw geometry and fully restrained on the four vertical sides. The interface between the bone and the screw is a frictional contact with frictional coefficient of 0.6, asymmetric behaviour, and contact stiffness updated for each iteration. The bone elements have the following properties: ρ = 1180kg/m^3, E = 17GPa, ν = 0.3, Yield σ = 100MPa, Ultimate σ = 110MPa and the titanium screw elements were set as the defined "*Titanium alloy*" by ANSYS®: ρ = 4620kg/m^3, E = 96GPa, ν = 0.3, Yield σ = 930MPa, Ultimate σ = 1070MPa.

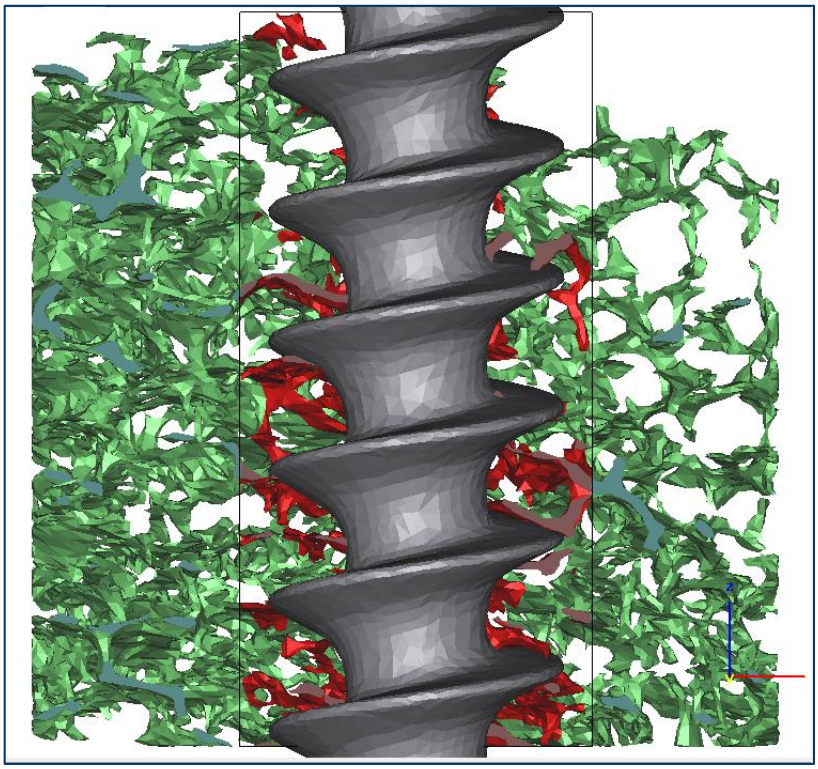

Figure 6-1: Cross section of the screw model with dual bone properties

The significant modification from this was the Young's modulus of the inner cancellous bone section (in red on Figure 6-1) which was modified in 30% steps from the original value of 17GPa to 22.1GPa and then to 27.2GPa.

6.1.a. Results

The reaction force of the 6 models analysed can be seen in Table 7 for a displacement of 0.2mm. There is a small variation (2.3% for 3.5mm and 11.3% for the 4.75mm) in the pull-out reaction force, notably an increase in pull-out strength related to the increase in material stiffness.

Table 7: Modified peri-implant bone model results (N)

	Young's modulus		
Peri-Diameter	17	22.1	27.2
3.5 mm	75.35	76.399	77.101
4.75 mm	76.204	81.167	85.089

Of first note is the reduction in reaction force of the models from the original (78.6N). This is due to the aforementioned compulsory re-meshing and manual correction of the mesh to enable import into ANSYS®. An example of the disfeaturing can be seen in Figure 6-2 where the automatic method would require a full manual re-construction, unfeasible as most changes would not be as noticeably different.

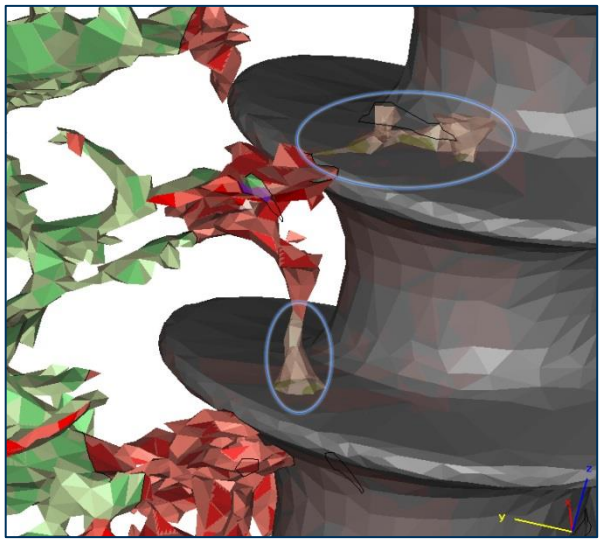

Figure 6-2: Re-meshing errors

Although this reduction will affect the exact magnitude of results, a comparative analysis can be made for the improvement: a 30% increase in the elastic modulus of a 3.5mm diameter of bone will improve pull-out by 1.4% to 76.4N while a 4.75mm diameter of augmented bone would improve pull-out by 6.5%. A further 30% increase in elastic modulus will have a lesser effect.

6.2. Cement as an intermediate solid

The second analysis which was part of this study investigated the augmentation effect of cement used as a bond between the screw and the cancellous bone. The models used for this analysis are shown in Figure 6-3 with a description of the contacts used.

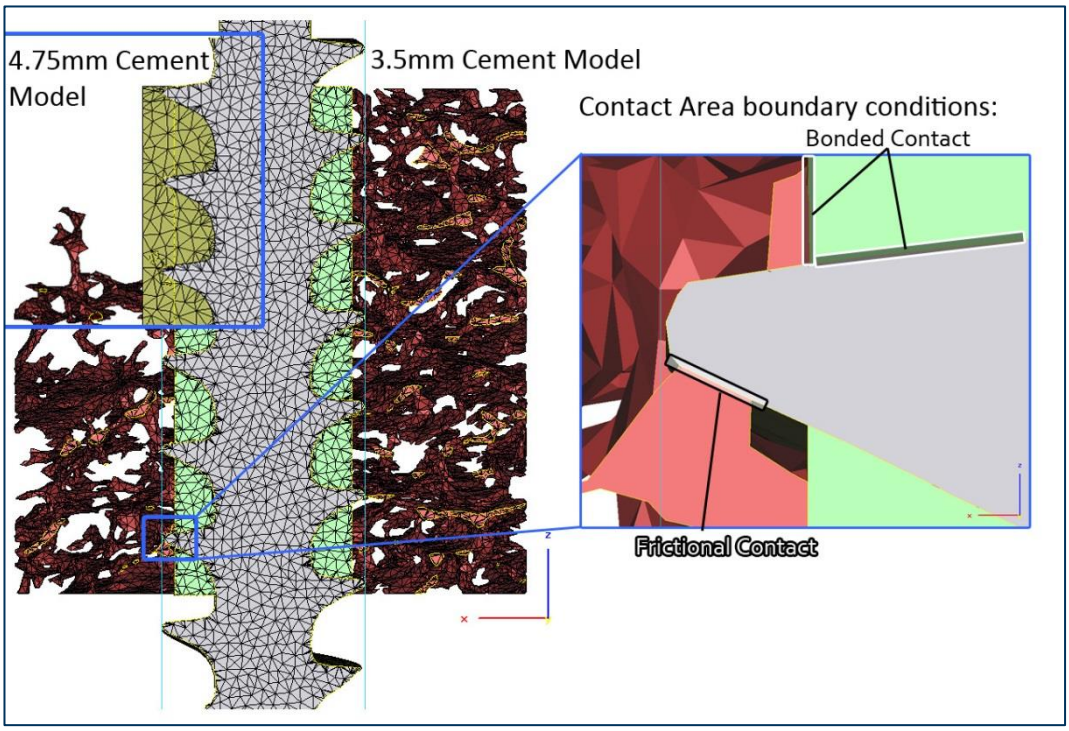

Figure 6-3: Cement augmentation model

These models used the same properties as the previous models: they were submitted to a vertical linearly ramped displacement of 0.2mm applied to the top of the screw geometry and fully restrained on the four vertical sides. The interface between the bone and the screw is a frictional contact with frictional coefficient of 0.6, asymmetric behaviour, and contact stiffness updated for each iteration. The bone elements have the following properties: ρ = 1180kg/m^3, E = 17GPa, ν = 0.3, Yield σ = 100MPa, Ultimate σ = 110MPa and the titanium screw elements were set as the defined "*Titanium alloy*" by ANSYS®: ρ = 4620kg/m^3, E = 96GPa, ν = 0.3, Yield σ = 930MPa, Ultimate σ = 1070MPa.

In addition, the cement was modelled with the properties of calcium phosphate: E = 1.5GPa, ν = 0.3, Yield σ = 16.3MPa (Brown *et al.*, 2013; Ikenaga *et al.*, 1998).

The cement and trabeculae interface as well as the cement and thread of the screw interface were both set as bonded contacts, as marked in Figure 6-3. Although a close approximation of cement augmentation, especially in the smaller diameter of cement, this model does not retain the trabecular struts which should be contained within the cement. In the 4.5mm cement model, this generates a buffer solid: an intermediate solid bonded to the cancellous bone on the exterior and acting as a continuum study of the screw on the inside, though shallow.

6.2.a. Results

The resulting reaction forces are compared to the original model run both frictionally as it was in the previous study, and as a fully bonded analysis. The results are shown in Figure 6-4.

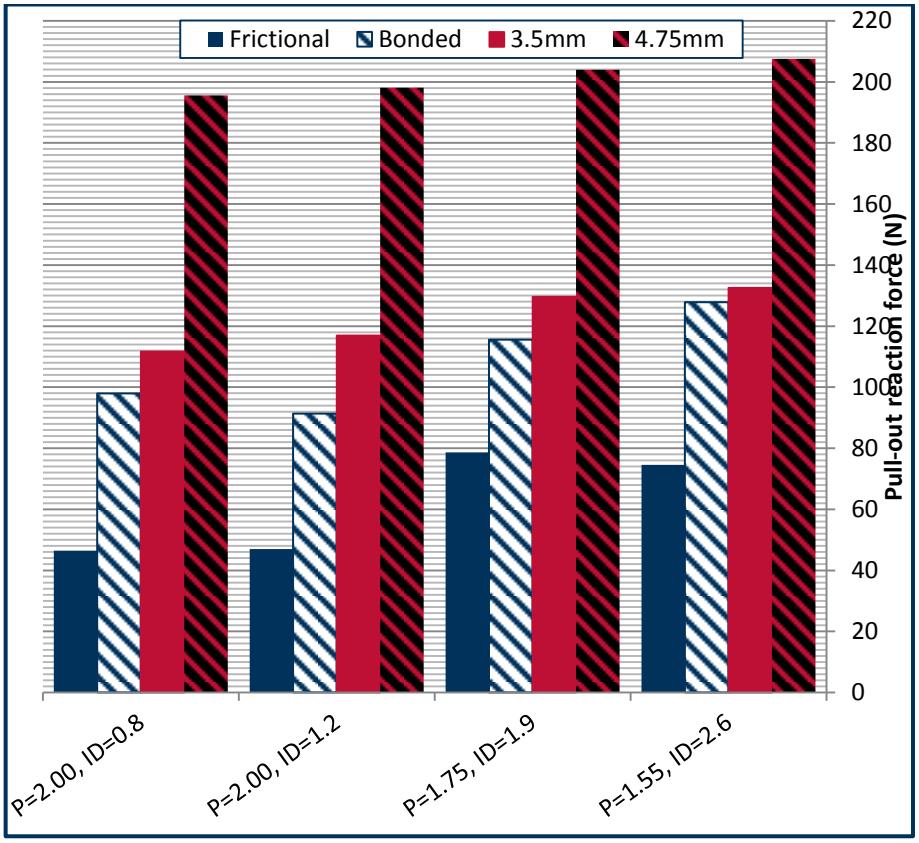

Figure 6-4: Cement augmentation models, reaction force comparison (N)

The results show a significant improvement of the pull-out force with 4.75mm of cement compared to the initial frictional analysis. It also shows a good

improvement of the 3.5mm of cement model compared to the frictional analysis with no cement. When the initial frictional model is modelled with a bonded contact between the screw and the bone however, the reaction forces are much closer to the 3.5mm of cement model.

A comparative study was then performed with the rotated models at a pitch of 2mm and inner diameters of 0.8 and 1.2mm (Figure 6-5). With 4.75mm of cement and the bonded models (cancellous bone and screw only, no cement), the reaction force is almost completely stabilised with a maximum of -0.45% and -3.15% of deviation, respectively. The bonded original models have a higher pull-out than the rotated models.

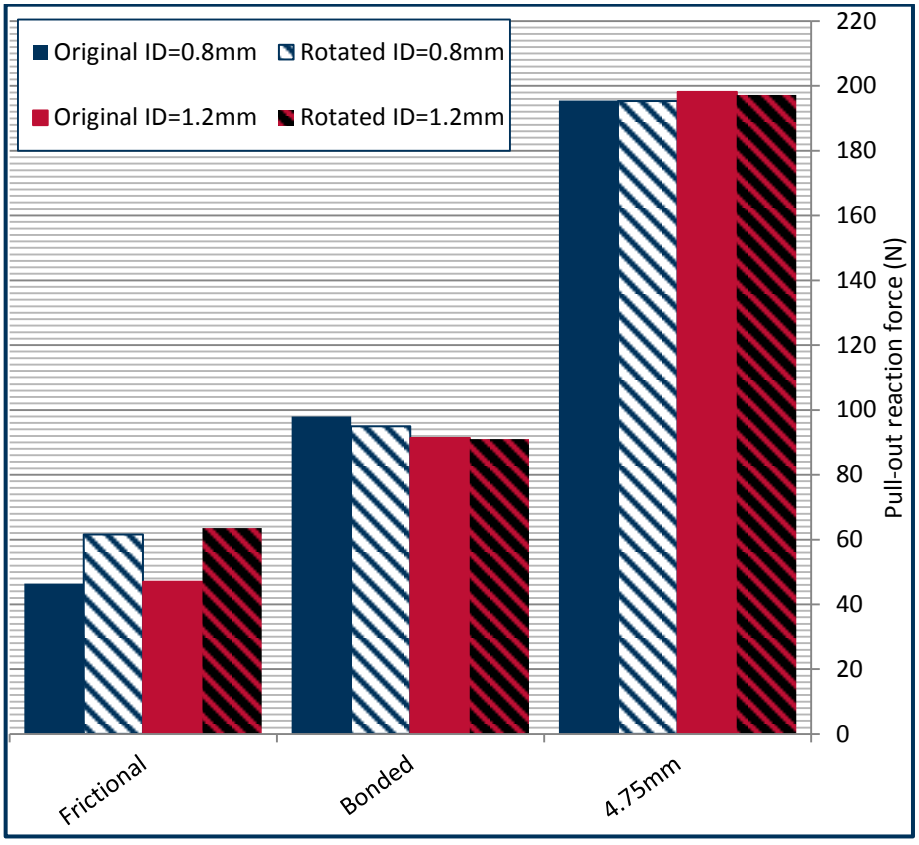

Figure 6-5: Screw rotation comparison, using reaction force (N)

This analysis was run with multiple cement elastic moduli, from a benchmarking 96 GPa, as this would represent a bonded cylinder of titanium which would yield the same pull-out forces regardless of TSF, to 0.1 which represents the material strength of Calcium Phosphate cement (Moreau, Weir and Xu, 2009). The results

of the reaction forces obtained from these models can be seen in Figure 6-6. The Young's Modulus of the cement is on an exponential scale.

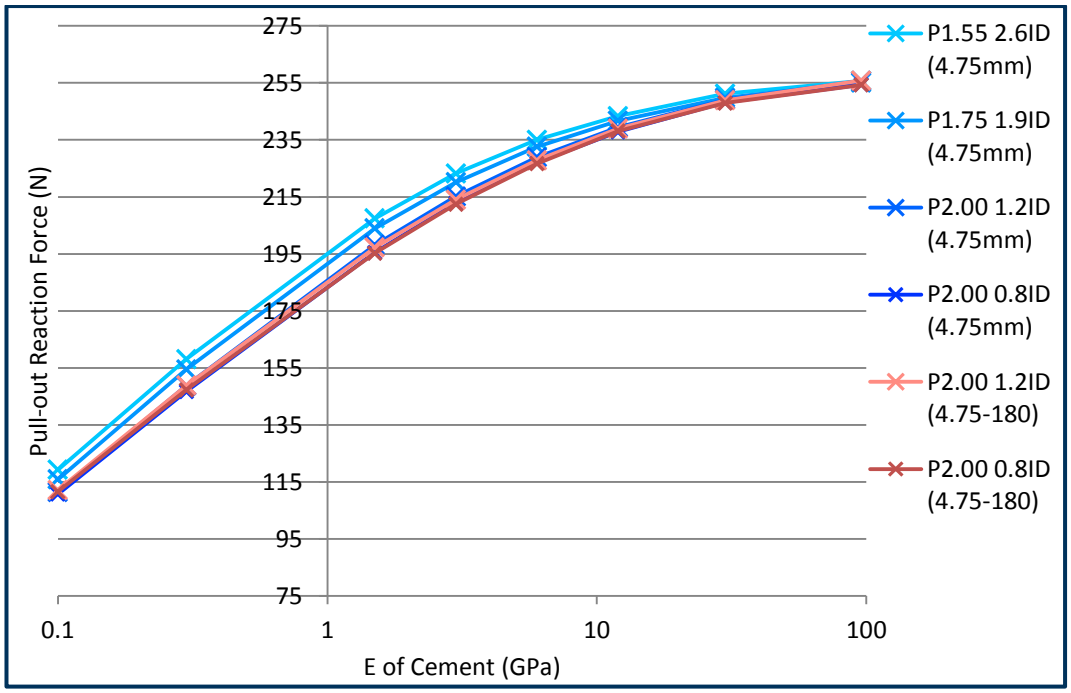

Figure 6-6: Reaction forces at varying elastic moduli (N)

6.3. Discussion

The first point of note in this study is that both analyses show stronger pull-out forces when the model is augmented. This effect is clearer in the modelled cement analysis as the absence of a third solid (cement) in the first analysis means that the result is not as significant due to the interface between the bone, though strengthened, and the screw. In the second analysis and modelled cement, the strength of the model would be reduced by the removal of trabeculae from within the cement, but in comparison to previous studies (Bennani Kamane, 2012), the interface between cement and screw was bonded which would in turn increase the strength of the model.

The variation in material elastic modulus in a selected area around the screw is shown to increase the pull-out reaction force as seen in Table 7. This is an approximation of the effect of cement augmentation but shows that local augmentation of the cancellous bone alone would improve pull-out strength, though not by a significant amount.

The second analysis is geometrically a closer approximation of cement augmentation, though not entirely adequate as trabecular struts within the cement were removed. With the cement as a continuum bonded to both the screw and the bone, the effects on the results are much more significant. These behave as expected, with the 3.5mm cement models of a lower Young's modulus providing lower pull-out forces than the bonded model, but higher than the frictional models used previously. These results also confirm the effect sustained by the rotation of the screw as when modelling 4.75mm of cement as an intermediate solid, the forces are almost identical (±1.2%).

In comparison to the variation of pull-out forces obtained by varying the geometry of the screw in Section 5.3, the results obtained from the models which included cement are significantly stronger while also removing the variation which was present at low inner diameter values. An augmentation as shallow as 3.5mm in diameter of cement around the screw, which would represent a 2.3mm layer of cement within the thread of the 1.2mm inner

diameter screw, can augment the model to a higher pull-out force than the bonded model without cement and almost double the pull-out force of the standard frictional model.

This study has demonstrated that augmentation will likely increase the holding power of screws in low-density cancellous bone although the idealised modelling and thus increased artificial stiffness should be taken into consideration.

7) Chapter 7 – Comparison of an Arthrex Pushlock with Sonic Fusion and a Predicate Device

This chapter will cover a study initially performed for comparison with a different type of implant related to Stryker® and is thus independent from the screw models performed previously.

The results obtained will be compared directly to previous work by Hughes (2014). The analysis will investigate pull-out forces in a comparative study, but remains an analysis of the effect of the peri-implant bone structure and interface, though instead of a screw implant design, a derived anchor model is used (Figure 7-1).

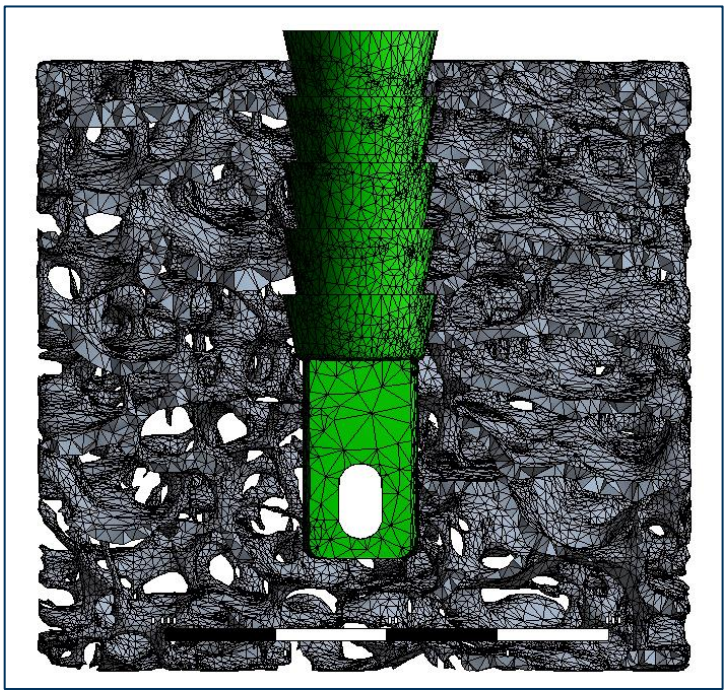

Figure 7-1: Arthrex Pushlock® model

Suture anchors are smaller screws or plugs with an eyelet, designed to attach a suture in order to repair tendons or ligaments by attaching them to bone instead of fracture repair (Hughes, 2014).

The models used for this analysis were made with surfaces directly imported from the surface meshes used by Hughes (2014) and the implant was inserted following the same method of surface intersection in 3-matic®. The bone

properties used were also identical and the elastic and strength properties of both the bone and PLDLLA ("Poly(L-lactide-co-D,L-lactide)") are assumed to be the same in tension and compression. The bone elements have the following properties: ρ = 1180kg/m^3, E = 17GPa, ν = 0.3, Yield σ = 100MPa, Ultimate σ = 110MPa (Rincón Kohli, 2003) and the PLDLLA implant elements have the following: E = 3GPa, ν = 0.3 (Black, 2005). These models were submitted to a vertical linearly ramped displacement of 0.2mm applied to the top of the screw geometry and fully restrained on the four vertical sides. The interface between the bone and the screw is a frictional contact with frictional coefficient of 0.6, asymmetric behaviour, and contact stiffness updated for each iteration, identical to the settings used by Hughes (2014). The analysis of the 2 devices were tested at 9 different locations to obtain a mean pull-out, but only 1 central location was analysed in the current comparison.

7.1. Results

The results obtained by Hughes (2014) will be listed below as subject of comparison. Table 8 shows the matching anchor position and the mean values obtained in the study.

The models used for the three sets of results listed below are described in much more depth in Chapter 7 of the thesis by Hughes (2014).

Table 8: Reaction forces (N), positions, and contact areas (mm^2) (Hughes, 2014)

Sonic Fusion model

X position	Y position	Force (N)	Contact Area (mm^2)
0	0	270.08	39.71
Mean		300.11	38.91
Std. Dev.		22.69	2.74

Bio Mini-revo® model

X position	Y position	Force (N)	Contact Area (mm^2)
0	0	254.84	14.93
Mean		259.71	15.81
Std. Dev.		14.79	2.37

Equivalent length Bio Mini-revo® model

X position	Y position	Force (N)	Contact Area (mm^2)
0	0	47.7	12.82
Mean		(17.96)	12.65
Std. Dev.		(15.98)	1.77

The results obtained for the Arthrex Pushlock® are listed in table 8 below.

Arthrex Pushlock® model, 17.5% BV/TV			8.3% BV/TV	
Displacement	Force (N)	Contact Area (mm^2)	Force (N)	Contact Area (mm^2)
0.2	309.72	10.96	109.63	6.65
0.1	148.68	10.96	52.90	6.65
0.15	229.65	10.96	81.22	6.65
0.18	278.38	10.96	98.27	6.65
0.35	553.07	10.96	195.16	6.65
0.45	732.54	10.96	252.25	6.65

The pull-out reaction force increases linearly with displacement.

7.2. Discussion and conclusion

From the results it can be seen that the Arthrex Pushlock® model has a greater pull-out force than the sonic fusion in the same location though only 3% higher than the mean value. It is also the model with the lowest contact area, which supports the assumption that contact area may not be a significant factor in the modelling of pull-out in discrete trabecular models. The increased pull-out strength against smallest contact area can be explained by the strong geometry of the device analysed. As a plug type of device however, the implant would deform upon insertion and the surrounding cancellous bone would not be an ideal match to the tapered ridges of the device. As such, the resulting pull-out force should be lower than the current result.

In comparison with the Bio Mini-revo® model however, which would be affected by the same idealised assumptions, the pull-out force is significantly (20%) higher though the contact area is lower. The conclusions for screw models and the effects of screw pitch and thread depth explain this difference, as the Bio Mini-revo® implant thread has a relatively low depth and larger pitch.

The different boundary conditions for the displacement of the implant have a linear effect on the pull-out force: Increasing displacement will increase the pull-out force. This is to be expected from a model with linear material properties, as the PLDLLA was only defined by Young's modulus and Poisson's ratio. The effect of a lower BV/TV is significant on the model, and the pull-out force is approximately a third of the value for the model with approximately twice the BV/TV. This also matches the results obtained in section 5.2 which show that BV/TV is a major factor in pull-out strength. Comparing the reaction forces of the equivalent length Bio Mini-revo® model and the 8.3% BV/TV model show further contrast of the thread pitch and depth, as the reaction force in the 8.3% BV/TV is more than double the highest equivalent length Bio Mini-revo® reaction forces while the contact area is approximately half due to the lower density.

In conclusion, this study has shown that sonic fusion may produce a holding power equivalent to that of an Arthrex Pushlock® anchor though both produce

approximately the same holding force. Sonic fusion requires less drill penetration into the bone however, and the Arthrex Pushlock® model was idealised at the contact surface, providing higher forces.

8) Chapter 8 – Conclusions and Further Work

8.1. Conclusions

This research has demonstrated the critical importance of modelling the microstructure of bone when modelling implants in cancellous bone. It has shown how the bone to implant interface is an important aspect of the discrete natured microstructure cancellous bone modelling. The results demonstrate an intrinsic variability of cancellous bone and how this can have a significant impact on implants.

The procedure for modelling implants in cancellous bone has been demonstrated including the recommended modelling technique to be used for the discrete modelling of cancellous bone.

In order to investigate the cut-out effect of femoral nail, this project has shown the importance of transient loading as it has a major effect on the magnitude and nature of the loads applied. It has also shown that FE models provide solutions that act very similarly to *in vivo* results, such as the scissoring of the two lag screws in the femoral nail, the stress distribution across the nail or the reduction of stress over load cycles.

The importance of lag screw placement was confirmed. The inferior-central or central-central cases are the optimum positions for the placement of lag screws, a Gamma3® lag screw in this case. The different positions of the lag screw on the neck fracture plane have been explored, discussed and evaluated. The difficulty in modelling in order to investigate cut-out in detail has been revealed and would need a multi-scale model which was not achievable at the time of writing.

The bone volume fraction has been shown to be the largest influence on pull-out reaction forces which confirms the very large negative effect osteoporosis has on bone strength. This effect is much larger than the variation of screw pitch which means that screw development is always eclipsed by an improvement of the peri-implant structure and bone density.

The parametric analysis of screw pitch and inner diameter shows a positive effect of a lower pitch and smaller thread depth. Previous studies show that increasing the thread depth would improve pull-out, but this is usually done by increasing the screw's outer diameter. The current study would conclude that a differentiation must be made between increasing the thread depth by increasing the outer diameter, and increasing the thread depth by decreasing the inner diameter. Another conclusion is the positive effect of a 30° proximal half angle, which improves pull-out and serves as validation for the screw model.

The parametric analysis also shows the variability of cancellous bone, where the difference of half a pitch in screw position can significantly alter pull-out strength. This further supports the assumption that every piece of implanted cancellous bone will be unique in results and a good reason for the use of FEA studies where an identical piece of bone can be used for analysis.

Augmentation was demonstrated to improve screw holding power. The research has shown that increasing the elastic modulus of bone, even in a small radius around the screw will improve pull-out. The augmentation with a layer of cement provides even higher strength and higher pull-out forces. Both models are idealised cancellous bone models where the Boolean operation of intersection would not represent in vitro screw insertion.

8.2. Further Work

Both software and hardware limitations will vary with time. Future models making use of the established process for accurate modelling of human trabecular bone may create much larger models involving larger sections of bone and greater contact areas in additions to micro-architecture accuracy. Emerging software or later versions of current modelling software might improve the modelling process and fix current issues with multi-scale modelling.

The different possible failure modes of the cancellous bone microstructure are a study which would be introduced by the screw design such as the half angle. Both the half angle and the pitch profile could have interesting effects of the modes of failure if increased accuracy was used.

The available 3d printing technology is also improving and would serve as a good alternative for physical testing or bone reinforcement as the accuracy and quality increases, and printing can now be done in calcium phosphate and collagen (Inzana *et al.*, 2014).

Published physical testing was examined during this project but there was no collaboration with clinical or physical testing. Working with a surgical team in conjunction with the FEA work would bring out clearer axes of research and needed improvement.

Finally, multiple models of real bone are needed to improve the FEA axe of implant research as the field relies principally on *in vitro* testing, but the variability of each bone sample is clearly affecting the results. An integration of patient CT scans with FE modelling on a case to case basis, which has been done selectively already, would both confirm FEA validation and provide a database of computational models. As the database is filled it may become a tool to estimate results for cases before implants are inserted physically using solution algorithms.

Digitalising medical interventions and assisting physical cases with the use of computers and software is an ongoing goal for the field of medicine.

9) References

Akan, K., Cift, H., Ozkan, K., Eceviz, E., Tasyikan, L. and Eren, A. (2011) 'Effect of osteoporosis on clinical outcomes in intertrochanteric hip fractures treated with a proximal femoral nail', *The Journal of international medical research,* 39(3), pp. 857-865.

Asnis, S.E., Ernberg, J.J., Bostrom, M.P., Wright, T.M., Harrington, R.M., Tencer, A. and Peterson, M. (1996) 'Cancellous bone screw thread design and holding power', *Journal of orthopaedic trauma,* 10(7), pp. 462-469.

Asnis, S.E. and Kyle, R.F. (1996) *Cannulated Screw Fixation: Principles and Operative Techniques.* 1st edn. New York: Springer-Verlag.

Banan, H., Al-Sabti, A., Jimulia, T. and Hart, A. (2002) 'The treatment of unstable, extracapsular hip fractures with the AO/ASIF proximal femoral nail (PFN)—our first 60 cases', *Injury,* 33(5), pp. 401-405.

Bartucci, E.J., Gonzalez, M.H., Cooperman, D.R., Freedberg, H.I., Barmada, R. and Laros, G.S. (1985) 'The effect of adjunctive methylmethacrylate on failures of fixation and function in patients with intertrochanteric fractures and osteoporosis', *The Journal of bone and joint surgery.American volume,* 67(7), pp. 1094-1107.

Baumgaertner, M.R., Curtin, S.L., Lindskog, D.M. and Keggi, J.M. (1995) 'The value of the tip-apex distance in predicting failure of fixation of peritrochanteric fractures of the hip', *The Journal of bone and joint surgery.American volume,* 77(7), pp. 1058-1064.

Bayraktar, H.H., Morgan, E.F., Niebur, G.L., Morris, G.E., Wong, E.K. and Keaveny, T.M. (2004) 'Comparison of the elastic and yield properties of human femoral trabecular and cortical bone tissue', *Journal of Biomechanics,* 37(1), pp. 27-35.

Bennani Kamane, P. (2012) *Finite element modelling of screw fixation in augmented and non-augmented cancellous bone*, PhD Thesis, Brunel University..

Bergmann, G., Deuretzbacher, G., Heller, M., Graichen, F., Rohlmann, A., Strauss, J. and Duda, G. (2001) 'Hip contact forces and gait patterns from routine activities', *Journal of Biomechanics,* 34(7), pp. 859-871.

Black, J. (2005) *Biological performance of materials: fundamentals of biocompatibility.4th Edition.* CRC Press. Boca Raton.

Bojan, A.J., Beimel, C., Taglang, G., Collin, D., Ekholm, C. and Jonsson, A. (2013) 'Critical factors in cut-out complication after Gamma Nail treatment of proximal femoral fractures', *BMC musculoskeletal disorders,* 14, pp. 1-2474-14-1.

Bridle, S.H., Patel, A.D., Bircher, M. and Calvert, P.T. (1991) 'Fixation of intertrochanteric fractures of the femur. A randomised prospective comparison of the gamma nail and the dynamic hip screw', *The Journal of bone and joint surgery.British volume,* 73(2), pp. 330-334.

Brighton, C.T. and Hunt, R.M. (1986) 'Histochemical localization of calcium in the fracture callus with potassium pyroantimonate. Possible role of chondrocyte mitochondrial calcium in callus calcification', *The Journal of bone and joint surgery.American volume,* 68(5), pp. 703-715.

Brown, C., Sinclair, R., Day, A., Hess, B. and Procter, P. (2013) 'An approximate model for cancellous bone screw fixation', *Computer methods in biomechanics and biomedical engineering,* 16(4), pp. 443-450.

Chapman, J., Harrington, R., Lee, K., Anderson, P., Tencer, A. and Kowalski, D. (1996) 'Factors affecting the pullout strength of cancellous bone screws', *Journal of Biomechanical Engineering,* 118(3), pp. 391-398.

Chen, T., Lung, C. and Cheng, C. (2009) 'Biomechanical comparison of a new stemless hip prosthesis with different shapes-a finite element analysis', *J Med Biol Eng,* 29(3), pp. 108-113.

Christodoulou, A., Terzidis, I., Ploumis, A., Metsovitis, S., Koukoulidis, A. and Toptsis, C. (2005) 'Supracondylar femoral fractures in elderly patients treated with the dynamic condylar screw and the retrograde intramedullary nail: a comparative study of the two methods', *Archives of orthopaedic and trauma surgery,* 125(2), pp. 73-79.

Coleman, M.N. and Colbert, M.W. (2007) 'Technical note: CT thresholding protocols for taking measurements on three-dimensional models', *American Journal of Physical Anthropology,* 133(1), pp. 723.

Cowin, S. (1986) 'Wolff's law of trabecular architecture at remodeling equilibrium', *Journal of Biomechanical Engineering,* 108(1), pp. 83-88.

Cowin, S.C. (2001) *Bone mechanics handbook.* 2nd Edition. CRC Press. Boca Raton.

Currey, J.D. (2002) *Bones: structure and mechanics.* Princeton University Press.

Currey, J.D. (1988) 'The effect of porosity and mineral content on the Young's modulus of elasticity of compact bone', *Journal of Biomechanics,* 21(2), pp. 131-139.

Currey, J.D. (1984) 'Effects of differences in mineralization on the mechanical properties of bone', *Philosophical transactions of the Royal Society of London.Series B, Biological sciences,* 304(1121), pp. 509-518.

Currie, C., Partridge, M., Plant, F., Roberts, J., Wakeman, R. and Williams, A. (2011) 'The National Hip Fracture Database National Report 2011', *British Geriatrics Society,* .

Dall'Oca, C., Maluta, T., Moscolo, A., Lavini, F. and Bartolozzi, P. (2010) 'Cement augmentation of intertrochanteric fractures stabilised with intramedullary nailing', *Injury,* 41(11), pp. 1150-1155.

Davis, T.R., Sher, J.L., Horsman, A., Simpson, M., Porter, B.B. and Checketts, R.G. (1990) 'Intertrochanteric femoral fractures. Mechanical failure after internal fixation', *The Journal of bone and joint surgery.British volume,* 72(1), pp. 26-31.

Den Hartog, B.D., Bartal, E. and Cooke, F. (1991) 'Treatment of the unstable intertrochanteric fracture. Effect of the placement of the screw, its angle of insertion, and osteotomy', *The Journal of bone and joint surgery.American volume,* 73(5), pp. 726-733.

Dick, C., Georgii, J., Burgkart, R. and Westermann, R. (2009) 'Stress tensor field visualization for implant planning in orthopedics', *Visualization and Computer Graphics, IEEE Transactions on,* 15(6), pp. 1399-1406.

Eriksson, F., Mattsson, P. and Larsson, S. (2002) 'The effect of augmentation with resorbable or conventional bone cement on the holding strength for femoral neck fracture devices', *Journal of orthopaedic trauma,* 16(5), pp. 302-310.

Fensky, F., Nüchtern, J., Kolb, J., Huber, S., Rupprecht, M., Jauch, S., Sellenschloh, K., Püschel, K., Morlock, M. and Rueger, J. (2013) 'Cement augmentation of the proximal femoral nail antirotation for the treatment of osteoporotic pertrochanteric fractures—a biomechanical cadaver study', *Injury,* 44(6), pp. 802-807.

Gabet, Y., Kohavi, D., Voide, R., Mueller, T.L., Müller, R. and Bab, I. (2010) 'Endosseous implant anchorage is critically dependent on mechanostructural determinants of peri-implant bone trabeculae', *Journal of Bone and Mineral Research,* 25(3), pp. 575-583.

Gausepohl, T., Möhring, R., Pennig, D. and Koebke, J. (2001) 'Fine thread versus coarse thread', *Injury,* 32, pp. 1-7.

Gefen, A. (2002) 'Optimizing the biomechanical compatibility of orthopedic screws for bone fracture fixation', *Medical engineering & physics,* 24(5), pp. 337-347.

Gibson, L. (1985) 'The mechanical behaviour of cancellous bone', *Journal of Biomechanics,* 18(5), pp. 317-328.

Gibson, L.J. and Ashby, M. (1982) 'The mechanics of three-dimensional cellular materials', *Proceedings of the Royal Society of London.A.Mathematical and Physical Sciences,* 382(1782), pp. 43-59.

Gibson, L.J. and Ashby, M.F. (1997) *Cellular solids: structure and properties.* 2nd Edition. Cambridge University Press. Cambridge.

Goodman, S.B., Bauer, T.W., Carter, D., Casteleyn, P.P., Goldstein, S.A., Kyle, R.F., Larsson, S., Stankewich, C., Swiontkowski, M.F.,Tencer, A.F., Yetkinler, D.N. and Poser, R.D. (1998) 'Norian SRS Cement Augmentation in Hip Fracture Treatment: Laboratory and Initial Clinical Results.', *Clinical Orthopaedics And Related Research,* 348, pp. 42-50.

Goodship, A. and Cunningham, J. (2001) 'Pathophysiology of functional adaptation of bone in remodelling and repair in-vivo'. *Bone Mechanics Handbook.* 2nd Edition. CRC Press. Boca Raton.

Große-Brauckmann, K. and Meinhard, W. (1996) 'The gyroid is embedded and has constant mean curvature companions', *Calculus of Variations and Partial Differential Equations,* 4(6), pp. 499-523.

Gundapaneni, D. and Goswami, T. (2014) 'Thermal isotherms in PMMA and cell necrosis during total hip arthroplasty', *J.Appl.Biomater.Funct.Mater.http://dxdoi.org/10.5301/jabfm,* [Epub ahead of print].

Gundle, R., Gargan, M. and Simpson, A. (1995) 'How to minimize failures of fixation of unstable intertrochanteric fractures', *Injury,* 26(9), pp. 611-614.

Guyton, J. (1998) 'Fractures of hip, acetabulum, and pelvis', *Campbell's operative orthopaedics.9th ed.St.Louis: Mosby,* , pp. 2181-2276.

Hara, T., Tanck, E., Homminga, J. and Huiskes, R. (2002) 'The influence of microcomputed tomography threshold variations on the assessment of structural and mechanical trabecular bone properties', *Bone,* 31(1), pp. 107-109.

Haynes, R., Pöll, R., Miles, A. and Weston, R. (1997) 'Failure of femoral head fixation: a cadaveric analysis of lag screw cut-out with the gamma locking nail and AO dynamic hip screw', *Injury,* 28(5), pp. 337-341.

Hou, S., Hsu, C., Wang, J., Chao, C. and Lin, J. (2004) 'Mechanical tests and finite element models for bone holding power of tibial locking screws', *Clinical Biomechanics,* 19(7), pp. 738-745.

Hou, F.J., Lang, S.M., Hoshaw, S.J., Reimann, D.A. and Fyhrie, D.P. (1998) 'Human vertebral body apparent and hard tissue stiffness', *Journal of Biomechanics,* 31(11), pp. 1009-1015.

Hughes, C.M. (2014) *A Finite Element Modelling Strategy for Suture Anchor Devices*, PhD Thesis, Brunel University..

Hughes, C., Bordush, A., Robioneck, B., Procter, P. and Brown, C. (2014) 'Bone Anchors—A Preliminary Finite Element Study of Some Factors Affecting Pullout', *Journal of Medical Devices,* 8(4), pp. 041006.

Huiskes, R., Weinans, H., Grootenboer, H., Dalstra, M., Fudala, B. and Slooff, T. (1987) 'Adaptive bone-remodeling theory applied to prosthetic-design analysis', *Journal of Biomechanics,* 20(11), pp. 1135-1150.

Ikenaga, M., Hardouin, P., Lemaitre, J., Andrianjatovo, H. and Flautre, B. (1998) 'Biomechanical characterization of a biodegradable calcium phosphate hydraulic cement: a comparison with porous biphasic calcium phosphate ceramics', *Journal of Biomedical Materials Research,* 40(1), pp. 139-144.

Inzana, J.A., Olvera, D., Fuller, S.M., Kelly, J.P., Graeve, O.A., Schwarz, E.M., Kates, S.L. and Awad, H.A. (2014) '3D printing of composite calcium phosphate and collagen scaffolds for bone regeneration', *Biomaterials,* 35(13), pp. 4026-4034.

Jacobs, C.R., Davis, B.R., Rieger, C.J., Francis, J.J., Saad, M. and Fyhrie, D.P. (1999) 'The impact of boundary conditions and mesh size on the accuracy of cancellous bone tissue modulus determination using large-scale finite-element modeling', *Journal of Biomechanics,* 32(11), pp. 1159-1164.

Jee, W.S. (2001) 'Integrated bone tissue physiology: anatomy and physiology', *Bone Mechanics Handbook.* 2nd Edition. CRC Press. Boca Raton.

Kane, P., Vopat, B., Heard, W., Thakur, N., Paller, D., Koruprolu, S. and Born, C. (2014) 'Is tip apex distance as important as we think? A biomechanical study examining optimal lag screw placement', *Clinical Orthopaedics and Related Research®,* 472(8), pp. 2492-2498.

Kanis, J.A., Delmas, P., Burckhardt, P., Cooper, C. and Torgerson, D. (1997) 'Guidelines for diagnosis and management of osteoporosis', *Osteoporosis International,* 7(4), pp. 390-406.

Karcher, H. (1989) 'The triply periodic minimal surfaces of Alan Schoen and their constant mean curvature companions', *Manuscripta mathematica,* 64(3), pp. 291-357.

Kawaguchi, S., Sawada, K. and Nabeta, Y. (1998) 'Cutting-out of the lag screw after internal fixation with the Asiatic gamma nail', *Injury,* 29(1), pp. 47-53.

Keaveny, T.M., Pinilla, T.P., Crawford, R.P., Kopperdahl, D.L. and Lou, A. (1997) 'Systematic and random errors in compression testing of trabecular bone', *Journal of Orthopaedic Research,* 15(1), pp. 101-110.

Kim, C.H., Zhang, H., Mikhail, G., Von Stechow, D., Müller, R., Kim, H.S. and Guo, X.E. (2007) 'Effects of thresholding techniques on μCT-based finite element models of trabecular bone', *Journal of Biomechanical Engineering,* 129(4), pp. 481-486.

Konstantinidis, L., Papaioannou, C., Hirschmüller, A., Pavlidis, T., Schroeter, S., Südkamp, N. and Helwig, P. (2013) 'Intramedullary nailing of trochanteric fractures: central or caudal positioning of the load carrier? A biomechanical comparative study on cadaver bones', *Injury,* 44(6), pp. 784-790.

Kuzyk, P.R., Zdero, R., Shah, S., Olsen, M., Waddell, J.P. and Schemitsch, E.H. (2012) 'Femoral head lag screw position for cephalomedullary nails: a biomechanical analysis', *Journal of orthopaedic trauma,* 26(7), pp. 414-421.

Kyle, R.F., Gustilo, R.B. and Premer, R.F. (1979) 'Analysis of six hundred and twenty-two intertrochanteric hip fractures', *The Journal of bone and joint surgery.American volume,* 61(2), pp. 216-221.

Ladd, A.J.C., Kinney, J.H., Haupt, D.L. and Goldstein, S.A. (1998) 'Finite-element modeling of trabecular bone: Comparison with mechanical testing and determination of tissue modulus', *Journal of Orthopaedic Research,* 16(5), pp. 622-628.

Lane, W.A. (1894) 'A Method of Treating Simple Oblique Fractures of the Tibia and Fibula more Efficient than those in Common Use', *Transactions of the Clinical Society of London,* 27, pp. 167.

Larsson, S., Friberg, S. and Hansson, L. (1990) 'Trochanteric Fractures: Influence of Reduction and Implant Position on Impaction and Complications.', *Clinical orthopaedics and related research,* 259, pp. 130-139.

Laskin, R.S., Gruber, M.A. and Zimmerman, A.J. (1979) 'Intertrochanteric fractures of the hip in the elderly: a retrospective analysis of 236 cases', *Clinical orthopaedics and related research,* 141, pp. 188-195.

Lee, T.C., Staines, A. and Taylor, D. (2002) 'Bone adaptation to load: Microdamage as a stimulus for bone remodelling', *Journal of anatomy,* 201(6), pp. 437-446.

Legrand, E., Chappard, D., Pascaretti, C., Duquenne, M., Krebs, S., Rohmer, V., Basle, M. and Audran, M. (2000) 'Trabecular bone microarchitecture, bone mineral density, and vertebral fractures in male osteoporosis', *Journal of Bone and Mineral Research,* 15(1), pp. 13-19.

Leung, K.S., So, W.S., Shen, W.Y. and Hui, P.W. (1992) 'Gamma nails and dynamic hip screws for peritrochanteric fractures. A randomised prospective study in elderly patients', *The Journal of bone and joint surgery.British volume,* 74(3), pp. 345-351.

Lindner, T., Kanakaris, N.K., Marx, B., Cockbain, A., Kontakis, G. and Giannoudis, P.V. (2009) 'Fractures of the hip and osteoporosis: the role of bone substitutes', *The Journal of bone and joint surgery.British volume,* 91(3), pp. 294-303.

Lucke, M., Burghardt, R.D., Siebenlist, S., Ganslmeier, A. and Stöckle, U. (2010) 'Medial migration of lag screw with intrapelvic dislocation in gamma nailing--a unique problem? A report of 2 cases', *Journal of orthopaedic trauma,* 24(2), pp. e6-e11.

Lyon, W.F., Cochran, J.R. and Smith, L. (1941) 'Actual Holding Power of various Screws in Bone', *Annals of Surgery,* 114(3), pp. 376-384.

Mainds, C.C. and Newman, R.J. (1989) 'Implant failures in patients with proximal fractures of the femur treated with a sliding screw device', *Injury,* 20(2), pp. 98-100.

McDonnell, P., Harrison, N., Lohfeld, S., Kennedy, O., Zhang, Y. and McHugh, P. (2010) 'Investigation of the mechanical interaction of the trabecular core with an external shell using rapid prototype and finite element models', *Journal of the mechanical behavior of biomedical materials,* 3(1), pp. 63-76.

McNamara, L.M. and Prendergast, P.J. (2007) 'Bone remodelling algorithms incorporating both strain and microdamage stimuli', *Journal of Biomechanics,* 40(6), pp. 1381-1391.

Miller, S.C., de Saint-Georges, L., Bowman, B.M. and Jee, W.S. (1989) 'Bone lining cells: structure and function', *Scanning microscopy,* 3(3), pp. 953-60; discussion 960-1.

Monahan, W.G. (1996) 'Fluoroscopic Procedures in Orthopaedics: Radiation Exposure of Patients and Personnel', *Cannulated Screw Fixation,* pp. 41-50. Springer. New York.

Moreau, J.L., Weir, M.D. and Xu, H.H. (2009) 'Self-setting collagen-calcium phosphate bone cement: Mechanical and cellular properties', *Journal of Biomedical Materials Research Part A,* 91(2), pp. 605-613.

Morgan, E.F. and Keaveny, T.M. (2001) 'Dependence of yield strain of human trabecular bone on anatomic site', *Journal of Biomechanics,* 34(5), pp. 569-577.

Mosekilde, L. (1990) 'Consequences of the remodelling process for vertebral trabecular bone structure: a scanning electron microscopy study (uncoupling of unloaded structures)', *Bone and mineral,* 10(1), pp. 13-35.

Mulholland, R. and Gunn, D. (1972) 'Sliding screw plate fixation of intertrochanteric femoral fractures.', *Journal of Trauma and Acute Care Surgery,* 12(7), pp. 581-591.

Müller, M.E., Koch, P., Nazarian, S. and Schatzker, J. (1990) *The comprehensive classification of fractures of long bones.* Springer-Verlag Berlin Heidelberg.

Mulvihill, B.M. and Prendergast, P.J. (2008) 'An algorithm for bone mechanoresponsiveness: Implementation to study the effect of patient-specific cell mechanosensitivity on trabecular bone loss', *Computer methods in biomechanics and biomedical engineering,* 11(5), pp. 443-451.

Mulvihill, B.M. and Prendergast, P.J. (2010) 'Mechanobiological regulation of the remodelling cycle in trabecular bone and possible biomechanical pathways for osteoporosis', *Clinical Biomechanics,* 25(5), pp. 491-498.

Namdari, S., Rabinovich, R., Scolaro, J., Baldwin, K., Bhandari, M. and Mehta, S. (2013) 'Absorbable and non-absorbable cement augmentation in fixation of intertrochanteric femur fractures: systematic review of the literature', *Archives of orthopaedic and trauma surgery,* 133(4), pp. 487-494.

Nazarian, A., Stauber, M., Zurakowski, D., Snyder, B.D. and Müller, R. (2006) 'The interaction of microstructure and volume fraction in predicting failure in cancellous bone', *Bone,* 39(6), pp. 1196-1202.

Niebur, G.L., Feldstein, M.J., Yuen, J.C., Chen, T.J. and Keaveny, T.M. (2000) 'High-resolution finite element models with tissue strength asymmetry accurately predict failure of trabecular bone', *Journal of Biomechanics,* 33(12), pp. 1575-1583.

Nishiura, T., Nozawa, M. and Morio, H. (2009) 'The new technique of precise insertion of lag screw in an operative treatment of trochanteric femoral fractures with a short intramedullary nail', *Injury,* 40(10), pp. 1077-1083.

Noor, S., Pridham, C., Fawcett, T., Barclay, M., Feng, Y., Hassan, O. and Pallister, I. (2013) 'Finite element analysis modelling of proximal femoral fractures, including post-fixation periprosthetic fractures', *Injury,* 44(6), pp. 791-795.

Oberg, E., Jones, F., Horton, H. and Ryffel, H. (1987) 'Working strength of bolts', *Machinery's Handbook,* pp. 1068-1069. Ryffel Industrial Press.

Parker, M.J. (1992) 'Cutting-out of the dynamic hip screw related to its position', J Bone Joint Surg Br, 74(4), pp. 625.

Parker, M.J. and Ali, S. (2010) 'Short versus long thread cannulated cancellous screws for intracapsular hip fractures: A randomised trial of 432 patients', *Injury,* 41(4), pp. 382-384.

Parker, M. and Johansen, A. (2006) 'Hip fracture', *British medical journal,* 7557, pp. 27.

Parmar, V., Kumar, S., Aster, A. and Harper, W.H. (2005) 'Review of methods to quantify lag screw placement in hip fracture fixation', *Acta Orthop Belg,* 71(3), pp. 260-263.

Perilli, E., Baleani, M., Öhman, C., Fognani, R., Baruffaldi, F. and Viceconti, M. (2008) 'Dependence of mechanical compressive strength on local variations in microarchitecture in cancellous bone of proximal human femur', *Journal of Biomechanics,* 41(2), pp. 438-446.

Pervez, H., Parker, M.J. and Vowler, S. (2004) 'Prediction of fixation failure after sliding hip screw fixation', *Injury,* 35(10), pp. 994-998.

Prendergast, P. and Taylor, D. (1990) 'Stress analysis of the proximo-medial femur after total hip replacement', *Journal of Biomedical Engineering,* 12(5), pp. 379-382.

Prendergast, P.J., Galibarov, P.E., Lowery, C. and Lennon, A.B. (2011) 'Computer simulating a clinical trial of a load-bearing implant: An example of an intramedullary prosthesis', *Journal of the Mechanical Behavior of Biomedical Materials,* 4(8), pp. 1880-1887.

Prendergast, P.J. and Taylor, D. (1992) 'Design of intramedullary prostheses to prevent bone loss: predictions based on damage-stimulated remodelling', *Journal of Biomedical Engineering,* 14(6), pp. 499-506.

Procter, P. (2013) 'Designing an Augmentation System', GRIBOI, Boston, 2013.

Procter, P., Bennani, P., Brown, C., Arnoldi, J., Pioletti, D. and Larsson, S. (2015) 'Variability of the pullout strength of cancellous bone screws with cement augmentation', *Clinical Biomechanics,* 30, pp. 500-506.

Rho, J., Zioupos, P., Currey, J. and Pharr, G. (2002) 'Microstructural elasticity and regional heterogeneity in human femoral bone of various ages examined by nano-indentation', *Journal of Biomechanics,* 35(2), pp. 189-198.

Rho, J., Tsui, T.Y. and Pharr, G.M. (1997) 'Elastic properties of human cortical and trabecular lamellar bone measured by nanoindentation', *Biomaterials,* 18(20), pp. 1325-1330.

Rice, J.C., Cowin, S.C. and Bowman, J.A. (1988) 'On the dependence of the elasticity and strength of cancellous bone on apparent density', *J.Biomechanics,* 21(2), pp. 155-168.

Riggs, B.L. and Melton, L.J. (1986) 'Involutional Osteoporosis', *N Engl J Med,* 314(26), pp. 1676-1686.

Rincón Kohli, L. (2003) 'Identification of a multiaxial failure criterion for human trabecular bone', PhD Thesis, Ecole polytechnique Federale de Lausanne..

Rizzoli, R. and Bonjour, J. (1999) 'Determinants of peak bone mass and mechanisms of bone loss', *Osteoporosis International,* 9(8), pp. S17-S23.

Scannell, P.T. and Prendergast, P.J. (2009) 'Cortical and interfacial bone changes around a non-cemented hip implant: Simulations using a combined strain/damage remodelling algorithm', *Medical engineering & physics,* 31(4), pp. 477-488.

Scherf, H. and Tilgner, R. (2009) 'A new high-resolution computed tomography (CT) segmentation method for trabecular bone architectural analysis', *American Journal of Physical Anthropology,* 140(1), pp. 39-51.

Schilcher, J., Michaëlsson, K. and Aspenberg, P. (2011) 'Bisphosphonate use and atypical fractures of the femoral shaft', *New England Journal of Medicine,* 364(18), pp. 1728-1737.

Schipper, I., Marti, R. and van der Werken, C. (2004) 'Unstable trochanteric femoral fractures: extramedullary or intramedullary fixation: review of literature', *Injury,* 35(2), pp. 142-151.

Schipper, I.B., Bresina, S., Wahl, D., Linke, B., van Vugt, A.B. and Schneider, E. (2002) 'Biomechanical evaluation of the proximal femoral nail', *Clinical orthopaedics and related research,* 405, pp. 277-286.

Schipper, I.B., Steyerberg, E.W., Castelein, R.M., van der Heijden, F.H., den Hoed, P.T., Kerver, A.J. and van Vugt, A.B. (2004) 'Treatment of unstable trochanteric fractures. Randomised comparison of the gamma nail and the proximal femoral nail', *The Journal of bone and joint surgery.British volume,* 86(1), pp. 86-94.

Schoen, A.H. (1970) *Infinite periodic minimal surfaces without self-intersections.* National Aeronautics and Space Administration. Washington, D.C. Technical Note.

Singh, M., Nagrath, A.R. and Maini, P.S. (1970) 'Changes in trabecular pattern of the upper end of the femur as an index of osteoporosis', *The Journal of bone and joint surgery.American volume,* 52(3), pp. 457-467.

Stoffel, K.K., Leys, T., Damen, N., Nicholls, R.L. and Kuster, M.S. (2008) 'A new technique for cement augmentation of the sliding hip screw in proximal femur fractures', *Clinical Biomechanics,* 23(1), pp. 45-51.

Sullivan, P.K., Smith, J.F. and Rozzelle, A.A. (1994) 'Cranio-orbital reconstruction: safety and image quality of metallic implants on CT and MRI scanning.', *Plastic and Reconstructive Surgery,* 94(5), pp. 589-596.

Taylor, M. and Prendergast, P.J. (2014) 'Four decades of finite element analysis of orthopaedic devices: Where are we now and what are the opportunities?', *Journal of Biomechanics,* 48(5), pp. 767-778.

Tencer, A.F., Asnis, S.E., Harrington, R.M. and Chapman, J.R. (1996) 'Biomechanics of cannulated and noncannulated screws', in *Cannulated Screw Fixation.* Springer, pp. 15-40.

Tortora, G.J. and Derrickson, B. (2013) *Essentials of anatomy and physiology.* 9th Edition. John Wiley & Sons. Singapore.

Turner, C.H., Rho, J., Takano, Y., Tsui, T.Y. and Pharr, G.M. (1999) 'The elastic properties of trabecular and cortical bone tissues are similar: results from two microscopic measurement techniques', *Journal of Biomechanics,* 32(4), pp. 437-441.

Ullrich, C.G., Binet, E.F., Sanecki, M.G. and Kieffer, S.A. (1980) 'Quantitative assessment of the lumbar spinal canal by computed tomography', *Radiology,* 134(1), pp. 137-143.

Van der Linden, J., Birkenhäger-Frenkel, D., Verhaar, J. and Weinans, H. (2001) 'Trabecular bone's mechanical properties are affected by its non-uniform mineral distribution', *Journal of Biomechanics,* 34(12), pp. 1573-1580.

van Rietbergen, B., Weinans, H., Huiskes, R. and Odgaard, A. (1995) 'A new method to determine trabecular bone elastic properties and loading using micromechanical finite-element models', *Journal of Biomechanics,* 28(1), pp. 69-81.

Vichard, P. and Gagneux, E. (1995) 'Il y a 100 ans: les premiers pas de l'ostéosynthèse des fractures', *Histoire des sciences médicales–Tome XXIX–n,* , pp. 2-1995.

Wang, C., Yettram, A., Yao, M. and Procter, P. (1998) 'Finite element analysis of a Gamma nail within a fractured femur', *Medical engineering & physics,* 20(9), pp. 677-683.

Wang, Y., Mori, R., Ozoe, N., Nakai, T. and Uchio, Y. (2009) 'Proximal half angle of the screw thread is a critical design variable affecting the pull-out strength of cancellous bone screws', *Clinical Biomechanics,* 24(9), pp. 781-785.

Weinan, E. (2011) *Principles of multiscale modeling.* 1st Edition. Cambridge University Press. Cambridge.

Wirth, A.J., Goldhahn, J., Flaig, C., Arbenz, P., Müller, R. and van Lenthe, G.H. (2011) 'Implant stability is affected by local bone microstructural quality', *Bone,* 49(3), pp. 473-478.

Wirth, A.J., Müller, R. and van Lenthe, H.G. (2012) 'The discrete nature of trabecular bone microarchitecture affects implant stability', *Journal of Biomechanics,* 45(6), pp. 1060-1067.

Wittenberg, R.H., Lee, K., Shea, M., White III, A.A. and Hayes, W.C. (1993) 'Effect of screw diameter, insertion technique, and bone cement augmentation of pedicular screw fixation strength.', *Clinical orthopaedics and related research,* 296, pp. 278-287.

World Health Organization (2003) *Prevention and management of osteoporosis: report of a WHO scientific group.* Diamond Pocket Books (P) Ltd.

Wu, C., Shih, C., Lee, M. and Tai, C. (1996) 'Biomechanical analysis of location of lag screw of a dynamic hip screw in treatment of unstable intertrochanteric fracture', *Journal of Trauma and Acute Care Surgery,* 41(4), pp. 699-702.

Wu, C. and Tai, C. (2010) 'Effect of lag-screw positions on modes of fixation failure in elderly patients with unstable intertrochanteric fractures of the femur', *Journal of Orthopaedic Surgery,* 18(2).

Zdero, R. and Schemitsch, E.H. (2009) 'The effect of screw pullout rate on screw purchase in synthetic cancellous bone', *Journal of Biomechanical Engineering,* 131(2), pp. 024501.

Zhang, Q., Tan, S. and Chou, S. (2004) 'Investigation of fixation screw pull-out strength on human spine', *Journal of Biomechanics,* 37(4), pp. 479-485.

Zioupos, P. and Currey, J. (1994) 'The extent of microcracking and the morphology of microcracks in damaged bone', *Journal of Materials Science,* 29(4), pp. 978-986.

Zioupos, P., Cook, R.B. and Hutchinson, J.R. (2008) 'Some basic relationships between density values in cancellous and cortical bone', *Journal of Biomechanics,* 41(9), pp. 1961-1968.

Zysset, P.K., Edward Guo, X., Edward Hoffler, C., Moore, K.E. and Goldstein, S.A. (1999) 'Elastic modulus and hardness of cortical and trabecular bone lamellae measured by nanoindentation in the human femur', *Journal of Biomechanics,* 32(10), pp. 1005-1012.

9.1. Bibliography

Asnis, S.E. and Kyle, R.F. (1996) *Cannulated Screw Fixation: Principles and Operative Techniques.* 1st edn. New York: Springer-Verlag.

Cowin, S.C. (2001) *Bone mechanics handbook.* 2nd Edition. CRC Press. Boca Raton.

Tortora, G.J. and Derrickson, B. (2013) *Essentials of anatomy and physiology.* 9th Edition. John Wiley & Sons. Singapore.

9.2. Additional Sources

Solidworks 2013®, Dassault Sytems®, Waltham, Massachusetts (2014)

ANSYS, ANSYS® Academic Research, Release 14 (2014)

MicroMRI Inc,. USA, (2014)

Mimics®v15.0, Materialise NV, Leuven, Belgium (2014)

SkyScan® (Bruker-MicroCT), Belgium, 2014

Appendix A

Materialise® instruction for the creation of cancellous bone models with implant insertion stage by stage.

Smooth

Smooth factor 0.7

Do not use compensation

Reduce triangles

Geometrical error 0.01

Flip Threshold angle 30

Ensure one shell

Mark shell, invert and delete other bits

Auto remesh

- Shape quality threshold 0.2 (then next time 0.3)
- Maximum geometrical error 0.02 (because small part and do not want triangles to be able to move very far)
- Do not control edge length
- Do not preserve surface contours

* using inspection to look at the number of triangles that have a shape quality of less than 0.2

Deal with intersecting and overlapping triangles

Delete intersecting triangles

Mark intersecting triangles (trial had 108)

select expand marked triangles and delete them

Mass hole filler

- Bad contour length of 5mm (or larger to ensure all are filled)

One was remaining so mark shell and invert again

Delete overlapping triangles

Mark overlapping triangles (trial had 8)

Select expand marked triangles and delete them

Mass hole filler as above

Second auto remesh

- Shape quality threshold to 0.3
- Maximum geometrical error 0.01
- Control edge length on, max edge length 0.3

Ensure one shell

Mark, invert and delete

Deal with intersecting and overlapping triangles

This time do not use hole filling as it may create more low quality triangles

Do it manually by marking, deleting and filling

Quality preserve reduce triangles

Use same parameters as automesh

Implanting Screw

*Can change the colour of the parts by selecting the surface and changing the colour in the lower menu. Cannot change internal colours of individual parts

** To ensure that the co-ordinate systems are the same go to edit update OCS to CS, method WCS

Auto Remesh

Remesh the screw to ensure that there are no local areas of high density mesh

- Shape quality threshold 0.3
- Max geometrical error 0.01
- Max edge length 0.2

Preserve surface contours

Create non-manifold assembly

Make sure screw is being inserted into the bone - not the other way round

Fix sharp triangles

- Mark and remove

- check filter distance and how this affects the geometry of the screw bone interface

Auto Remesh

Using the same shape quality thresholds as have been used on the 2 components previously

If they are different then for max geometrical error use the lowest of the two parts and for max edge length use the largest.

Deal with intersecting and overlapping triangles

Delete intersecting triangles

Mark intersecting triangles (trial had 2)

Select expand marked triangles and delete them

Delete overlapping triangles

Mark overlapping triangles (trial had 11)

Select expand marked triangles and delete them

If deleting wee bits make sure the interface belongs to the screw.

Checking for holes at the interface

Remeshing > Create non-manifold curves

Curve list. Non manifold curves-3

3 is the number of surfaces that the edge belongs to. Normally this is 1 for a triangle on a surface but is more at the interface when surfaces are joining. All of these should be 'closed', if they are not there is a hole so fix it. Non-manifold curves-4 should be ok.)

Other holes not at the interface can be found by bad edges in the normal view.